Sede Amministrativa

Università degli Studi di Padova

Dipartimento di Fisica e Astronomia "G. Galilei"

Corso di dottorato di ricerca in Physics

XXXIV ciclo

Low-Dimensional Quantum Gases in Curved and Flat Geometries

Coordinatore

Ch.mo Prof. Franco Simonetto

Supervisore

Ch.mo Prof. Luca Salasnich

Dottorando

Andrea Tononi

a Federica

"At that time the wind was blowing and the banner was moving. One monk said that the wind was moving, while another monk said the banner was moving. They argued on and on, so I went forward and said, 'It is not the wind that is moving, and it is not the banner that is moving. It is your minds that are moving'."

— quote from [1], appearing as the foreword of Wong Kar-wai's movie *Ashes of time*.

Abstract

Low-dimensional quantum gases, produced by confining and cooling atoms in two- or in one-dimensional configurations, display a rich variety of equilibrium and nonequilibrium properties. The emerging experimental techniques for controlling both their geometry and their topology, by trapping these systems, for instance, in rings or in hollow shells, offer a promising route for the investigation of quantum many-body physics in curved spatial domains. In this thesis, we discuss the quantum statistical properties of spherically-symmetric bosonic shells, analyzing the phenomena of Bose-Einstein condensation and of superfluidity in the finite-size two-dimensional regime. Adopting the functional integral formulation of quantum field theory, we obtain the finite-temperature equation of state of these shell-shaped systems, and, with similar techniques, also of two-dimensional flat superfluids, both bosonic and fermionic. Moreover, we quantitatively analyze the hydrodynamic excitations at finite temperature, which consist of the first and second sound in flat superfluids, and which are the main probe of the Berezinskii-Kosterlitz-Thouless superfluid transition. We conclude our analysis by studying bright solitons in one-dimensional Bose-Bose mixtures, and discussing the quench dynamics of tunneling quasicondensate tubes.

This thesis contains a revised and coherent presentation of the results discussed in these papers and preprints:

- A. Tononi and L. Salasnich,
  Bose-Einstein Condensation on the Surface of a Sphere,
  Physical Review Letters **123**, 160403 (2019).
- A. Tononi, Y. Wang, and L. Salasnich,
  Quantum Solitons in Spin-Orbit Coupled Bose-Bose Mixtures,
  Physical Review A **99**, 063618 (2019).
- A. Tononi, F. Toigo, S. Wimberger, A. Cappellaro, and L. Salasnich,
  Dephasing-rephasing dynamics of one-dimensional tunneling quasicondensates,
  New Journal of Physics **22**, 073020 (2020).
- A. Tononi, F. Cinti, and L. Salasnich,
  Quantum bubbles in microgravity,
  Physical Review Letters **125**, 010402 (2020).
- K. Furutani, A. Tononi, and L. Salasnich
  Sound modes in collisional superfluid Bose gases,
  New Journal of Physics **23**, 043043 (2021).
- A. Tononi, A. Cappellaro, G. Bighin, and L. Salasnich,
  Propagation of first and second sound in a two-dimensional Fermi superfluid,
  Physical Review A **103**, L061303 (2021).
- A. Tononi, A. Pelster, and L. Salasnich,
  Topological superfluid transition in bubble-trapped condensates,
  arXiv:2104.04585.

To preserve the unity of the thesis, other publications will not be discussed in detail. Among them:

- A. Tononi, A. Cappellaro, and L. Salasnich,
  Condensation and superfluidity of dilute Bose gases with finite-range interaction,
  New Journal of Physics **20**, 125007 (2018).
- A. Tononi,
  Zero-Temperature Equation of State of a Two-Dimensional Bosonic Quantum Fluid with Finite-Range Interaction,
  Condensed Matter **4(1)**, 20 (2019).

Contents

1

Introduction

1.1 Background

We can picture the research in physics as a collective enterprise of a heterogeneous community that, implementing shared rules and beliefs, constructs and maintains an idealized description of reality. Some special beliefs, that we call *paradigms*[1], are considered sufficiently general and convincing – in other words, fundamental – that they constitute the theoretical basis to interpret the experiments. Paradigms are typically simple and, in a certain sense, correct ideas that guide future research and which are continuously put in a new perspective by new evidences. Indeed, the "creation of a thing, and creation plus full understanding of a correct idea of the thing, are very often parts of one and the same indivisible process and cannot be separated without bringing the process to a stop" [2]. As other fundamental concepts in quantum mechanics, the phenomenon of Bose-Einstein condensation, which constitutes the core of the present thesis, has undergone this scientific process.

Quantum mechanics, indeed, was not fully established when Einstein, following a paper by Bose [3], discussed the phenomenon of condensation in a series of papers in 1924 [4] and 1925 [5]. The exclusion principle was indeed discovered by Pauli only in 1924 [6], and the classification of the particles as bosons and fermions was still unknown. It is thus fair to say that Einstein idea was visionary and, at the same time, rather rudimentary. Many years were necessary for the "full understanding of the correct idea" of Bose-Einstein condensation and, to a certain extent, the process is still ongoing.

[1] Here we define the word paradigm adopting, among two broad possibilities [7], the narrower sense intended by T. Kuhn [8].

When the experiments with liquid Helium of Kapitza [9] emerged in the 30's, London interpreted the superfluid properties as a manifestation of the phenomenon of Bose-Einstein condensation [10]. Landau, on the contrary, considered Bose-Einstein condensation as a pathological condition of a noninteracting Bose gas [11], and described the observations only in terms of superfluidity [12], developing previous theoretical analyses by Tisza [13–15].

The Bogoliubov theory [16] and following theoretical works have established the existence of a Bose-Einstein condensate phase in interacting superfluid bosons, but the heredity of Landau is still present, as the relation between Bose-Einstein condensation and superfluidity is still not completely settled [17]. The tension among these concepts, indeed, continues to emerge in the scientific process in which new possibilities in terms of interactions, geometry, system size, spatial dimension, etc. challenge the previous theoretical concepts, and theories are stretched to reach the "full understanding" of the paradigm.

The key elements, which turned the study of Bose-Einstein condensation into a structured field with heterogeneous ramifications, are the tunability and the versatility of the experiments. The experimental milestone, from which the present diversity originates, was the discovery of Bose-Einstein condensation in 1995 [18–20], obtained by confining alkali-metal atoms and cooling them at nK-range temperatures. Rather than being a fortuitous chance, the first observation of Bose-Einstein condensation was the outcome of progressive technical advances in cooling and trapping of neutral atoms, which were mainly obtained in the 70's and in the 80's. Among them, we remind the Zeeman slower [21], and the laser cooling to produce optical molasses [22–24], combined with the trapping techniques by means of optical and magnetic potentials [25–27]. With the development of sub-Doppler cooling [28, 29] and magneto-optical traps [30], most of the technical advances were ready: the use of evaporative cooling [31, 32] allowed to reach a sufficiently high phase-space density and observe the macroscopic occupation of the condensate state [18, 19].

Nowadays, it is possible to tune and control experimentally all the different contributions of the many-body Hamiltonian: from kinetic and potential terms, to the interaction ones, i. e. engineering both weakly- and strongly-interacting systems with either short- or long-range interactions [33–35]. In perspective, these convenient features make ultracold atoms a reliable platform for the future development of quantum simulators and quantum computers [36–38]. Moreover, by strongly constraining the dynamics of an atomic gas along one (or two) spatial directions [39], i. e. decoupling the transverse dynamics from the in-plane (or in-line) degrees of freedom, ultracold atoms allow to test and develop quantum many-body physics in low spatial dimensions [40, 41].

1.2 This thesis

In this thesis, we discuss the physics of systems of ultracold atoms in low dimensions, analyzing their equilibrium and nonequilibrium properties in the temperature and density regimes where quantum degeneracy occurs. We will analyze both flat geometries, as atomic gases in box potentials or in elongated tubes, and curved configurations, as bosonic atoms confined on spherical or on ellipsoidal surfaces. Most of the results regard bosonic atoms, but also fermionic systems and their crossover from the Bardeen-Cooper-Schrieffer state to a Bose-Einstein condensate (BCS-BEC) will be analyzed. Let us provide a brief introduction to the systems and the phenomena that will be discussed in detail in the following chapters.

Shell-shaped condensates

In the field of quantum gases, most of the experimental and of the theoretical results concerning one- and two-dimensional systems, are obtained in flat geometries, as pancake or cigar-like shapes [42]. The idea of studying a curved quantum gas can be initially traced in a 2001 seminal paper by Zobay and Garraway [43], who analyzed the magnetic confinement of atomic gases with a combination of a static field and of a radiofrequency field. By properly engineering the trap parameters, it was shown that these radiofrequency-induced adiabatic potentials can trap the atoms in a shell-shaped configuration, but only if the gravitational force can be counterbalanced or neglected.

A new impulse to study theoretically these bubble-trapped condensates follows the development of several microgravity facilities to cool and confine the atomic condensates in microgravity conditions. Among them, we remind NASA-JPL Cold Atom Laboratory (CAL) [44, 45], on board of the International Space Station, drop towers [46–48], rockets [49], and a free falling elevator [50]. Experiments on bubble-trapped condensates are currently being carried on in CAL [51, 52], and will probably continue with BECCAL [53], a future microgravity facility on the International Space Station. Thus, the experimental work has driven the need of theoretical predictions, and the present thesis discusses some of the first theoretical results derived for these systems [54, 55]. In particular, considering bubble-trapped condensates in the two-dimensional thin-shell limit, we will analyze Bose-Einstein condensation and superfluidity in the spherically-symmetric case. Moreover, we will discuss the physics of prolate ellipsoidal shells [56], offering important predictions for the upcoming experiments, and we will analyze the equilibrium phase diagram of these systems.

To underline the rising interest on bubble-trapped condensates, and to provide

a synopsis of the state of the art on this topic, we list and briefly comment the main themes that have been studied recently in bubble-trapped condensates. The most promising issue is probably vortex physics [57–59], which, together with the system thermodynamics and the adiabatic expansion [60], will be the object of careful investigation on CAL. Some works have analyzed the zero-temperature hydrodynamic excitations [61–63], while others have focused on the properties of dipolar bosons [64,65]. Also the supersolidity of few-body systems was discussed [66], and a general zero-temperature framework to study quantum gases on manifolds was introduced in Ref. [67]. Finally, Bose-Bose mixtures on a spherical surface and their stability has been analyzed [68].

From our perspective, the research on curved quantum gases is still underdeveloped, and the future discoveries in this subfield will improve our general understanding of Bose-Einstein condensation and superfluidity in ultracold quantum gases.

Hydrodynamic excitations and sound modes

The two-fluid model of Landau and Tisza, developed to interpret the rich physics of superfluid Helium [9], provides a long-wavelength hydrodynamic description of a quantum liquid [12], which is modeled as a mixture of a normal fluid and of a superfluid. Due to the presence of two components, one of the main predictions of the model is the existence of two branches of hydrodynamic excitations. A major part of the present thesis is devoted to the study of the hydrodynamic modes in uniform two-dimensional superfluids which, in the box-trapped case, propagate as sound waves.

Interestingly, the measurement of the *first* and *second* sound velocities in a two-dimensional system provides a direct evidence of the superfluid transition, which, in the context of magnetic systems, was discussed by Berezinskii [69], Kosterlitz and Thouless [70–72] (BKT). The BKT transition, in which the superfluid properties are suppressed by the thermal proliferation of vortices, does not lead to any discontinuity of the thermodynamic potentials, but consists of the universal jump of the superfluid density at a critical temperature identified by Kosterlitz and Nelson [73].

While the BKT transition has already been observed in superfluid Helium [74], which is a strongly-interacting system, the first evidences in weakly-interacting bosonic superfluids were initially indirect [75]. A clear experimental proof was obtained just a few months ago [76], by measuring the first and second sound velocities in box-trapped superfluid bosons. In this thesis, we will compare our theoretical results with the experiment of Ref. [76], and we will obtain further

predictions for future investigations.

In general, the observation of the hydrodynamic excitations in weakly-interacting quantum gases confirms the validity of the two-fluid description, and demonstrates the superfluid nature of the system. In the present work, we will also analyze the propagation of sound in two-dimensional uniform fermions across the BKT transition. In particular, we will compare our finite-temperature theory with the experiment of Ref. [77], and we will discuss our results across the crossover from weakly-bound BCS pairs to the BEC regime of composite bosons [78, 79]. With the same goal, we will consider a shell-shaped bosonic superfluid, and we will study the finite-temperature hydrodynamic excitations of the system. Their experimental characterization, indeed, can prove that the superfluid transition occurs also in topologically-nontrivial compact shells, and that it is driven by the BKT mechanism of the vortex-antivortex unbinding.

One-dimensional bosonic gases

In physics, one-dimensional models are usually implemented to analyze a simplified version of a complicated three-dimensional system. However, as the field of ultracold quantum gases demonstrates, one-dimensional geometries can provide new perspectives on quantum and statistical mechanics, since new and unexpected phenomena emerge in these systems [80].

In this thesis, for instance, we will study the static and dynamic properties of bright solitons in one-dimensional quantum gases. These configurations emerge as the ground-state solution of the Gross-Pitaevskii equation [81, 82], a nonlinear Schrödinger-like equation that describes the one-dimensional gas and, therefore, requires its transverse confinement. In particular, among different possible platforms to realize these states, we will consider one-dimensional Bose-Bose mixtures, obtained by confining ultracold atoms in different hyperfine states. On this specific setup, it is important to highlight the seminal papers of Refs. [83, 84], that set a new paradigm in the study of quantum mixtures by pointing out the emergence of self-bound states from the competition between the mean-field energy and quantum fluctuations. Droplet and solitonic states occur, indeed, due to the different density dependence of mean-field and beyond-mean-field energy contributions, whose specific properties depend on the spatial dimension and can be controlled experimentally.

We will also investigate the phase dynamics of two tunneling 1D Bose gases, either in a head-to-tail tunneling configuration, or in a side-by-side one [85]. This fundamental line of research has a long tradition, dating back to the analysis of

tunneling in independent Bose-Einstein condensates [86–88], and its development will lead to a better understanding of nonequilibrium quantum statistical physics.

2

Fundamental results and formalism overview

In this chapter, we provide a brief overview of the main models and techniques that we will adopt to analyze the static and dynamic properties of quantum gases. The chapter contains also the discussion of a few results, considered of fundamental importance, on Bose-Einstein condensation and on superfluidity. Their derivation is carried on in a consistent manner with respect to the perspective adopted in this thesis.

2.1 Bose-Einstein condensation

The transition of a many-body system of identical particles to a Bose-Einstein condensate occurs when a macroscopic fraction of the particles occupies the lowest-energy single-particle state. The simplest realization of this transition takes place in noninteracting bosons, which, historically, was the case analyzed by Einstein [4, 5]. Clearly, in the absence of interactions between the particles, the condensate phase must emerge from the quantum statistical properties, which we now discuss, of a large number of bosons that constitute the system.

We begin our analysis by considering a system of noninteracting particles confined in a spatial domain V, which we assume to be sufficiently larger with respect to the particle size. Working in the grand canonical ensemble, we suppose that the system is in thermal equilibrium with a bath of temperature T. In the noninteracting case, this condition can be established by turning off the interparticle interactions once that the thermalization of the interacting system has occurred. Moreover, we

suppose that the system is in chemical equilibrium with the external reservoir of chemical potential μ, so that the number of particles displays small fluctuations around its mean value N. Considering a single particle, we denote the kinetic part of the Hamiltonian with $\hat{h}_{\rm kin}$, and we suppose that the external potential $\hat{h}_{\rm pot}$, which acts on the particle confined in V, also imposes proper boundary conditions at the domain boundary ∂V. The Schrödinger equation of the particle reads

$$(\hat{h}_{\rm kin} + \hat{h}_{\rm pot})\, \phi_\alpha = \epsilon_\alpha\, \phi_\alpha, \tag{2.1}$$

where ϕ_α are the eigenfunctions, labelled by the quantum numbers α, and ϵ_α are the eigenenergies. In the following, we suppose that the solution of this eigenproblem is known, i. e., that ϕ_α and ϵ_α are known for each α. After reducing the problem to this single solvable unit, we now construct the quantum statistical properties of the many-body system.

Given the state with fixed quantum number α, we denote with $p_0^{(\alpha)}$, $p_1^{(\alpha)}$, ... $p_r^{(\alpha)}$, ... the probabilities that it is occupied by 0, 1, ... r, ... bosons. Our goal is to determine, in conditions of thermal and chemical equilibrium, the average number of bosons N_α that occupies the state α, which is given by

$$N_\alpha = \sum_{r=0}^{\infty} r\, p_r^{(\alpha)}, \tag{2.2}$$

and which is determined by the $p_r^{(\alpha)}$. According to the original derivation of Bose [3] and Einstein [4], i. e. imposing that the entropy S is maximum for a fixed temperature T and for a fixed chemical potential μ, these probabilities are given by

$$p_0^{(\alpha)} = B, \qquad p_1^{(\alpha)} = B\, e^{-\beta(\epsilon_\alpha - \mu)}, \qquad ... \qquad p_r^{(\alpha)} = B\, e^{-\beta(\epsilon_\alpha - \mu)\, r}, \qquad ... \tag{2.3}$$

where $\beta = 1/(k_{\rm B} T)$, with $k_{\rm B}$ the Boltzmann constant, and B is a positive constant. To determine B, we impose that the total probability of occupating the state α is equal to one, i. e. $\sum_{r=0}^{\infty} p_r^{(\alpha)} = 1$, and we find that $B = 1 - e^{-\beta(\epsilon_\alpha - \mu)}$. We now calculate the sum over r in the definition of N_α, obtaining

$$N_\alpha = \frac{1}{e^{\beta\,(\epsilon_\alpha - \mu)} - 1}, \tag{2.4}$$

which is the Bose-Einstein distribution. We emphasize that, to have positive probabilities $p_r^{(\alpha)}$ and positive occupation numbers N_α, the chemical potential must satisfy the inequality $\mu < \epsilon_{\bar{\alpha}}$, with $\epsilon_{\bar{\alpha}} = \min_\alpha(\epsilon_\alpha)$ the single-particle ground-state energy. In particular, when $\epsilon_{\bar{\alpha}} = 0$, as in the cases discussed in the next subsections, the chemical potential can assume only negative values: $\mu < 0$.

The phenomenon of Bose-Einstein condensation consists in the macroscopic occupation of the lowest-energy single-particle state $\bar{\alpha}$ by a macroscopic fraction of the atoms in the system [5]. In general, this condition can be achieved by following two slightly different procedures: either fixing the particle number and decreasing the temperature, or fixing the temperature and increasing the particle number. Actually, working in the grand canonical ensemble, the particle number is determined by the chemical potential, and the relevant thermodynamic variables are therefore T and μ. Let us rewrite the total number of bosons as

$$N = N_{\bar{\alpha}} + \tilde{N}, \tag{2.5}$$

with

$$N_{\bar{\alpha}} = \frac{1}{e^{\beta\,(\epsilon_{\bar{\alpha}} - \mu)} - 1}, \qquad \tilde{N} = \sum_{\alpha \neq \bar{\alpha}} \frac{1}{e^{\beta\,(\epsilon_{\alpha} - \mu)} - 1}, \tag{2.6}$$

where $N_{\bar{\alpha}}$ are the particles in the lowest-energy single particle state $\bar{\alpha}$, and $\tilde{N}$ is the number of particles in the excited states $\alpha \neq \bar{\alpha}$.

If $\mu \to \epsilon_{\bar{\alpha}}^{-}$ at a fixed temperature T, the number of particles $\tilde{N}$ tends to the critical atom number N_c from below. Strictly speaking, depending on the dimensionality of the system and on its (infinite or finite) size, N_c could be infinite when $\mu = \epsilon_{\bar{\alpha}}$. Thus, the following discussion applies only to the case in which N_c is finite. When this occurs, since the chemical potential μ controls the total number of particles N, for μ larger than a critical value μ_c we find that $N > N_c$. Therefore, in the regime of $\mu_c < \mu < \epsilon_{\bar{\alpha}}$ a macroscopic number of particles $N_{\bar{\alpha}}$ occupies the condensate state $\bar{\alpha}$. The total number of bosons N becomes infinite for $\mu = \epsilon_{\bar{\alpha}}^{-}$, when the condensate state $\bar{\alpha}$ becomes infinitely occupied.

Thermodynamics of the noninteracting Bose gas

In the grand canonical ensemble, the thermodynamics of a noninteracting Bose gas can be derived from the grand canonical partition function $\mathcal{Z}$, which reads [89]

$$\mathcal{Z} = \sum_{N=0}^{\infty} z^N \, \mathcal{Q}_N(V,T), \tag{2.7}$$

where $z = e^{\beta\mu}$ is the fugacity. In this expression, we introduce the canonical partition function of the N-particle system as

$$\mathcal{Q}_N(V,T) = \sum_{\substack{\{N_\alpha\} \\ N = \sum_\alpha N_\alpha}} e^{-\beta E_{\{N_\alpha\}}}, \tag{2.8}$$

which is calculated as the sum, over all possible occupation numbers $\{N_\alpha\}$ satisfying the constraint $N = \sum_\alpha N_\alpha$, of the Boltzmann factors $e^{-\beta E_{\{N_\alpha\}}}$, where $E_{\{N_\alpha\}} = \sum_\alpha N_\alpha \epsilon_\alpha$. After a few steps [89], the grandcanonical partition function can be rewritten as

$$\mathcal{Z} = \prod_\alpha \sum_{N_\alpha=0}^{\infty} \left[e^{-\beta(\epsilon_\alpha-\mu)}\right]^{N_\alpha}, \tag{2.9}$$

and, calculating the sum, we find

$$\mathcal{Z} = \prod_\alpha \frac{1}{1-e^{-\beta(\epsilon_\alpha-\mu)}}, \tag{2.10}$$

which, assuming that the solution of eigenproblem of Eq. (2.1) is known, is also a known function of T and μ. The grand canonical potential $\Omega = U - TS - \mu N$, with U the internal energy, can be calculated from the grand canonical partition function as $\Omega = -\beta^{-1}\ln(\mathcal{Z})$, obtaining

$$\Omega = \frac{1}{\beta}\sum_\alpha \ln\left[1-e^{-\beta(\epsilon_\alpha-\mu)}\right], \tag{2.11}$$

and, using standard thermodynamic relations, also the other thermodynamic functions can be obtained. For instance, the number of atoms is given by

$$N = -\left(\frac{\partial\Omega}{\partial\mu}\right)_{V,T} = \sum_\alpha \frac{1}{e^{\beta\,(\epsilon_\alpha-\mu)}-1}, \tag{2.12}$$

which coincides with the result of Eq. (2.5). Moreover, the entropy reads

$$S = -\left(\frac{\partial\Omega}{\partial T}\right)_{\mu,V} = k_{\mathrm{B}}\sum_\alpha \left\{\frac{\beta\,(\epsilon_\alpha-\mu)}{e^{\beta\,(\epsilon_\alpha-\mu)}-1} - \ln\left[1-e^{-\beta(\epsilon_\alpha-\mu)}\right]\right\}, \tag{2.13}$$

while the internal energy U can be calculated from $U = \Omega + TS + \mu N$, and reads

$$U = \sum_\alpha \frac{\epsilon_\alpha}{e^{\beta\,(\epsilon_\alpha-\mu)}-1}. \tag{2.14}$$

Finally, the pressure is defined as

$$P = -\left(\frac{\partial\Omega}{\partial V}\right)_{\mu,T}, \tag{2.15}$$

which, for a uniform system, coincides with the simple relation $P = -\Omega/V$.

2.1.1 Noninteracting bosons in a uniform 3D box

We consider a noninteracting Bose gas confined in a cubic box of volume $V = L^3$. The solution of the single-particle eigenproblem of Eq. (2.1) yields the eigenergies

$$\epsilon_{\mathbf{k}} = \frac{\hbar^2 k^2}{2m}, \tag{2.16}$$

where, due to the imposition of periodic boundary conditions on the eigenfunctions $\phi_{\mathbf{k}} = e^{i\mathbf{k}\cdot\mathbf{x}}/\sqrt{V}$, the wave vector is given by $\mathbf{k} = (2\pi/L)(n_x, n_y, n_z)$, with $n_x, n_y, n_z \in \mathbb{Z}$. In this configuration, Bose-Einstein condensation occurs in the state $\bar{\alpha} = \mathbf{0}$, in which the wave vector $\mathbf{k}$ is zero. To get an analytical insight on this problem, we set the chemical potential to $\mu = \epsilon_{\mathbf{0}} = 0$, and we ignore the fact that $N_{\mathbf{0}}$ diverges.

Implementing Eq. (2.5) for $N_{\mathbf{0}} = 0$, we obtain a relation between the critical temperature of Bose-Einstein condensation $T_{\mathrm{BEC}}^{(0)}$ and the total number of atoms $N = \tilde{N} = N_c$, over which the condensate state is macroscopically occupied. In particular

$$N = 8 \sum_{n_x=1}^{\infty} \sum_{n_y=1}^{\infty} \sum_{n_z=1}^{\infty} \frac{1}{e^{\epsilon_{\mathbf{k}}/(k_{\mathrm{B}} T_{\mathrm{BEC}}^{(0)})} - 1}, \tag{2.17}$$

where, in the sum, we are neglecting the terms with one null quantum number and the others nonzero, and the terms with two null quantum numbers and the other nonzero. For sufficiently large V these contributions are irrelevant, and the discrete wave vectors $\mathbf{k}$ can be thought, in this limit, as a continuum of values. In this case, we can substitute the sum with an integral:

$$\sum_{n_x=1}^{\infty} \sum_{n_y=1}^{\infty} \sum_{n_z=1}^{\infty} \to \frac{L^3}{(2\pi)^3} \int_{2\pi/L}^{\infty} \mathrm{d}k_x \int_{2\pi/L}^{\infty} \mathrm{d}k_y \int_{2\pi/L}^{\infty} \mathrm{d}k_z \tag{2.18}$$

and the lower bounds, i. e. $2\pi/L$, can actually be approximated with 0. Before doing this substitution, let us briefly discuss the case of a large but finite volume. Since the distance between the energy levels $\epsilon_{\mathbf{k}}$ increases with the quantum numbers n_x, n_y, n_z, the continuum approximation of Eq. (2.18) seems to become invalid. At the same time, the Bose-Einstein distribution cuts off the higher-energy states, and the semiclassical approximation works well.

If we evaluate Eq. (2.17) analytically, by performing the wave vector integrals Eq. (2.18) in the thermodynamic limit and using spherical coordinates, we find the critical density

$$\frac{N}{L^3} = \zeta(3/2) \left(\frac{m k_{\mathrm{B}} T_{\mathrm{BEC}}^{(0)}}{2\pi\hbar^2} \right)^{3/2}, \tag{2.19}$$

where $\zeta(x)$ is Riemann's zeta function. Inverting Eq. (2.19), we finally obtain

$$T_{\mathrm{BEC}}^{(0)} = \frac{2\pi}{[\zeta(3/2)]^{2/3}} \frac{\hbar^2 n^{2/3}}{m k_{\mathrm{B}}}, \tag{2.20}$$

which is the critical temperature of a noninteracting Bose gas with number density $n = N/L^3$ in a uniform box. We stress again that this relation between the critical temperature $T_{\mathrm{BEC}}^{(0)}$ and n holds in the thermodynamic limit of $N, L^3 \to \infty$, with n fixed.

2.1.2 Noninteracting bosons in a uniform 2D box

Let us now calculate the critical temperature of a bosonic gas confined in a uniform square box with area $V = L^2$. Similarly to the cubic case, the eigenergies are given by $\epsilon_k = \hbar^2 k^2/(2m)$, where $\mathbf{k} = (2\pi/L)(n_x, n_y)$ is the two-dimensional wave vector, with $n_x, n_y \in \mathbb{Z}$. In this context, the analogous of Eq. (2.17) reads

$$N = 4 \sum_{n_x=1}^{\infty} \sum_{n_y=1}^{\infty} \frac{1}{e^{\epsilon_k/(k_{\mathrm{B}} T_{\mathrm{BEC}}^{(0)})} - 1}, \tag{2.21}$$

and, assuming that the energy levels are finely spaced in the region where the Bose-Einstein distribution is nonzero, we write

$$\frac{N}{L^2} = \int_{2\pi/L}^{\infty} \frac{\mathrm{d}k_x}{(2\pi)} \int_{2\pi/L}^{\infty} \frac{\mathrm{d}k_y}{(2\pi)} \frac{1}{e^{\epsilon_k/(k_{\mathrm{B}} T_{\mathrm{BEC}}^{(0)})} - 1}, \tag{2.22}$$

where, as in the three-dimensional case, we have substituted the sum with an integral. However, in contrast with the three-dimensional case, here we cannot consider the thermodynamic limit and set the lower bound $2\pi/L$ of the integrals to 0. Indeed, a simple numerical test shows that, for a nonzero critical temperature $T_{\mathrm{BEC}}^{(0)}$, the critical density $n = N/L^2$ is finite only if the system size L^2 is finite. More quantitatively, in the thermodynamic limit of $L^2 \to \infty$, and assuming $T_{\mathrm{BEC}}^{(0)} > 0$, the critical density of Eq. (2.22) diverges in the infrared as $\int_0^{\infty} \mathrm{d}k/k$. This divergence is a manifestation of the Hohenberg-Mermin-Wagner theorem [90, 91], which, in this context, states that there cannot be Bose-Einstein condensation at finite temperature in a two-dimensional system at the thermodynamic limit.

For a finite-size system, both the critical density and the critical temperature are finite, and the precise calculation of these quantities requires the numerical evaluation of the sum in Eq. (2.21). However, an approximated result, which neglects subleading corrections scaling with the inverse system size, can be obtained

expressing the integral of Eq. (2.22) in polar coordinates, in which the radial component of the wave vector is integrated in the interval $[4\sqrt{\pi}/L, \infty[$[1]. In this case, repeating the same steps of the previous section, we find

$$k_B T_{\mathrm{BEC}}^{(0)} \approx 2\pi \frac{\hbar^2 n}{m} \left\{ \frac{8\pi\hbar^2}{m L^2 k_{\mathrm{B}} T_{\mathrm{BEC}}^{(0)}} - \ln\left[e^{8\pi\hbar^2/(mL^2 k_{\mathrm{B}} T_{\mathrm{BEC}}^{(0)})} - 1 \right] \right\}^{-1}, \tag{2.23}$$

which is an implicit equation relating the critical temperature $T_{\mathrm{BEC}}^{(0)}$ with the two-dimensional number density n. The analysis of this result confirms our previous considerations, namely, that n cannot be finite in the limit of infinite system size $L^2 \to \infty$ unless $T_{\mathrm{BEC}}^{(0)} \to 0$.

2.1.3 Noninteracting bosons on the surface of a sphere

We now describe Bose-Einstein condensation of noninteracting bosons confined on the surface of a sphere of radius R. We parametrize the surface of the sphere, whose area is given by $V = 4\pi R^2$, with the spherical coordinates $\{\theta, \varphi\} \in [0, \pi] \times [0, 2\pi]$. For this configuration, the single-particle Schrödinger equation of Eq. (2.1) can be written as

$$\frac{\hat{L}^2}{2mR^2} \, \mathcal{Y}_l^{m_l}(\theta, \varphi) = \epsilon_l \, \mathcal{Y}_l^{m_l}(\theta, \varphi), \tag{2.24}$$

where

$$\hat{L}^2 = -\hbar^2 \left[\frac{1}{\sin\theta} \frac{\partial}{\partial\theta} \left(\sin\theta \frac{\partial}{\partial\theta} \right) + \frac{1}{\sin^2\theta} \frac{\partial^2}{\partial\varphi^2} \right], \tag{2.25}$$

is the angular momentum operator in spherical coordinates, $\mathcal{Y}_l^{m_l}(\theta, \varphi)$ are the spherical harmonics, labelled by the main quantum number of the angular momentum l, and by the magnetic quantum number $m_l = -l, -l+1, ...l-1, l$. The eigenenergies ϵ_l, which are degenerate in m_l, read

$$\epsilon_l = \frac{\hbar^2 l(l+1)}{2mR^2}, \tag{2.26}$$

and the lowest-energy condensate state $\bar{\alpha}$ corresponds to $l = 0$, $m_l = 0$, so that $\epsilon_0 = 0$.

[1]The integral in Eq. (2.22) cannot be expressed in polar coordinates in a straightforward way, due to the squared shape of the cutoffed area $(-2\pi/L, 2\pi/L) \times (-2\pi/L, 2\pi/L)$. Our choice of the infrared cutoff for the radial wave vector coordinate, i. e. $k_{\mathrm{c}} = 4\sqrt{\pi}/L$, allows to keep the cutoffed area constant.

The relation between the critical temperature of Bose-Einstein condensation $T_{\mathrm{BEC}}^{(0)}$ and the number of atoms N is given by

$$N = \sum_{l=1}^{\infty} \sum_{m_l=-l}^{l} \frac{1}{e^{\epsilon_l/(k_{\mathrm{B}} T_{\mathrm{BEC}}^{(0)})} - 1}, \tag{2.27}$$

where we set the chemical potential to $\mu = \epsilon_0 = 0$. To obtain an analytical result for $T_{\mathrm{BEC}}^{(0)}$, in analogy to the previous cases, we substitute the sum with an integral, i. e. $\sum_{l=1}^{\infty} \sum_{m_l=-l}^{l} \to \int_1^{\infty} \mathrm{d}l\,(2l+1)$ [92], finding

$$\frac{N}{4\pi R^2} = \frac{m k_{\mathrm{B}} T_{\mathrm{BEC}}^{(0)}}{2\pi\hbar^2} \left\{ \frac{\hbar^2}{m R^2 k_{\mathrm{B}} T_{\mathrm{BEC}}^{(0)}} - \ln\left[e^{\hbar^2/(m R^2 k_{\mathrm{B}} T_{\mathrm{BEC}}^{(0)})} - 1 \right] \right\}, \tag{2.28}$$

which allows to calculate the critical number of atoms for a given critical temperature. The critical temperature can be obtained by solving the following equation [54]

$$k_B T_{\mathrm{BEC}}^{(0)} = 2\pi \frac{\hbar^2 n}{m} \left\{ \frac{\hbar^2}{m R^2 k_{\mathrm{B}} T_{\mathrm{BEC}}^{(0)}} - \ln\left[e^{\hbar^2/(m R^2 k_{\mathrm{B}} T_{\mathrm{BEC}}^{(0)})} - 1 \right] \right\}^{-1}, \tag{2.29}$$

where we define the two-dimensional number density of the spherical Bose gas as $n = N/(4\pi R^2)$. In Fig. (2.1) we plot the dimensionless critical temperature as a function of the parameter nR^2, obtained by solving numerically Eq. (2.29). The critical temperature, for a fixed density n, is finite for a finite radius of the sphere R, and it tends to 0 in the limit of $R \to \infty$. As seen in the two-dimensional flat case, this behavior is consistent with the prescription of the Mermin-Wagner-Hohenberg theorem.

Note that it is not possible to identify the critical temperature in the spherical case with Eq. (2.23), i. e. the analogous result for the two-dimensional box, by simply substituting $4\pi R^2 = L^2$ into Eq. (2.29). Indeed, even by doing this, a factor of 2 remains in the expressions and prevents their identification. The presence of this factor signals the different value of the infrared energy cutoff in the two cases: while in the spherical case the first state above the condensate has the energy $\hbar^2/(mR^2)$, in the spherical one we assumed $\hbar^2 k_{\mathrm{c}}^2/(2m) = 8\pi\hbar^2/(mL^2)$, and these, even setting $4\pi R^2 = L^2$, differ by a factor 2.

At temperatures lower than $T_{\mathrm{BEC}}^{(0)}$, determined by Eq. (2.29), the condensate state is occupied by a macroscopic fraction of bosons n_0/n, with $n_0 = N_0/(4\pi R^2)$. The condensate fraction reads [54]

$$\frac{n_0}{n} = 1 - \frac{1 - k_{\mathrm{B}} T \frac{m R^2}{\hbar^2} \ln\left[e^{\hbar^2/(m R^2 k_{\mathrm{B}} T)} - 1 \right]}{1 - k_{\mathrm{B}} T_{\mathrm{BEC}}^{(0)} \frac{m R^2}{\hbar^2} \ln\left[e^{\hbar^2/(m R^2 k_{\mathrm{B}} T_{\mathrm{BEC}}^{(0)})} - 1 \right]}\,, \tag{2.30}$$

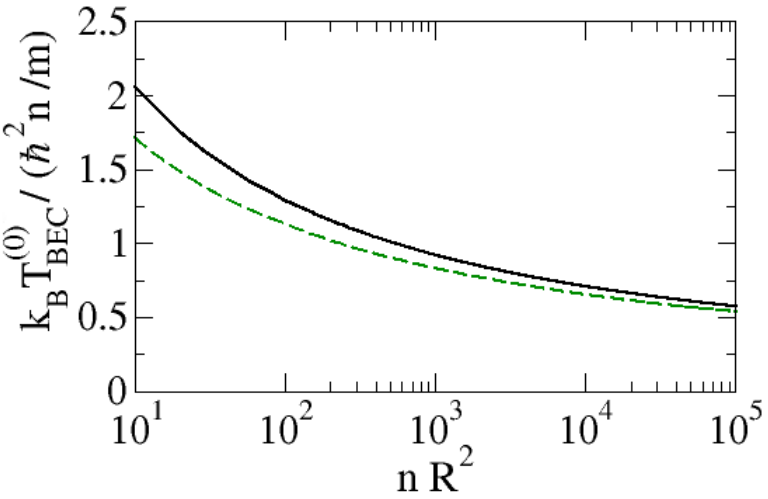

Figure 2.1: Critical temperature of noninteracting bosons on the surface of a sphere (black line), plotted as a function of the parameter nR^2. The green dashed line represents the direct evaluation of the sum of Eq. (2.27), showing that the analytical result improves for larger values of nR^2. Note that the critical temperature tends logarithmically to zero in the thermodynamic limit. From Ref. [54].

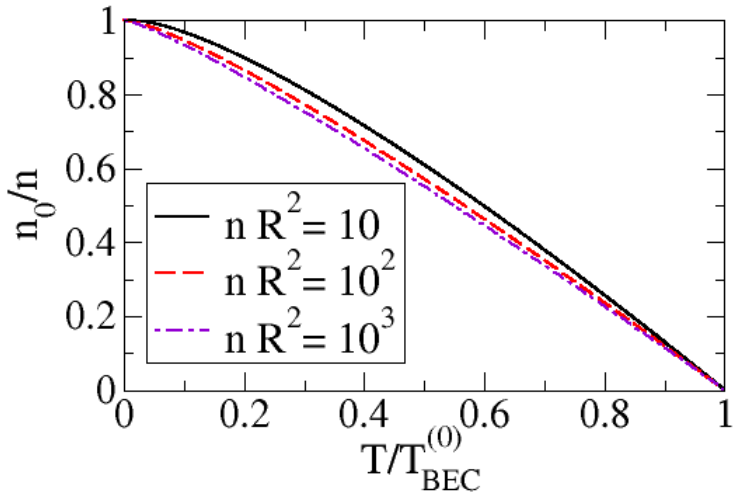

Figure 2.2: Condensate fraction of noninteracting bosons on the surface of a sphere plotted as a function of the adimensional temperature $T/T^{(0)}_{\mathrm{BEC}}$ for different values of nR^2. From Ref. [54].

which can be calculated evaluating the sum in Eq. (2.5) and following the analogous of the procedure adopted for the critical temperature. In Fig. 2.2, we plot n_0/n for different values of the parameter nR^2.

2.2 Functional integral of a many-body bosonic system

The quantum statistical properties of a many-body system, due to the interaction between the particles, cannot be determined in a straightforward manner from the solution of the single-particle eigenvalue equation. In the formalism of first quantization, the solution of the N-body bosonic problem requires the proper symmetrization of the wave function of the system, and the complexity of the problem increases exponentially with N. Second quantization offers an elegant way to reformulate the problem, including the quantum statistics in the properties of operators, and focusing only on the occupation numbers of the different states. In this section, starting from the second-quantized Hamiltonian of a system of bosons, we express the grand canonical partition function as a coherent-state functional integral of a bosonic complex field.

We consider a many-body system of interacting bosons, whose grand canonical partition function $\mathcal{Z}$ is given by

$$\mathcal{Z} = \mathrm{Tr}\big[e^{-\beta(\hat{H}-\mu\hat{N})}\big], \tag{2.31}$$

where $\hat{H}$ is the many-body Hamiltonian of the system, and $\hat{N}$ is the number operator. We express $\hat{H}$ and $\hat{N}$ in terms of the field operator $\hat{\psi}(\mathbf{r})$ in second quantization, which annihilates a boson at the spatial coordinate $\mathbf{r}$. In particular, considering a generic D-dimensional system of bosons in the hypervolume V, the Hamiltonian reads

$$\begin{aligned}\hat{H} = &\int_V \mathrm{d}\mathbf{r}\, \hat{\psi}^\dagger(\mathbf{r})\bigg[-\frac{\hbar^2\nabla^2}{2m} + U(\mathbf{r})\bigg]\hat{\psi}(\mathbf{r}) \\ &+ \frac{1}{2}\int_V \mathrm{d}\mathbf{r}\int_V \mathrm{d}\mathbf{r}'\, \hat{\psi}^\dagger(\mathbf{r})\hat{\psi}^\dagger(\mathbf{r}')V(\mathbf{r}-\mathbf{r}')\hat{\psi}(\mathbf{r}')\hat{\psi}(\mathbf{r}),\end{aligned} \tag{2.32}$$

where $U(\mathbf{r})$ is the external potential, and $V(\mathbf{r}-\mathbf{r}')$, with a slight abuse of notation, is also the two-body interaction potential between the particles. Moreover, we write

$$\hat{N} = \int_V \mathrm{d}\mathbf{r}\, \hat{\psi}^\dagger(\mathbf{r})\hat{\psi}(\mathbf{r}), \tag{2.33}$$

which is the number operator in second quantization.

Since the grand canonical partition function is the trace of the operator $e^{-\beta(\hat{H}-\mu\hat{N})}$, it can be calculated by summing the expectation values of this operator over all the possible states of a proper basis. For this scope, we choose the basis of generalized coherent states $|\psi\rangle$, which are defined as the eigenstates of the field operator $\hat{\psi}(\mathbf{r})\,|\psi\rangle = \psi(\mathbf{r})\,|\psi\rangle$. These states are normalized by construction, but are not orthogonal, and, calculating the trace in Eq. (2.31) in this basis [93], we get

$$\mathcal{Z} = \int \prod_{\mathbf{r}} \frac{\mathrm{d}\bar{\psi}_0(\mathbf{r})\mathrm{d}\psi_0(\mathbf{r})}{2\pi i}\ \langle\psi_0|\, e^{-\beta(\hat{H}-\mu\hat{N})}\,|\psi_0\rangle\,, \tag{2.34}$$

where, in the following, we will express the measure of the integral in a compact form as $\mathrm{d}[\bar{\psi}_0, \psi_0]$. To proceed further, we reinterpret the expectation value $\langle\psi_0|\, e^{-\beta(\hat{H}-\mu\hat{N})}\,|\psi_0\rangle$ as the probability amplitude of a system with Hamiltonian $\hat{H} - \mu\hat{N}$ that propagates in the imaginary time interval $\tau \in [0, \beta\hbar]$. Specifically: the many-body system starts at time 0 in the initial state $|\psi_0\rangle$, evolves under the action of the operator $e^{-\,(\tau/\hbar)(\hat{H}-\mu\hat{N})}$, and ends at time $\beta\hbar$ in the same state $|\psi_0\rangle$. Exploring this fruitful analogy, the partition function of a many-body system can be calculated as a Feynman path integral [94]. Thus, we split β into many imaginary time intervals $\Delta\tau$, by writing $\beta = M\Delta\tau/\hbar$, with $M \gg 1$. In this way, the exponential $e^{-\frac{M\Delta\tau}{\hbar}(\hat{H}-\mu\hat{N})}$ can be split into the product of M exponentials, committing for each subdivision an error of $\mathrm{o}(\Delta\tau^2)$, which is negligible for sufficiently large M. Inserting $M-1$ coherent-state identities between the M exponentials, the field operators inside $\hat{H} - \mu\hat{N}$ are substituted by the classical fields $\psi(\mathbf{r}, j\Delta\tau) =: \psi(\mathbf{r}, \tau)$, and this occurs for each time step $j\Delta\tau$, with $j = 0, ..., M$. Besides this generic description, we do not enter into the details of the calculations, which can be found in Refs. [93, 95, 96], and we report now the final results.

The grand canonical partition function of a many-body system of interacting bosons is given by

$$\mathcal{Z} = \int \mathcal{D}[\bar{\psi}, \psi]\ e^{-\frac{S[\bar{\psi},\psi]}{\hbar}}, \tag{2.35}$$

where the Euclidean action S, i. e. the action in imaginary time, is defined as

$$S[\bar{\psi}, \psi] = \int_0^{\beta\hbar} \mathrm{d}\tau \int_V \mathrm{d}\mathbf{r}\, \mathcal{L}(\bar{\psi}, \psi), \tag{2.36}$$

and the Euclidean Lagrangian $\mathcal{L}$ reads

$$\mathcal{L} = \bar{\psi}(\mathbf{r}, \tau)\left(\hbar\partial_\tau - \frac{\hbar^2\nabla^2}{2m} - \mu\right)\psi(\mathbf{r}, \tau) + \frac{1}{2}\int_V \mathrm{d}\mathbf{r}'\, |\psi(\mathbf{r}', \tau)|^2 V(\mathbf{r}-\mathbf{r}')|\psi(\mathbf{r}, \tau)|^2. \tag{2.37}$$

Note that the measure of the functional integral is defined as

$$\mathcal{D}[\bar{\psi},\psi] = \prod_{j=0}^{M} \mathrm{d}[\bar{\psi}_j,\psi_j], \tag{2.38}$$

namely, as the product of the integration measures for all the intermediate imaginary-time steps.

Let us now interpret broadly our result for the partition function. Within this formalism, we are calculating $\mathcal{Z}$ as a sum over all possible configurations of the classical field $\psi(\mathbf{r},\tau)$ which describes a specific trajectory of the system in the imaginary time interval $[0,\hbar\beta]$. The factor $e^{-S[\bar{\psi},\psi]/\hbar}$ assigns a different weight, throughout the value of the action $S[\bar{\psi},\psi]$, to the different configurations. The quantum nature of the system, embodied by the bosonic statistics, is included through the periodic boundary conditions in imaginary time, which determine the specific form of the trace in Eq. (2.34). The functional integral representation of the partition function is equivalent to the general definition of $\mathcal{Z}$, thus, it does not involve any approximation. At the same time, it constitutes an intuitive description in terms of a complex bosonic field and allows for a practical implementation of approximated calculations [97, 98].

2.3 Functional integral of a many-body fermionic system

The majority of the results of this thesis concerns systems of bosonic ultracold atoms. However, we will later analyze the phenomenon of sound propagation in Fermi superfluids, which requires the knowledge of the system thermodynamics. In this section, in analogy with what we have done in the bosonic case, we implement a coherent-state functional integral formulation of the grand canonical partition function of a fermionic system. For this scope, we need to implement explicitly Eq. (2.31), specifying the second-quantized Hamiltonian and the number operators of the fermions.

Let describe a system of uniform fermions confined in the D-dimensional hyper-volume V. If we would consider a single fermionic species, i. e. fermions in a single hyperfine state, the Pauli principle would prevent s-wave interactions to occur. To avoid this limitation, we suppose to have an equal mixture of fermionic atoms in two different hyperfine states, labelled with the index $\sigma = \{\uparrow,\downarrow\}$, and we assume an attractive contact interaction between fermions with opposite spins.

The grand-canonical Hamiltonian, written in terms of the second-quantized field operator $\hat{\psi}_\sigma(\mathbf{r})$, is given by

$$\hat{H} - \mu\hat{N} = \sum_{\sigma=\uparrow,\downarrow} \int_V \mathrm{d}\mathbf{r} \left[\hat{\psi}^\dagger_\sigma(\mathbf{r}) \left(-\frac{\hbar^2\nabla^2}{2m} - \mu \right) \hat{\psi}_\sigma(\mathbf{r}) + g\ \hat{\psi}^\dagger_\uparrow(\mathbf{r}) \hat{\psi}^\dagger_\downarrow(\mathbf{r}) \hat{\psi}_\downarrow(\mathbf{r}) \hat{\psi}_\uparrow(\mathbf{r}) \right], \tag{2.39}$$

where m is the atomic mass, μ is the chemical potential, and g is the s-wave contact interaction strength between fermions with opposite spins. Note that, by tuning the Feshbach resonance with the application of a static magnetic field [99], it is possible to change the strength g and study the crossover from BCS pairs of weakly-interacting fermions to a bosonic BEC made of tightly-bound composite molecules [79]. The grand canonical partition function $\mathcal{Z}$, according to its definition of Eq. (2.31), is given by

$$\mathcal{Z} = \int \prod_{\sigma=\uparrow,\downarrow} \prod_{\mathbf{r}} \mathrm{d}\bar{\psi}_\sigma(\mathbf{r}) \mathrm{d}\psi_\sigma(\mathbf{r})\ \langle -\psi |\, e^{-\beta(\hat{H}-\mu\hat{N})}\, |\psi\rangle\,, \tag{2.40}$$

where we are calculating the trace in the basis of generalized fermionic coherent states [93, 95]. The latter are the eigenstates of the fermionic field operator with eigenvalue $\psi_\sigma(\mathbf{r})$, namely

$$\hat{\psi}_\sigma(\mathbf{r})\, |\psi\rangle = \psi_\sigma(\mathbf{r})\, |\psi\rangle\,, \tag{2.41}$$

and the fermionic statistics results in the non commutativity of the complex fermionic field $\psi_\sigma(\mathbf{r})$, which assumes the values of Grassmann anticommuting numbers [95]. The construction of the functional integral in the fermionic case is similar to that of the bosonic case, with the crucial difference that the fermionic Grassmann field satisfies antiperiodic conditions at the boundaries of the imaginary time interval, i. e. $\psi_\sigma(\mathbf{r}, 0) = -\psi_\sigma(\mathbf{r}, \beta\hbar)$. Keeping in mind this distinction, which stems from the fermionic quantum statistics, we now report the results, while the full derivation can be found in Ref. [95].

The grand canonical partition function of a system of fermions across the BCS-BEC crossover reads [100]

$$\mathcal{Z} = \int \mathcal{D}[\bar{\psi}_\sigma, \psi_\sigma]\ e^{-\frac{S[\bar{\psi}_\sigma, \psi_\sigma]}{\hbar}}, \tag{2.42}$$

where the Euclidean action is defined as

$$S[\bar{\psi}_\sigma, \psi_\sigma] = \int_0^{\beta\hbar} \mathrm{d}\tau \int_V \mathrm{d}\mathbf{r}\, \mathcal{L}(\bar{\psi}_\sigma, \psi_\sigma), \tag{2.43}$$

and the Euclidean Lagrangian reads

$$\mathcal{L} = \sum_{\sigma=\uparrow,\downarrow} \bar{\psi}_\sigma(\mathbf{r}, \tau) \left(\hbar\partial_\tau - \frac{\hbar^2\nabla^2}{2m} - \mu \right) \psi_\sigma(\mathbf{r}, \tau) + g\, \bar{\psi}_\uparrow(\mathbf{r}, \tau)\, \bar{\psi}_\downarrow(\mathbf{r}, \tau)\, \psi_\downarrow(\mathbf{r}, \tau)\, \psi_\uparrow(\mathbf{r}, \tau), \tag{2.44}$$

where the imaginary-time dependence of the fermionic field emerges from the construction of the functional integral, and

$$\mathcal{D}[\bar{\psi},\psi] = \prod_{\sigma=\uparrow,\downarrow}\prod_{\mathbf{r}}\prod_{j=0}^{M} \mathrm{d}\bar{\psi}_\sigma(\mathbf{r}, j\beta\hbar/M)\,\mathrm{d}\psi_\sigma(\mathbf{r}, j\beta\hbar/M), \tag{2.45}$$

with $M \to \infty$, is the measure of the integral.

The grand canonical partition function of Eq. (2.42) has been obtained without further approximations with respect to the Hamiltonian in second quantization. As a natural consequence, due to the quartic dependence of the Lagrangian on the fermionic field, it is not possible to calculate exactly the functional integral. To facilitate the development of an approximated theory, we introduce the bosonic pairing field $\Delta(\mathbf{r},\tau)$, which pairs fermions with opposite spins and, therefore, represents the Cooper pairs in the system [101]. In particular, after defining

$$\Delta(\mathbf{r},\tau) = g\psi_\downarrow(\mathbf{r},\tau)\,\psi_\uparrow(\mathbf{r},\tau), \tag{2.46}$$

and analogously for the complex conjugate field $\bar{\Delta}$, we perform the following Hubbard-Stratonovich transformation [100, 102]

$$\begin{aligned}\exp\left[-\int_0^{\beta\hbar}\mathrm{d}\tau\int_V \mathrm{d}\mathbf{r}\, g\,\bar{\psi}_\uparrow(\mathbf{r},\tau)\bar{\psi}_\downarrow(\mathbf{r},\tau)\psi_\downarrow(\mathbf{r},\tau)\psi_\uparrow(\mathbf{r},\tau)\right] = \\ \exp\left\{\int_0^{\beta\hbar}\mathrm{d}\tau\int_V \mathrm{d}\mathbf{r}\left[\frac{\bar{\Delta}(\mathbf{r},\tau)\Delta(\mathbf{r},\tau)}{g} + \bar{\psi}_\uparrow(\mathbf{r},\tau)\bar{\psi}_\downarrow(\mathbf{r},\tau)\Delta(\mathbf{r},\tau)\right.\right. \\ \left.\left. +\bar{\Delta}(\mathbf{r},\tau)\psi_\downarrow(\mathbf{r},\tau)\psi_\uparrow(\mathbf{r},\tau)\right]\right\}\end{aligned} \tag{2.47}$$

which, despite the disadvantage of introducing an additional field, allows us to get a Gaussian integral in the fermionic fields. Indeed, the partition function has been transformed in this way as [103]

$$\begin{aligned}\mathcal{Z} = \int\mathcal{D}[\bar{\psi}_\sigma,\psi_\sigma]\int\mathcal{D}[\bar{\Delta},\Delta]\exp\left\{-\int_0^{\beta\hbar}\mathrm{d}\tau\int_V\mathrm{d}\mathbf{r}\right[\\ \sum_{\sigma=\uparrow,\downarrow}\bar{\psi}_\sigma(\mathbf{r},\tau)\left(\hbar\partial_\tau - \frac{\hbar^2\nabla^2}{2m} - \mu\right)\psi_\sigma(\mathbf{r},\tau) \\ \left. - \frac{\bar{\Delta}(\mathbf{r},\tau)\Delta(\mathbf{r},\tau)}{g} - \bar{\psi}_\uparrow(\mathbf{r},\tau)\bar{\psi}_\downarrow(\mathbf{r},\tau)\Delta(\mathbf{r},\tau) - \bar{\Delta}(\mathbf{r},\tau)\psi_\downarrow(\mathbf{r},\tau)\psi_\uparrow(\mathbf{r},\tau)\right]\right\}.\end{aligned} \tag{2.48}$$

which is an alternative form with respect to Eq. (2.42) that does not involve any further approximation.

In the following chapters, we will describe how to derive the system thermodynamics, by developing an approximated calculation of $\mathcal{Z}$.

2.4 Landau two-fluid model

An interacting quantum gas in a regime of quantum degeneracy displays the property of superfluidity. This peculiar phenomenon, which consists in the capability of a quantum liquid to flow through narrow capillaries without friction, was first discovered in experiments with Helium-II by Kapitza [9]. In a seminal paper, published in 1941, Landau formulated a complete theory to describe this and other experimental properties of Helium-II [12], developing the concepts previously introduced by Tisza [13–15].

The behavior of a superfluid, which is intrinsically quantum mechanical, can be explained with a semiclassical two-fluid model. The main idea is that the fluid can be thought as composed by two parts: the superfluid part, which is not viscous and has zero entropy, and the normal part, which behaves like a viscous fluid. At sufficiently low temperatures, therefore, the hydrodynamic behavior of a many-body system consists in the superposition of the superfluid motion (i. e. a portion of the fluid in the same coherent state), and of the motion of the bosonic excitations, constituting the normal fluid. Notably, the two fluids do not exchange momentum with each other: there is no internal friction between the normal fluid and the superfluid one, neither within the superfluid itself. It is also important to stress that the fluids are not separable, but must be thought as the simultaneous capability of a quantum system to display two different and independent motions.

To develop an hydrodynamic description, we suppose that the thermodynamic quantities fluctuate around the average value that they assume at thermodynamic equilibrium. Thus, we require that, during the dynamics, the system is always in local equilibrium, so that the thermodynamic functions acquire an additional dependence on space and on time. Under these assumptions, let us briefly introduce and comment the equations of Landau-Tisza two-fluid model [12]. We consider a system of mass density ρ, such that

$$\rho = \rho_n + \rho_s, \tag{2.49}$$

where ρ_s is the mass density of the superfluid part of the fluid and ρ_n is the mass density of the normal part of the fluid. The total mass current results from the superposition of the normal flow and of the superflow, namely

$$\mathbf{j} = \rho_n \mathbf{v}_n + \rho_s \mathbf{v}_s, \tag{2.50}$$

where $\mathbf{v}_n$ is the normal fluid velocity and $\mathbf{v}_s$ is the superfluid velocity. The conservation of mass is expressed by the continuity equation

$$\frac{\partial \rho}{\partial t} + \nabla \cdot \mathbf{j} = 0, \tag{2.51}$$

and the conservation of momentum is described by

$$\frac{\partial j_i}{\partial t} + \frac{\partial \Pi_{ik}}{\partial x_k} = 0, \tag{2.52}$$

with we define the tensor $\Pi_{ik} = P\,\delta_{ik} + \rho_n v_{n,i} v_{n,k} + \rho_s v_{s,i} v_{s,k}$, with P the pressure of the fluid. As a consequence of the irrotational nature of the superfluid velocity, i. e. $\nabla \times \mathbf{v}_s = 0$, the superfluid motion is reversible, and entropy is carried only by the normal part of the fluid. Therefore, the continuity equation for the entropy density $\rho\tilde{s}$ can be written as

$$\frac{\partial \rho\tilde{s}}{\partial t} + \rho\tilde{s}\,\nabla \cdot \mathbf{v}_n = 0, \tag{2.53}$$

where $\tilde{s} = S/M$ is the entropy per unit mass of fluid M described in this model.

To close the system of equations of the two-fluid model, another relation is needed. It is the Newton equation of the superfluid, obtained by equating the acceleration of the superfluid, i. e. $\mathrm{d}\mathbf{v}_s/\mathrm{d}t$, to the force per unit of mass necessary to accelerate it. The latter quantity is equal to $-\nabla(\partial U/\partial M)_{S,V}$, where U is the internal energy and $(\partial U/\partial M)_{S,V}$ is the potential energy per unit of mass associated to the motion of the sole superfluid. Now, considering the thermodynamic relation $(\partial U/\partial M)_{S,V} = (\partial G/\partial M)_{P,T}$, we conveniently discuss the derivative of G, the Gibbs free energy, rather than that of U. We write G as $G_0 + \mathbf{P}^2/(2M_n)$, with G_0 the free energy of the stationary fluid, $\mathbf{P} = M_n(\mathbf{v}_n - \mathbf{v}_s)$ the momentum of the normal fluid, and $M_n \propto M$ the normal fluid mass. Differentiating G with respect to M, and putting all the elements together, Landau obtained the following equation [12]

$$\frac{\partial \mathbf{v}_s}{\partial t} = -\nabla\left[\frac{G_0}{M} + \frac{{\mathbf{v_s}}^2}{2} - \frac{1}{2}(\mathbf{v}_n - \mathbf{v}_s)^2 \frac{\rho_n}{\rho_n + \rho_s}\right], \tag{2.54}$$

where the Lagrangian derivative has been expressed in terms of the Eulerian one as $\mathrm{d}\mathbf{v}_s/\mathrm{d}t = \partial\mathbf{v}_s/\partial t + \nabla(\mathrm{v}_s^2/2)$. Note that G_0 satisfies the Gibbs-Duhem relation $G_0 = \mu N$, with μ the chemical potential of the stationary fluid. Thus, interpreting the mass M as $M = mN$, with m the mass of the identical microscopic constituents of the fluid, the term G_0/M in Eq. (2.54) is equal to μ/m.

Having introduced the equations of the two-fluid model, we specify that all the thermodynamic quantities depend on space and time: $\rho(\mathbf{r},t)$, $\rho_n(\mathbf{r},t)$, $\rho_s(\mathbf{r},t)$, $\mathbf{j}(\mathbf{r},t)$, $\mathbf{v}_n(\mathbf{r},t)$, $\mathbf{v}_s(\mathbf{r},t)$, $P(\mathbf{r},t)$, $S(\mathbf{r},t)$, $G_0(\mathbf{r},t)$. For simplicity, their explicit dependence is omitted unless it becomes necessary.

2.4.1 Sound propagation in a quantum fluid

Within the phenomenological description of the two-fluid model, a quantum liquid admits two different kinds of hydrodynamic excitations. If the system is uniformly confined in a D-dimensional box $V = L^D$, these excitations are labelled by a wave vector and correspond to sound waves: the *first* and the *second* sound. In this case, the velocity with which these waves propagate is simply defined as the constant of proportionality between the frequency of these modes and the wave vector itself.

Starting from the equations of the two-fluid model, we derive here the Landau biquadratic equation for the calculation of the sound velocities. In particular, we will limit our derivation to the case in which the superfluid and the normal fluid velocities are small, thus neglecting all the $\mathrm{o}(v^2)$ terms, and we consider the linearized equations [12]

$$\frac{\partial \rho}{\partial t} + \nabla \cdot \mathbf{j} = 0, \tag{2.55}$$

$$\frac{\partial \rho \tilde{s}}{\partial t} + \rho \tilde{s}\, \nabla \cdot \mathbf{v}_n = 0, \tag{2.56}$$

$$\frac{\partial \mathbf{j}}{\partial t} + \nabla P = 0, \tag{2.57}$$

$$\frac{\partial \mathbf{v}_s}{\partial t} + \nabla \left(\frac{G}{M} \right) = 0, \tag{2.58}$$

where, in the last equation, we omit the subindex 0 in the stationary Gibbs free energy. Deriving Eq. (2.55) with respect to t and substituting it into Eq. (2.57) we get

$$\frac{\partial^2 \rho}{\partial t^2} = \nabla^2 P, \tag{2.59}$$

which is the familiar wave equation of a single classical fluid. Indeed, if the system would be composed only by one species, Eq. (2.59) would describe a wave where pressure fluctuations induce density fluctuations and vice versa.

However, a system composed by two fluids hosts two sounds, and this additional degree of freedom is encoded in the equation

$$\frac{\partial^2 \tilde{s}}{\partial t^2} = \tilde{s}^2 \frac{\rho_s}{\rho_n} \nabla^2 T, \tag{2.60}$$

which, if it were decoupled from the previous equation, would describe the propagation of temperature fluctuations that induce entropy fluctuations.

We now briefly discuss how to obtain Eq. (2.60), by reviewing the original derivation of Landau [12]. We substitute $\partial \rho / \partial t$ of Eq. (2.55) into Eq. (2.56) and, employing

the relations (2.49) and (2.50), we get

$$\frac{\partial \tilde{s}}{\partial t} = \tilde{s}\,\frac{\rho_s}{\rho}\,\nabla\cdot(\mathbf{v}_s - \mathbf{v}_n). \tag{2.61}$$

Then, differentiating with respect to time, we rewrite this differential identity as

$$\frac{\partial^2 \tilde{s}}{\partial t^2} = \tilde{s}\,\frac{\rho_s}{\rho}\,\nabla\cdot\left[\frac{\partial(\mathbf{v}_s - \mathbf{v}_n)}{\partial t}\right], \tag{2.62}$$

where we neglect higher order terms in the velocities. As can be seen differentiating the Gibbs-Duhem relation $G = \mu N$ and considering $M = mN$, we have $\mathrm{d}(G/M) = m^{-1}\mathrm{d}\mu = -\tilde{s}\,\mathrm{d}T + \rho^{-1}\,\mathrm{d}P$. From this relation it follows that

$$\nabla P = \rho\tilde{s}\,\nabla T + \rho\,\nabla(G/M), \tag{2.63}$$

and, inserting $\nabla(G/M)$ from Eq. (2.58), ∇P from Eq. (2.57) and using again Eqs. (2.49) and (2.50), we obtain

$$\rho_n\,\frac{\partial(\mathbf{v}_s - \mathbf{v}_n)}{\partial t} = \rho\tilde{s}\,\nabla T. \tag{2.64}$$

Finally, the wave equation (2.60) can be obtained calculating the divergence of Eq. (2.64) and inserting it into Eq. (2.61).

The sound velocities can be calculated by expanding Eqs. (2.59) and (2.60) for small perturbations around the equilibrium configuration, namely

$$\tilde{s} = \tilde{s}_0 + \tilde{s}', \qquad \rho = \rho_0 + \rho', \qquad P = P_0 + P', \qquad T = T_0 + T', \tag{2.65}$$

where the primed quantities represent small fluctuations with respect to the uniform and constant equilibrium values and, therefore, depend on the coordinates $(\mathbf{r}, t)$. In particular, the fluctuation fields are not independent from each other, and, knowing the equation of state, it is possible to determine two of the thermodynamic variables by fixing two of the others. For instance, we write

$$\rho' = \left(\frac{\partial\rho}{\partial T}\right)_P T' + \left(\frac{\partial\rho}{\partial P}\right)_T P' \qquad \tilde{s}' = \left(\frac{\partial\tilde{s}}{\partial T}\right)_P T' + \left(\frac{\partial\tilde{s}}{\partial P}\right)_T P', \tag{2.66}$$

where the derivatives are calculated using the equilibrium values. Employing these equations to eliminate ρ' and $\tilde{s}'$ and decomposing each fluctuation field $P'(\mathbf{r}, t)$ and $T'(\mathbf{r}, t)$ in the basis of plane waves $\exp[i\omega(t - x/c)]$, where c is the sound wave velocity and ω its frequency, the equations of sound become

$$\begin{cases} P'(\omega)\big[-c^2\big(\frac{\partial\rho}{\partial P}\big)_T + 1\big] + T'(\omega)\big[-c^2\big(\frac{\partial\rho}{\partial T}\big)_P\big] = 0, \\ P'(\omega)\big[-c^2\big(\frac{\partial\tilde{s}}{\partial P}\big)_T\big] + T'(\omega)\big[-c^2\big(\frac{\partial\tilde{s}}{\partial T}\big)_P + \tilde{s}^2\,\frac{\rho_s}{\rho_n}\big] = 0, \end{cases} \tag{2.67}$$

where $P'(\omega)$ and $T'(\omega)$ are the amplitudes of the Fourier components of the pressure and temperature fluctuation fields. To find a nontrivial solution of the system, we impose that its determinant is zero, obtaining an equation for the velocity of sound, namely

$$c^4\left[\left(\frac{\partial\rho}{\partial P}\right)_T\left(\frac{\partial\tilde{s}}{\partial T}\right)_P-\left(\frac{\partial\rho}{\partial T}\right)_P\left(\frac{\partial\tilde{s}}{\partial P}\right)_T\right]-c^2\left[\left(\frac{\partial\tilde{s}}{\partial T}\right)_P+\tilde{s}^2\frac{\rho_s}{\rho_n}\left(\frac{\partial\rho}{\partial P}\right)_T\right] +\tilde{s}^2\frac{\rho_s}{\rho_n}=0, \tag{2.68}$$

which is a biquadratic equation for the velocity c of the sound waves. To put it in a standard form we need to invert the coefficient of the c^4 term, which, using the Jacobian notation [104], can be rewritten in the following equivalent ways: either as

$$\frac{\partial(\rho,\tilde{s})}{\partial(P,T)}=\frac{\partial(\rho,\tilde{s})/\partial(\rho,T)}{\partial(P,T)/\partial(\rho,T)}=\frac{\tilde{c}_V}{T(\partial P/\partial\rho)_T}, \tag{2.69}$$

where $\tilde{c}_V$ is the specific heat at constant volume per unit of mass M, or as

$$\frac{\partial(\rho,\tilde{s})}{\partial(P,T)}=\frac{\partial(\rho,\tilde{s})/\partial(P,\tilde{s})}{\partial(P,T)/\partial(P,\tilde{s})}=\left(\frac{\partial\tilde{s}}{\partial T}\right)_P\left(\frac{\partial\rho}{\partial P}\right)_{\tilde{s}}. \tag{2.70}$$

From the previous relations, we finally obtain the Landau equation of sound, namely

$$c^4-c^2\left[\left(\frac{\partial P}{\partial\rho}\right)_{\tilde{s}}+\frac{T\tilde{s}^2\rho_s}{\tilde{c}_V\rho_n}\right]+\frac{\rho_s T\tilde{s}^2}{\rho_n\tilde{c}_V}\left(\frac{\partial P}{\partial\rho}\right)_T=0, \tag{2.71}$$

which relates the sound velocity c to the equilibrium thermodynamics of a quantum liquid. Note that this biquadratic equation admits only two linearly independent solutions, and the degeneracy is associated to the positive or negative speed with respect to the direction of propagation.

To simplify the notation, in the coefficients of the equation of sound we introduce the definition of the following velocities:

$$v_A=\sqrt{\left(\frac{\partial P}{\partial\rho}\right)_{\tilde{s}}},\quad v_T=\sqrt{\left(\frac{\partial P}{\partial\rho}\right)_T},\quad v_L=\sqrt{\frac{\rho_s T\tilde{s}^2}{\rho_n\tilde{c}_V}}, \tag{2.72}$$

which are, respectively, the adiabatic velocity v_A, the isothermal velocity v_T and the Landau velocity v_L. Depending on the thermodynamics of the physical system considered and on the temperature regime, it may occur that the general solutions of Eq. (2.71) are well approximated by these expressions. Before analyzing specific systems, we write the Landau equation as

$$c^4-\left(v_A^2+v_L^2\right)c^2+v_L^2v_T^2=0, \tag{2.73}$$

and we explicitly calculate its general solutions, namely

$$\begin{aligned} c_1 &= \left[\frac{v_A^2+v_L^2}{2} + \sqrt{\left(\frac{v_A^2+v_L^2}{2}\right)^2 - v_L^2 v_T^2}\right]^{1/2}, \\ c_2 &= \left[\frac{v_A^2+v_L^2}{2} - \sqrt{\left(\frac{v_A^2+v_L^2}{2}\right)^2 - v_L^2 v_T^2}\right]^{1/2}, \end{aligned} \tag{2.74}$$

which are the velocities of the first and second sound. Note that, by definition, the first sound propagates with a higher velocity with respect to the second one.

At the critical temperature at which the superfluid density vanishes, the Landau velocity v_L and, consequently, the second sound velocity c_2, become zero. Therefore, only the first sound can propagate in this high-temperature regime, and its velocity c_1 coincides with the usual adiabatic sound velocity v_A. Actually, v_A is usually derived as the solution of Eq. (2.59), which encodes the interplay of pressure and density fluctuations. In the standard discussion of sound waves, thus, there is not an analogous of the sound equation (2.60), and only Eq. (2.59) is adopted. Indeed, in a classical fluid, heat propagates in a diffusive manner rather than as a wave. On the contrary, in a superfluid system, heat can propagate as a wave, as a consequence of the zero entropy of the superfluid component. In general, the pressure-density oscillations of a superfluid and entropy-temperature ones are not mutually independent: c_1 and c_2 are the result of these combined phenomena and, indeed, are obtained by putting Eqs. (2.59) and (2.60) together.

In the thesis, we will discuss the propagation of sound in different physical systems, whose thermodynamic and superfluid properties produce a different qualitative and quantitative behavior of the sound modes. To facilitate that analysis, it is historically and scientifically relevant to discuss the propagation of sound in superfluid ^{4}He. In this system, the adiabatic compressibility $\kappa_{\tilde{s}} = \rho^{-1}(\partial\rho/\partial P)_{\tilde{s}}$ and the isothermal one $\kappa_T = \rho^{-1}(\partial\rho/\partial P)_T$ are approximately the same. As a consequence, also the adiabatic and the isothermal velocities, as can be seen from their definitions, are approximately equal: $v_A \approx v_T$. In this case, the velocities of the sound modes of Eq. (2.74) can be approximated as

$$c_1 \approx v_A, \qquad c_2 \approx v_L, \tag{2.75}$$

which explains the notation of the "Landau" velocity, for the additional (second) sound velocity that he originally identified.

In liquid helium, the first sound propagates with v_A and is, therefore, a pure density wave in which the normal fluid and the superfluid propagate in phase. The second sound, instead, propagates with v_L and constitutes a pure heat wave, in which the

normal fluid and the superfluid oscillate with opposite phase. Thus, the pressure-density oscillations of ^{4}He are essentially decoupled from the temperature-entropy ones. This statement can be expressed mathematically as $(\partial\tilde{s}/\partial P)_T = (\partial\rho/\partial T)_P = 0$, where the equality follows from known Maxwell relations. It is also easy to verify that when these partial derivatives are zero, the equations of the system (2.67) are decoupled and, the same expressions for c_1 and c_2 of Eq. (2.75) can be obtained from this complementary perspective.

2.5 Magnetic trapping of ultracold atomic gases

Ultracold atoms undergo the phase transition of Bose-Einstein condensation when the phase-space density exceeds a critical value. This phenomenon was observed for the first time in 1995, by cooling atomic gases with the combined use of laser and evaporative cooling techniques. These experiments relied on the magnetic and optical confinement of the sample, which could not be cooled in the nK temperature range if held in physical containers. In this section, we discuss briefly the basic ideas to confine atoms with magnetic traps. We avoid analyzing the pre-cooling stage in magneto-optical traps and the evaporative cooling (for details on this topic see [105]), and the short analysis implemented here aims to provide a background for discussing radiofrequency-induced adiabatic potentials.

Let us discuss how weakly-interacting bosonic gases are confined. In these systems, the interactions are so weak that, to describe the trapping mechanism, it is sufficient to understand how a single atom interacts with the magnetic field. Given a static space-dependent magnetic field $\mathbf{B}_0(\mathbf{r})$, the potential energy of an atom interacting with the field reads

$$U(\mathbf{r}) = -\boldsymbol{\mu}\cdot\mathbf{B}_0(\mathbf{r}), \tag{2.76}$$

where $\boldsymbol{\mu}$ is the magnetic dipole moment of the atom. This dipole moment is proportional to the total angular momentum operator $\hat{\mathbf{F}} = \hat{\mathbf{I}} + \hat{\mathbf{J}}$, which is given by the sum of the nuclear spin $\hat{\mathbf{I}}$ and of the angular momentum of the electrons $\hat{\mathbf{J}}$. In particular, we write $\boldsymbol{\mu} = -g_F\mu_{\mathrm{B}}\hat{\mathbf{F}}/\hbar$, where μ_{B} is Bohr's magneton and g_F is the Landé factor [106]. The projection of $\hat{\mathbf{F}}$ on the local direction of the magnetic field is quantized as $\hbar m_F$, where $m_F = -F, ..., +F$ is the magnetic quantum number which, for bosonic atoms, assumes only integer values. Therefore, the space-dependent energy levels of the atom, which result from the interaction of its magnetic dipole moment with the magnetic field, are given by

$$u_{m_F}(\mathbf{r}) = m_F g_F\,\mu_{\mathrm{B}}|\mathbf{B}_0(\mathbf{r})|. \tag{2.77}$$

By properly engineering the static magnetic field to have a minimum at a certain position, the atoms with $m_F g_F > 0$, usually called low-field-seeking states, will be subject to the force $-\nabla u_{m_F}(\mathbf{r})$ directed towards the trap minimum. To confine the atoms, a possible magnetic field configuration is the quadrupole field $\mathbf{B}_0(\mathbf{r}) \propto (x, y, -2z)$, which however suffers from losses of atoms due to the likely occurrence of Majorana spin-flips at the trap minimum [105]. Other static magnetic field configurations include the Ioffe-Pritchard trap and cloverleaf traps (see, for more details, Refs. [105, 107] and the references therein).

The atoms are typically confined in magnetic conservative traps after the stage of laser cooling, in which the optical molasses reach a temperature in the mK range and densities of $10^{12}\,\mathrm{cm}^{-3}$. To produce a Bose-Einstein condensate, it is however necessary to further decrease the temperature: this is typically done by letting the most energetic atoms escape from the trap, allowing the system to thermalize at a lower temperature. This technique is called evaporative cooling, and the loss of energetic atoms is realized by coupling, via a radiofrequency magnetic field, the potential of low-field seeking states with repulsive potentials in the regions far from the trap minimum.

But adopting the setup used to perform the evaporative cooling, it is also possible to engineer radiofrequency-induced adiabatic potentials that trap the atoms in a spatially-confined superposition of their hyperfine states. Let us consider an atom in a region of space where both a static magnetic field $\mathbf{B}_0(\mathbf{r})$ and a time-dependent magnetic field $\mathbf{B}_{\mathrm{rf}}(\mathbf{r}, t)$ are nonzero. Due to the static magnetic field, the atom precesses around the local direction of the static field with the Larmor frequency

$$\omega_{\mathrm{L}}(\mathbf{r}) = \frac{|g_F|\mu_{\mathrm{B}}|\mathbf{B}_0(\mathbf{r})|}{\hbar}, \tag{2.78}$$

which depends on the spatial position. Due to the radiofrequency field $\mathbf{B}_{\mathrm{rf}}(\mathbf{r}, t)$, whose frequency is given by ω_{rf}, tunneling between different magnetic sublevels can occur, and it is more likely to happen in the regions where $\omega_{\mathrm{L}}(\mathbf{r}) \approx \omega_{\mathrm{rf}}$. Thus, when both fields are present, the atoms can be confined or repelled in *dressed* magnetic levels which correspond to a superposition of the *bare* energy levels of Eq. (2.77). By writing the Hamiltonian of the interaction between the magnetic fields in the rotating wave approximation, and moving to the frame rotating at ω_{rf}, the radiofrequency-induced adiabatic potentials read [106]

$$U_{M_F}(\mathbf{r}) = M_{\mathrm{F}}\sqrt{[\hbar\omega_{\mathrm{L}}(\mathbf{r}) - \hbar\omega_{\mathrm{rf}}]^2 + [\hbar\Omega_{\mathrm{r}}(\mathbf{r})]^2}, \tag{2.79}$$

where M_F labels the dressed magnetic state, while

$$\Omega_{\mathrm{r}}(\mathbf{r}) = \frac{|g_F|\mu_{\mathrm{B}}|\mathbf{B}^{\perp}_{\mathrm{rf}}(\mathbf{r})|}{2\hbar} \tag{2.80}$$

is the Rabi frequency among the bare levels, with $\mathbf{B}_{\rm rf}^{\perp}(\mathbf{r})$ the component of $\mathbf{B}_{\rm rf}(\mathbf{r},t)$ perpendicular to $\mathbf{B}_0(\mathbf{r})$ in the position $\mathbf{r}$.

Considering a system confined optically along two spatial directions, the potential $U_{M_F}(\mathbf{r})$ consists of a double well potential, as it is illustrated in Ref. [108]. In two dimensions, $U_{M_F}(\mathbf{r})$ confines the atoms on a ring, while in three-dimensions, the atoms will be confined around a two-dimensional shell-shaped surface [43]. We will analyze more in detail the latter configuration in the next chapter, adopting the formalism developed insofar to analyze the physics of shell-shaped Bose gases.

3

Quantum physics of shell-shaped Bose gases

In this chapter, which contains the central results of the thesis, we analyze the physics of two-dimensional shell-shaped Bose gases. To investigate experimentally the properties of this atomic configuration, it is necessary to implement a magnetic confinement with radiofrequency-induced adiabatic potentials, whose basic details are discussed in section 2.5. We model explicitly these external potentials as [43]

$$U_{\mathrm{bubble}}(\mathbf{r}) = M_{\mathrm{F}}\sqrt{[u(\mathbf{r}) - \hbar\Delta]^2 + (\hbar\Omega_{\mathrm{r}})^2}, \tag{3.1}$$

where M_{F} is the magnetic quantum number of the dressed state populated by the atoms, Δ and Ω_{r} are tunable frequencies, and $u(\mathbf{r}) = m(\omega_x^2 x^2 + \omega_y^2 y^2 + \omega_z^2 z^2)/2$ is the bare harmonic trap with frequencies $\omega_{x,y,z}$. The set of points which minimize the potential $U_{\mathrm{bubble}}(\mathbf{r})$ corresponds to the surface of a triaxial ellipsoid, whose equation reads $(\omega_x^2 x^2 + \omega_y^2 y^2 + \omega_z^2 z^2) = 2\hbar\Delta/m$. When the energy contribution associated to the trapping potential is sufficiently stronger than the mean kinetic and interaction energy, the particles will be confined across the surface of this ellipsoid.

Actually, the first experiments with radiofrequency-induced adiabatic potentials [109] featured an additional gravitational potential contribution $mg_{\mathrm{grav}}z$, with g_{grav} the acceleration of gravity. In the presence of gravity, thus, it is only possible to produce flat condensates [109, 110], or to engineer ring-shaped traps [111–114]. To confine the atomic cloud in fully-closed shells, it is necessary to carry on the experiments in microgravity facilities, as the Cold Atom Lab [44, 51, 52], or in free-falling experiments conducted in a drop tower [46] or in a falling elevator [50]. Most of the work of the current chapter is devoted to studying the physics of shell-

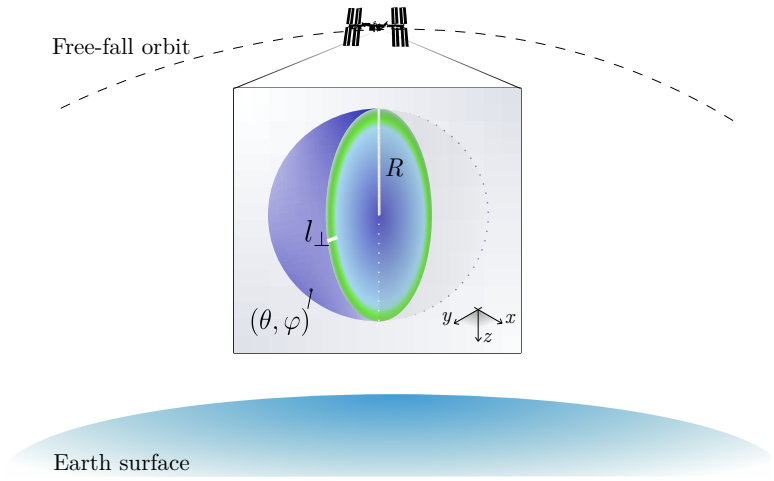

Figure 3.1: Typical configuration of a spherically-symmetric shell-shaped condensate, obtained by trapping an atomic gas with a radiofrequency-induced adiabatic potential in microgravity. From Ref. [55].

shaped condensates in microgravity and, therefore, we will neglect the gravitational potential energy $mg_{\rm grav}z$.

When all the harmonic frequencies are equal, i. e. $\omega_{x,y,z} = \omega_{\rm r}$, the trapping configuration is spherically symmetric. In this case, and considering the limit of $\Delta \gg \Omega_{\rm r}$, the potential of Eq. (3.1) can be approximated as the radially-shifted harmonic trap

$$U_{\rm thin} = \frac{m}{2}\omega_\perp^2 (r - R)^2, \tag{3.2}$$

where $\omega_\perp = \omega_{\rm r}(2M_F\Delta/\Omega_{\rm r})^{1/2}$ is the transverse frequency, and $R = [2\hbar\Delta/(m\omega_r^2)]^{1/2}$ is the radius of the sphere. In the initial sections of this chapter, we will analyze the thermodynamic properties of a system of interacting bosonic atoms confined on a spherically-symmetric thin shell, see Fig. 3.1. However, instead of describing a three-dimensional system of bosonic particles confined in the external potential of Eq. (3.2), we will adopt the formalism of functional integration (see section 2.2) to model a uniform Bose gas on the surface of a sphere. This explicit discussion of the trapping potential, however, is useful to check if a purely two-dimensional formalism is adequate. Indeed, the typical energies of the 2D phenomena we will analyze must always be lower than the energy of the transverse confinement $\hbar\omega_\perp$.

The properties of ellipsoidal shells will be discussed only in the last section, where we formulate several theoretical predictions for the ongoing microgravity experiments on the Cold Atom Laboratory [51, 52].

3.1 Bose-Einstein condensation and thermodynamics

Let us consider a spherically-symmetric two-dimensional Bose gas, obtained by confining a system of atomic bosons on the surface of a thin spherical shell. We implement here a two-dimensional description of the thermodynamic properties of the system, based on the coherent state functional integral formulation of quantum field theory developed in the section 2.2.

3.1.1 Derivation of the grand potential

At the equilibrium, the quantum statistical properties of the Bose gas can be derived from the grand canonical partition function $\mathcal{Z}$, which reads

$$\mathcal{Z} = \int \mathcal{D}[\bar{\psi}, \psi]\, e^{-\frac{S[\bar{\psi},\psi]}{\hbar}}, \tag{3.3}$$

where we define the Euclidean action S of a spherical gas as

$$S[\bar{\psi}, \psi] = \int_0^{\beta\hbar} \mathrm{d}\tau \int_0^{2\pi} \mathrm{d}\varphi \int_0^{\pi} \mathrm{d}\theta\, \sin\theta\, R^2\, \mathcal{L}(\bar{\psi}, \psi). \tag{3.4}$$

and $\mathcal{L}$ is the Euclidean Lagrangian. We limit ourselves to the description of bosons with a zero-range interaction of strength g_0, for which $\mathcal{L}$ reads

$$\mathcal{L} = \bar{\psi}(\theta, \varphi, \tau)\left(\hbar\partial_\tau + \frac{\hat{L}^2}{2mR^2} - \mu\right)\psi(\theta, \varphi, \tau) + \frac{g_0}{2}|\psi(\theta, \varphi, \tau)|^4, \tag{3.5}$$

where the kinetic part contains the angular momentum operator in spherical coordinates

$$\hat{L}^2 = -\hbar^2\left[\frac{1}{\sin\theta}\frac{\partial}{\partial\theta}\left(\sin\theta\frac{\partial}{\partial\theta}\right) + \frac{1}{\sin^2\theta}\frac{\partial^2}{\partial\varphi^2}\right], \tag{3.6}$$

and the radius of the sphere R is considered a fixed constant.

Note that, to avoid discussing the details of the external potential, we are directly implementing the description of a two-dimensional Bose gas on a spherical manifold. The connection between our theory and the experiments, and the discussion of the trapping parameters requires the modeling in this space of the bare contact interaction strength g_0 between the bosons. We will make this connection in section 3.1.3 and, for now, we derive a general theory in which g_0 is a generic parameter.

The standard Bogoliubov-Popov theory of a two-dimensional Bose gas [115], and particularly its implementation with the functional integral, can be extended to the spherical case. The main technical differences concern the different geometry, which produces different quantum numbers in the implementation of the Bogoliubov transformations. We decompose the bosonic field as

$$\psi(\theta,\varphi,\tau) = \psi_0 + \eta(\theta,\varphi,\tau), \tag{3.7}$$

where, as in the noninteracting problem studied in section 2.1.3, the condensate state ψ_0 is represented by the $l = 0$, $m_l = 0$ mode of the field. The complex fluctuation field $\eta(\theta,\varphi,\tau)$ contains all the components $\{l, m_l\} \neq \{0, 0\}$, and can therefore be written as

$$\begin{aligned}
\eta(\theta,\varphi,\tau) &= \sum_{\omega_n} \sum_{l=1}^{\infty} \sum_{m_l=-l}^{l} \frac{\eta(l,m_l,\omega_n)}{R}\, e^{-i\omega_n\tau}\, \mathcal{Y}^l_{m_l}(\theta,\varphi), \\
\bar{\eta}(\theta,\varphi,\tau) &= \sum_{\omega_n} \sum_{l=1}^{\infty} \sum_{m_l=-l}^{l} \frac{\bar{\eta}(l,m_l,\omega_n)}{R}\, e^{i\omega_n\tau}\, \mathcal{Y}^{l\,\dagger}_{m_l}(\theta,\varphi),
\end{aligned} \tag{3.8}$$

where $\omega_n = 2\pi n/(\beta\hbar)$ are the Matsubara frequencies, and where the factor R is introduced to adimensionalize the components.

We substitute the field decomposition (3.7) into the Lagrangian of Eq. (3.5), and we neglect the contributions containing cubic and quartic powers of the fluctuation field, finding [54]

$$\mathcal{L} = \mathcal{L}_0 + \mathcal{L}_{\rm g}, \tag{3.9}$$

where the mean-field Lagrangian is given by

$$\mathcal{L}_0 = -\mu\psi_0^2 + \frac{g_0}{2}\psi_0^4, \tag{3.10}$$

and where the Gaussian Lagrangian reads

$$\begin{aligned}
\mathcal{L}_g = {} & \bar{\eta}(\theta,\varphi,\tau)\left(\hbar\partial_\tau + \frac{\hat{L}^2}{2mR^2} - \mu + 2g_0\psi_0^2\right)\eta(\theta,\varphi,\tau) \\
& + g_0\psi_0^2\left[\bar{\eta}(\theta,\varphi,\tau)\bar{\eta}(\theta,\varphi,\tau) + \eta(\theta,\varphi,\tau)\eta(\theta,\varphi,\tau)\right].
\end{aligned} \tag{3.11}$$

By expanding the fluctuation field as in Eq. (3.8), we express the action of Eq. (3.4) as a sum over ω_n, l and m_l, and, using the property of orthonormality of the spherical harmonics $\delta_{ll'}\delta_{m_l m_l'} = \int_0^{2\pi} \mathrm{d}\varphi \int_0^{\pi} \mathrm{d}\theta \sin\theta\, \mathcal{Y}^{l'*}_{m_l'}(\theta,\varphi)\mathcal{Y}^l_{m_l}(\theta,\varphi)$, we obtain

$$S = S_0 + S_{\rm g}, \tag{3.12}$$

where $S_0 = 4\pi R^2 \beta\hbar\,(-\mu\psi_0^2 + g\psi_0^4/2)$ is the mean-field action. The Gaussian action $S_{\rm g}$ can be written in the following matricial form

$$S_{\rm g}[\bar{\eta},\eta] = \frac{\beta\hbar}{2}\sum_{\omega_n}\sum_{l=1}^{\infty}\sum_{m_l=-l}^{l}\begin{bmatrix}\bar{\eta}(l,m_l,\omega_n)\\ \eta(l,-m_l,-\omega_n)\end{bmatrix}^T \mathbf{M}\begin{bmatrix}\eta(l,m_l,\omega_n)\\ \bar{\eta}(l,-m_l,-\omega_n)\end{bmatrix}, \tag{3.13}$$

where the elements of the matrix $\mathbf{M}$ are defined as

$$\begin{aligned}\mathbf{M}_{11} &= -i\hbar\omega_n + \epsilon_l - \mu + 2g_0\psi_0^2,\\ \mathbf{M}_{22} &= +i\hbar\omega_n + \epsilon_l - \mu + 2g_0\psi_0^2,\\ \mathbf{M}_{12} &= \mathbf{M}_{21} = (-1)^{m_l} g_0\psi_0^2,\end{aligned} \tag{3.14}$$

and $\epsilon_l = \hbar^2 l(l+1)/(2mR^2)$ are the energy levels of a free particle on the sphere. Having neglected the non-Gaussian terms in the Lagrangian, it is possible to calculate the partition function by performing the Gaussian functional integral of the action $S_{\rm g}$. Here we simply report the final result for the grand potential

$$\Omega = -\beta^{-1}\ln\mathcal{Z} = \Omega_0 + \Omega_{\rm g}, \tag{3.15}$$

where

$$\Omega_0 = 4\pi R^2\left(-\mu\psi_0^2 + \frac{g_0}{2}\psi_0^4\right) \tag{3.16}$$

is the mean-field grand potential, and with

$$\Omega_{\rm g}(\mu,\psi_0^2) = \frac{1}{2\beta}\sum_{\omega_n}\sum_{l=1}^{\infty}\sum_{m_l=-l}^{l}\ln\{\beta^2[\hbar^2\omega_n^2 + E_l^2(\mu,\psi_0^2)]\}, \tag{3.17}$$

the Gaussian beyond-mean-field grand potential. In the previous expression, we define $E_l(\mu,\psi_0^2)$ as

$$E_l(\mu,\psi_0^2) = \sqrt{(\epsilon_l - \mu + 2g_0\psi_0^2)^2 - g_0^2\psi_0^4}, \tag{3.18}$$

which represents the excitation spectrum of the quasiparticles.

The last steps consist in calculating the sum over the Matsubara frequencies in Eq. (3.17), namely, the sum of the discrete frequencies $\omega_n = 2\pi n/(\beta\hbar)$ over all $n \in \mathbb{Z}$. To perform this operation, we multiply the logarithm by the convergence factor $e^{i\omega_n\Delta\tau}$, with $\Delta\tau \to 0^+$. The reason for including this term lies in the construction of the functional integral, where the field $\bar{\psi}$ is evaluated at a time infinitesimally higher than the field ψ (infinitesimally for $M \to \infty$ imaginary time slices) [103, 116, 117]. With this operation, the sum in Eq. (3.17) converges, producing two Gaussian contributions, one is temperature-independent, the other

depends on temperature [117]. We report the final result for the effective grand potential $\Omega(\mu, \psi_0^2)$, which reads [54]

$$\begin{aligned}\Omega(\mu,\psi_0^2) = 4\pi R^2\big(-\mu\psi_0^2 + g_0\psi_0^4/2\big) + \frac{1}{2}\sum_{l=1}^{\infty}\sum_{m_l=-l}^{l}[E_l(\mu,\psi_0^2) - \epsilon_l - \mu] \\ + \frac{1}{\beta}\sum_{l=1}^{\infty}\sum_{m_l=-l}^{l}\ln\big[1 - e^{-\beta E_l(\mu,\psi_0^2)}\big],\end{aligned} \tag{3.19}$$

and where the counterterms at the first line appear due to the convergence-factor regularization. The classical field ψ_0 can be determined imposing that it extremizes the grand canonical potential, i. e. $\partial\Omega/\partial\psi_0 = 0$. This condition, defining the condensate density as $n_0 = \psi_0^2$, leads to the following relation

$$n_0(\mu) = \frac{\mu}{g_0} - \frac{1}{4\pi R^2}\sum_{l=1}^{\infty}\sum_{m_l=-l}^{l}\frac{2\epsilon_l + \mu}{E_l^{\mathrm{B}}}\left(\frac{1}{2} + \frac{1}{e^{\beta E_l^{\mathrm{B}}} - 1}\right), \tag{3.20}$$

where we treat the Gaussian contributions perturbatively, considering them as small contributions with respect to the mean-field term [118, 119]. In the previous relation, we define the Bogoliubov spectrum as

$$E_l^{\mathrm{B}} = \sqrt{\epsilon_l(\epsilon_l + 2\mu)}, \tag{3.21}$$

which is obtained neglecting the higher-order beyond-mean-field corrections of Eq. (3.20).

Substituting the previous equation into the effective grand potential, we finally obtain the grand canonical potential Ω as a function of the chemical potential

$$\Omega[\mu, n_0(\mu)] = \Omega_0[\mu, n_0(\mu)] + \Omega_{\mathrm{g}}^{(0)}[\mu, n_0(\mu)] + \Omega_{\mathrm{g}}^{(T)}[\mu, n_0(\mu)], \tag{3.22}$$

where we define the mean-field grand potential as

$$\Omega_0[\mu, n_0(\mu)] = -(4\pi R^2)\,\frac{\mu^2}{2g_0}, \tag{3.23}$$

and the beyond-mean-field Gaussian contributions at zero and at finite temperature, respectively, as

$$\Omega_{\mathrm{g}}^{(0)}[\mu, n_0(\mu)] = \frac{1}{2}\sum_{l=1}^{\infty}\sum_{m_l=-l}^{l}(E_l^{\mathrm{B}} - \epsilon_l - \mu), \tag{3.24}$$

$$\Omega_{\mathrm{g}}^{(T)}[\mu, n_0(\mu)] = \frac{1}{\beta}\sum_{l=1}^{\infty}\sum_{m_l=-l}^{l}\ln(1 - e^{-\beta E_l^{\mathrm{B}}}). \tag{3.25}$$

In the next sections, we will compute Ω explicitly, but before that, let us calculate the critical temperature of Bose-Einstein condensation of a interacting Bose gas on the surface of a sphere.

3.1.2 Critical temperature and condensate fraction

Let us calculate the critical temperature and the condensate fraction in terms of the bare interaction strength g_0. In the next subsection, we will discuss the scattering theory of a Bose gas on the surface of a sphere, to connect our field-theoretical description with the experiments.

According to standard thermodynamic relations, we calculate the number density as

$$n(\mu) = -\frac{1}{4\pi R^2}\frac{\partial\Omega[\mu, n_0(\mu)]}{\partial\mu}, \tag{3.26}$$

where the grand potential is given by Eq. (3.22). To calculate the condensate fraction n_0/n we aim to obtain a perturbative expression of the density as a function of the condensate density, i. e. $n(n_0)$. For this scope, we express the chemical potential in the previous equation as $\mu = g_0 n_0 + ...$ by inverting Eq. (3.20), and $n(n_0)$ reads

$$n(n_0) = n_0 + f_g^{(0)}(n_0) + f_g^{(T)}(n_0), \tag{3.27}$$

where we define the beyond-mean-field Gaussian contribution to the density at zero and at finite temperature respectively, as

$$f_g^{(0)}(n_0) = \frac{1}{4\pi R^2}\frac{1}{2}\sum_{l=1}^{\infty}\sum_{m_l=-l}^{l}\left\{\frac{\epsilon_l + g_0 n_0}{E_l[\mu(n_0), n_0]} - 1\right\}, \tag{3.28}$$

$$f_g^{(T)}(n_0) = \frac{1}{4\pi R^2}\sum_{l=1}^{\infty}\sum_{m_l=-l}^{l}\frac{\epsilon_l + g_0 n_0}{E_l[\mu(n_0), n_0]}\frac{1}{e^{\beta E_l[\mu(n_0), n_0]} - 1}. \tag{3.29}$$

In Ref. [54], to obtain an analytical expression of n_0/n and motivated by some applications of variational perturbation theory at the lowest order [118, 119], we made use of the approximation $n_0 \approx n$ in Eqs. (3.28) and (3.29). By doing so, performing, as in the noninteracting case of the previous chapter, the integral over l instead of the sum, we get

$$f_g^{(0)}(n) = \frac{m g_0 n}{4\pi\hbar^2} + \frac{1}{4\pi R^2}\left(1 - \sqrt{1 + \frac{2 g_0 m n R^2}{\hbar^2}}\right), \tag{3.30}$$

$$f_g^{(T)}(n) = \frac{1}{2\pi R^2}\sqrt{1 + \frac{2 g_0 m n R^2}{\hbar^2}} - \frac{m k_{\mathrm{B}} T}{2\pi\hbar^2}\ln\left(e^{\frac{\hbar^2}{m R^2 k_{\mathrm{B}} T}\sqrt{1 + \frac{2 g_0 m n R^2}{\hbar^2}}} - 1\right), \tag{3.31}$$

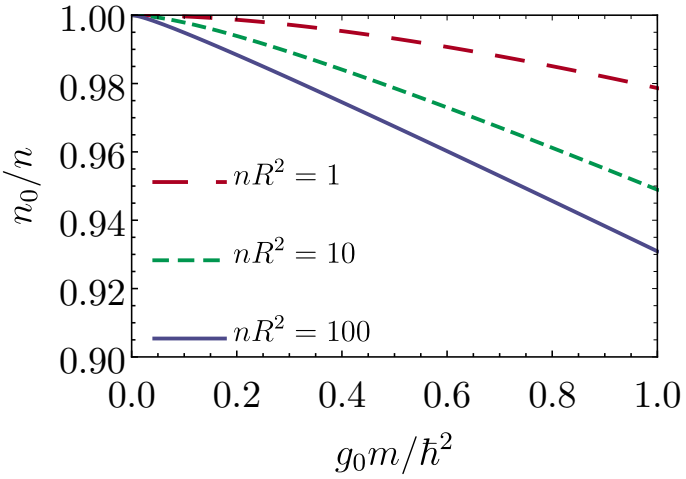

Figure 3.2: Condensate fraction of interacting bosons on the surface of a sphere at zero temperature, plotted as a function of the adimensional interaction strength $g_0 m/\hbar^2$ and for different nR^2.

and putting all these contributions together into Eq. (3.27), we simply divide by the density n to calculate the condensate fraction of a Bose gas on the surface of a sphere. We find

$$\begin{aligned}\frac{n_0}{n} =& 1 - \frac{m g_0}{4\pi\hbar^2} - \frac{1}{4\pi R^2 n}\left(1 + \sqrt{1 + \frac{2 g_0 m n R^2}{\hbar^2}}\right) \\ &+ \frac{m k_{\mathrm{B}} T}{2\pi\hbar^2 n} \ln\left(e^{\frac{\hbar^2}{m R^2 k_{\mathrm{B}} T}\sqrt{1+\frac{2 g_0 m n R^2}{\hbar^2}}} - 1\right),\end{aligned} \tag{3.32}$$

which is a valid approximation of the condensate fraction for sufficiently low interactions. At zero temperature, taking into account that $x \ln(e^{b/x} - 1) \xrightarrow{x \to 0} b$ for $b > 0$, the condensate fraction is given by

$$\frac{n_0}{n}(T = 0) = 1 - \frac{m g_0}{4\pi\hbar^2} - \frac{1}{4\pi R^2 n}\left(1 - \sqrt{1 + \frac{2 g_0 m n R^2}{\hbar^2}}\right), \tag{3.33}$$

which is shown in Fig. 3.2, plotted as a function of $m g_0/\hbar^2$, for different choices of the parameter nR^2.

In the thermodynamic limit in which $N, R \to \infty$ with n fixed, the quantum statistical properties of an infinite sphere must be equivalent to those of a flat two-dimensional system. In that limit (and working at zero temperature) we obtain $n_0/n = 1 - m g_0/(4\pi\hbar^2)$, a result equivalent to the condensate fraction calculated by Schick for a 2D Bose gas [120]. When considering a finite radius of the sphere,

instead, the zero-temperature condensate fraction, at the leading order in the small interaction parameter $mg_0/\hbar^2$, is given by

$$\frac{n_0}{n}(T=0) \sim 1 - \frac{nR^2}{8\pi}\left(\frac{mg_0}{\hbar^2}\right)^2. \tag{3.34}$$

so that the finite-radius quantum depletion scales quadratically with the interaction strength.

The critical temperature of the interacting Bose gas on a sphere T_{BEC} can be calculated imposing that $n_0/n = 0$ into Eq. (3.32), and we obtain

$$k_{\mathrm{B}}T_{\mathrm{BEC}} = \frac{\frac{2\pi\hbar^2 n}{m} - \frac{g_0 n}{2}}{\frac{\hbar^2}{2mR^2 k_{\mathrm{B}}T_{\mathrm{BEC}}}\left(1+\sqrt{1+\frac{2g_0 mnR^2}{\hbar^2}}\right) - \ln\left(e^{\frac{\hbar^2}{mR^2 k_{\mathrm{B}}T_{\mathrm{BEC}}}\sqrt{1+\frac{2g_0 mnR^2}{\hbar^2}}} - 1\right)}. \tag{3.35}$$

which is an implicit analytical expression for T_{BEC}. We emphasize that the critical temperature of the noninteracting case $T^{(0)}_{\mathrm{BEC}}$, reported at Eq. (2.29), is reproduced by putting $g_0 = 0$ in this expression.

In Figs. 3.3 and 3.4, we plot the adimensional critical temperature (red dashed line) as a function of the adimensional contact interaction strength $mg_0/\hbar^2$. Due to the finite system size, Bose-Einstein condensation occurs at finite temperature and, due to the peculiar form of the superfluid density, we expect that for small enough radii, a shell-shaped condensate displays a phase of Bose-Einstein condensation without superfluidity. The superfluid transition, modeled for Fig. 3.3 in a simplified way with the Kosterlitz-Nelson criterion [73], will be discussed more in detail in section 3.4, but these findings are qualitatively unchanged.

3.1.3 Scattering theory on a sphere

In the typical experiments with weakly-interacting Bose-Einstein condensates, there is a single length that controls the physics of the system, the *s*-wave scattering length. This quantity, which can be usually tuned with Feshbach resonances, is linked to the contact interaction strength with the scattering theory.

In this section, with the goal of discussing the thermodynamics of spherical bubble-trapped condensates, we analyze the scattering theory of particles confined on a spherical surface. In particular, we will restrict our discussion to a large sphere with $R \gg \xi$, where ξ is the healing length of the system, which we will later define precisely. To analyze the scattering of two identical particles on a sphere, interacting with the interaction operator $\hat{V}$, we can consider the motion of a

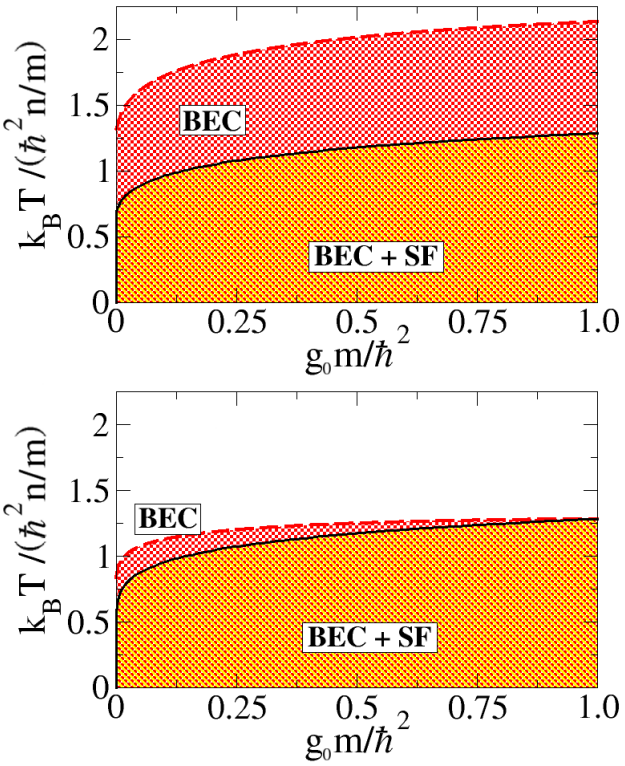

Figure 3.3: Phase diagram of a Bose gas confined on the surface of a sphere, considering $nR^2 = 10^2$ in the top panel, and $nR^2 = 10^4$ in the bottom one. The red dashed line represents the critical temperature of Eq. (3.35), properly rescaled with physical constants, under which the condensate fraction of the system is nonzero and the system is a Bose-Einstein condensate (BEC). Under the black solid line, determined by the temperature at which the superfluid density satisfies the Kosterlitz-Nelson criterion [54], the system is also superfluid (SF). Interestingly, our theory suggests that a sufficiently small sphere displays a superfluid phase in which the system is not condensate due to BKT physics. This prediction holds also for the more refined modeling of section 3.4. From Ref. [54].

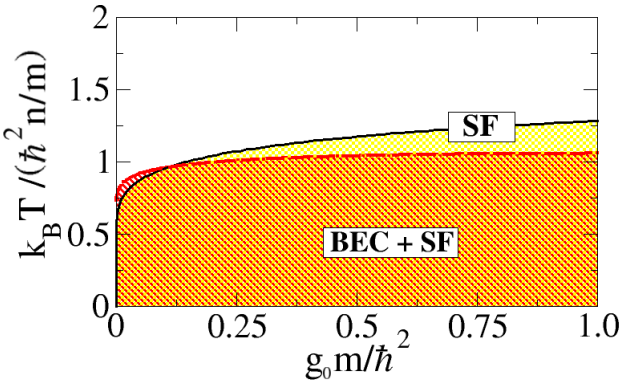

Figure 3.4: Phase diagram of a spherical bosonic film for $nR^2 = 10^5$, which shows the same quantities with respect to Fig. 3.3. Given the larger value of nR^2, which, for a fixed density n, corresponds to a larger condensate, the phase diagram is more similar to that of a conventional infinite 2D superfluid. In that case, even if the system is superfluid below the BKT critical temperature, there is no Bose-Einstein condensation at finite temperature.

single particle with reduced mass $m/2$ in the potential $\hat{V}$. In the absence of scattering, the free Hamiltonian of the particle with reduced mass would be given by $\hat{H}_0 = \hat{L}^2/(mR^2)$, with $\hat{L}$ the angular momentum operator, and the energy eigenstates read $E_{l_0} = \hbar^2 l_0(l_0+1)/(mR^2)$, with l_0 a quantized positive integer. The free eigenfunctions are the spherical harmonics $\mathcal{Y}_l^{m_l}(\theta,\varphi) = \langle \theta,\varphi | \, l, m_l \rangle$, where the brakets satisfy the following relations

$$\sum_{l=0}^{\infty} \sum_{m_l=-l}^{l} |l, m_l\rangle \langle l, m_l| = 1, \qquad \int_0^{2\pi} \mathrm{d}\varphi \int_0^{\pi} \mathrm{d}\theta \, \sin\theta \, |\theta,\varphi\rangle \langle \theta,\varphi| = 1. \tag{3.36}$$

The full Hamiltonian $\hat{H}_0 + \hat{V}$ has the eigenstates $|\Psi_{l_0}\rangle$, which are in principle unknown, and we define the transition operator $\hat{\mathcal{T}}$ through the relation

$$\hat{\mathcal{T}} \, |l, m_l\rangle = \hat{V} \, |\Psi_{l_0}\rangle \, , \tag{3.37}$$

namely, as the operator whose action on the eigenstates of the free Hamiltonian is equivalent to the action of the interaction operator on the eigenstates of the full Hamiltonian. The Schrödinger equation $(\hat{H}_0 + \hat{V}) \, |\Psi_{l_0}\rangle = E_{l_0} \, |\Psi_{l_0}\rangle$ can be formally solved as

$$|\Psi_{l_0}\rangle = |l_0, m_{l_0}\rangle + \frac{1}{E_{l_0} - \hat{H}_0 + i\eta} \, \hat{V} \, |\Psi_{l_0}\rangle \, , \tag{3.38}$$

where $\eta \to 0^+$ is a small vanishing parameter included to regularize the calculations, since the eigenvalues of $\hat{H}_0$ coincide with E_{l_0}. Acting with $\hat{V}$ on the left, we find the Lippmann-Schwinger equation [121, 122]

$$\hat{\mathcal{T}} = \hat{V} + \hat{V}\,\frac{1}{E_{l_0} - \hat{H}_0 + i\eta}\,\hat{\mathcal{T}}, \tag{3.39}$$

where we used the definition of the transition operator.

Considering the contact interaction between bosons $\hat{V} = (g_0/R^2)\,|\theta,\varphi\rangle\,\langle\theta,\varphi|$, where g_0 is exactly the amplitude introduced in the functional integral calculations, we calculate the scattering amplitude $\mathcal{T}_{l',l_0} = \langle l', m_l'|\,\hat{\mathcal{T}}\,|l_0, m_{l_0}\rangle$ by averaging Eq. (3.39). We obtain

$$\mathcal{T}_{l',l_0} = \frac{g_0}{4\pi R^2}\,\delta_{l'l_0}\,\delta_{m_l' m_{l_0}} + \frac{g_0}{4\pi R^2}\sum_{l=0}^{\infty}\sum_{m_l=-l}^{l}\frac{\mathcal{T}_{l',l_0}}{E_{l_0} - E_l + i\eta}\,\delta_{l'l}\,\delta_{m_l' m_l} \tag{3.40}$$

where we also inserted the identity (3.36) at the right-hand side and integrated over the angles. The recursive solution of Eq. (3.40) would generate the infinite Born series of terms at the right-hand side [123] and, to avoid that, we implement some approximations. We first bring the second term on the right to the left, and we calculate the sum over all possible l' and m_l', finding

$$\sum_{l'=0}^{\infty}\sum_{m_l'=-l'}^{l'}\left[\mathcal{T}_{l',l_0} - \frac{g_0}{4\pi R^2}\frac{\mathcal{T}_{l',l_0}}{E_{l_0} - E_{l'} + i\eta}\right] = \frac{g_0}{4\pi R^2}. \tag{3.41}$$

Then, we limit to the regime of low-energy scattering in which the matrix element $\mathcal{T}_{l',l_0} = \langle l', m_l'|\,\hat{V}\,|\Psi_{l_0}\rangle$ is nonzero only when the state $|l', m_l'\rangle$ is near the state $|l, m_l\rangle$. In this case, we can approximate the first term in Eq. (3.41) as

$$\mathcal{T}_{l',l_0} \approx \mathcal{T}(E_{l_0} + i\eta)\,\delta_{l'l_0}\,\delta_{m_l' m_{l_0}}, \tag{3.42}$$

where $\mathcal{T}(E_{l_0} + i\eta)$ is the on-shell $\mathcal{T}$ matrix described in Ref. [124], and in the second term in Eq. (3.41) we assume

$$\mathcal{T}_{l',l_0} \approx \mathcal{T}(E_{l_0} + i\eta), \tag{3.43}$$

where the Kronecker deltas are now absent because the factor $[E_{l_0} - E_{l'} + i\eta]^{-1}$ acts already as a smeared delta function. With these approximations, Eq. (3.41) leads to

$$\frac{1}{\mathcal{T}(E_{l_0} + i\eta)} = \frac{4\pi R^2}{g_0} + \sum_{l=0}^{\infty}\sum_{m_l=-l}^{l}\frac{1}{E_l - E_{l_0} - i\eta}, \tag{3.44}$$

which relates the on-shell $\mathcal{T}$ matrix with the contact interaction strength g_0. Following Refs. [125,126], instead of the summation at the right-hand side of the previous equation, we integrate over l up to an ultraviolet cutoff l_c. Thus, calling $\mathcal{T}(E_{l_0}+i\eta)$ as $\mathcal{T}_{l_c}(E_{l_0}+i\eta)$ to remind ourselves of the cutoff, we get

$$\mathcal{T}_{l_c}(E_{l_0}+i\eta) = -\frac{\hbar^2}{2mR^2}\,\frac{1}{-\frac{2\pi\hbar^2}{mg_0}+\frac{1}{2}\ln\left[\frac{l_0(l_0+1)}{l_c(l_c+1)}\right]-i\frac{\pi}{2}}, \tag{3.45}$$

where the limit of $\eta\to 0^+$ is performed after the integration.

Our goal is to find a relation between the contact interaction strength g_0, and the cutoff l_c. In particular, we will also include this cutoff in the zero temperature grand potential and, by using the relation between g_0 and l_c, we will be able to get a renormalized cutoff-independent grand potential Ω. For low-energy scattering, the on-shell $\mathcal{T}$ matrix can be thought a renormalized interaction strength, and is proportional to the s-wave scattering amplitude $f(l_0)$, which is given by [127]

$$f(E_{l_0}) = -\frac{4\hbar^2}{m}\frac{1}{\cot\delta_0(E_{l_0})-i}, \tag{3.46}$$

where, differently from Ref. [127], we have multiplied by a factor $-\sqrt{i/(8\pi k)}$ to get the flat-case scaling of $f(E_{l_0})$ at large distances. In the scattering amplitude, the phase shift $\delta_0(E_{l_0})$ of the partial s-wave reads

$$\cot\delta_0(E_{l_0}) = -\frac{2}{\pi}[Q_{l_0}(\cos\theta_0)+B^{-1}], \tag{3.47}$$

where $Q_{l_0}(\cos\theta_0)$ is the Legendre associated function of second kind, θ_0 is the range of the potential, and B^{-1} is a constant which depends on high-energy scattering properties. As in Ref. [128], the parameter B^{-1} can be fixed introducing the s-wave scattering length, and we set $B^{-1}=\ln(\theta_0/\theta_s)$, with θ_s the s-wave scattering angle. Note that we can define a_s, i. e. the two-dimensional s-wave scattering length *on the sphere*, as $a_s = R\,\theta_s$. For a sufficiently large spherical surface, such that the potential range θ_0 is very small and l_0 is much larger than the zero-point motion, the scattering amplitude can be expanded as [127]

$$f(E_{l_0}) = -\frac{2\pi\hbar^2}{m}\frac{1}{\ln\left(\frac{l_0\theta_s e^{\gamma}}{2}\right)-i\frac{\pi}{2}}. \tag{3.48}$$

As anticipated, we impose that $\mathcal{T}_{l_c}(E_{l_0}+i\eta) = f(E_{l_0})/(4\pi R^2)$ at the leading order in l_0, and thus, from Eqs. (3.45), (3.48), we find the contact interaction strength

$$g_0 = -\frac{2\pi\hbar^2}{m}\frac{1}{\ln[\sqrt{l_c(l_c+1)}\,a_s e^{\gamma}/(2R)]}, \tag{3.49}$$

expressed as a function of the cutoff l_c, and of the s-wave scattering length on the sphere.

Before of concluding the discussion of scattering on a spherical surface, we remark that the results of Eqs. (3.48) and (3.49) are obtained assuming a large radius of the sphere. From a quantitative point of view, we thus suppose that the radius is much larger than the healing length ξ, which can be modeled as

$$\xi = \sqrt{\frac{\hbar^2}{2m g_{2D} n}}, \tag{3.50}$$

where we can estimate g_{2D} as the mean-field contact interaction strength in two-dimensional weakly-interacting condensates, namely

$$g_{2D} = -\frac{4\pi\hbar^2}{m}\frac{1}{\ln(n a_s^2)}. \tag{3.51}$$

Strictly speaking, the two-dimensional s-wave scattering length in g_{2D} refers to a flat two-dimensional system, while the length appearing in Eq. (3.49) refers to scattering on the spherical surface. These quantities are in principle different, and the hypothesis of working in the large-radius regime justifies the use of relations obtained for flat condensates. In particular, it is within this spirit that we assume for a_s the value calculated in works on quasi two-dimensional condensates [129], namely

$$a_s = 2\sqrt{\frac{\pi}{C}} \exp\left(-\sqrt{\frac{\pi}{2}}\frac{l_\perp}{a_{3D}} - \gamma_{\mathrm{E}} \right) l_\perp, \tag{3.52}$$

where γ_{E} is the Euler-Mascheroni constant, $C = 0.915$ is calculated solving numerically the two-body problem, $l_\perp$ is the shell thickness, and a_{3D} is the s-wave scattering length in three-dimensions. We emphasize that all these quantities are known and, in particular, that $l_\perp = \sqrt{\hbar/(m\omega_\perp)}$, with $\omega_\perp$ defined in Eq. (3.2) in terms of the trap frequencies.

3.1.4 Thermodynamics

After discussing the scattering properties of a spherical Bose gas, we are ready to derive the regularized grand potential. The zero-temperature contributions to the grand potential of Eq. (3.22) can be expressed as

$$\frac{\Omega^{(0)}}{4\pi R^2} = -\frac{\mu^2}{2g_0} + \frac{1}{2}\int_1^{l_c} \mathrm{d}l\,(2l+1)\,(E_l^{\mathrm{B}} - \epsilon_l - \mu), \tag{3.53}$$

where we integrate instead of summing, and where we include an ultraviolet cutoff l_c. The integral can be performed analytically, and its logarithmic divergence in the parameter l_c is balanced exactly by the same scaling of the bare interaction g_0, as can be seen in Eq. (3.49). Including also the finite-temperature contribution of Eq. (3.22), we get

$$\frac{\Omega}{4\pi R^2} = -\frac{m\mu^2}{8\pi\hbar^2}\left\{\ln\left[\frac{4\hbar^2}{m(\mu+E_1^{\mathrm{B}}+\epsilon_1)a_s^2\,e^{2\gamma+1}}\right]+\frac{1}{2}\right\}+\frac{mE_1^{\mathrm{B}}}{8\pi\hbar^2}(E_1^{\mathrm{B}}-\epsilon_1-\mu) + \frac{1}{4\pi R^2}\frac{1}{\beta}\sum_{l=1}^{\infty}\sum_{m_l=-l}^{l}\ln(1-e^{-\beta E_l^{\mathrm{B}}}), \tag{3.54}$$

which is the grand potential per unit of area of a spherically symmetric Bose gas. Note that $E_1^B=\sqrt{\epsilon_1[\epsilon_1+2\mu]}$, with $\epsilon_1=\hbar^2/(mR^2)$, and in the thermodynamic limit in which $R\to\infty$ we have $E_1^{\mathrm{B}},\epsilon_1\to 0$. In this limit, and at a one-loop level, our grand potential coincides with the one obtained in Refs. [125, 126] where an infinite and uniform Bose gas is studied.

We calculate the number of atoms in the condensate deriving the grand potential with respect to the chemical potential μ. We obtain

$$\frac{N}{4\pi R^2} = \frac{m\mu}{4\pi\hbar^2}\ln\left[\frac{4\hbar^2}{m(\mu+E_1^B+\epsilon_1)\,a_s^2\,e^{2\gamma+1}}\right]+\frac{m\mu}{4\pi\hbar^2}\frac{E_1^B+\epsilon_1}{\mu+E_1^B+\epsilon_1} + \frac{1}{4\pi R^2}\sum_{l=1}^{\infty}\sum_{m_l=-l}^{l}\frac{\epsilon_l}{E_l^B}\frac{1}{e^{\beta E_l^B}-1}, \tag{3.55}$$

whose finite-size contributions, as occurs for the grand potential, vanish in the thermodynamic limit.

The typical experiments with Bose-Einstein condensates are done with a fixed number of particles and, therefore, are not compatible with a description in the grand canonical ensemble: the systems are not exchanging particles with an external reservoir. It is however simpler to calculate the partition function in this ensemble, and the spurious fluctuations in the number of atoms do not usually prevent the correct description of the experiments, provided that the number of particles is sufficiently large. Despite these considerations, it is formally inconsistent to fix a temperature-independent value of the chemical potential when, on the contrary, it is the number of atoms that is kept fixed. The correct procedure is, in this case, to perform the following Legendre transformation:

$$F(T,V,N)=\mu(T,V,N)N+\Omega[T,V,\mu(T,V,N)], \tag{3.56}$$

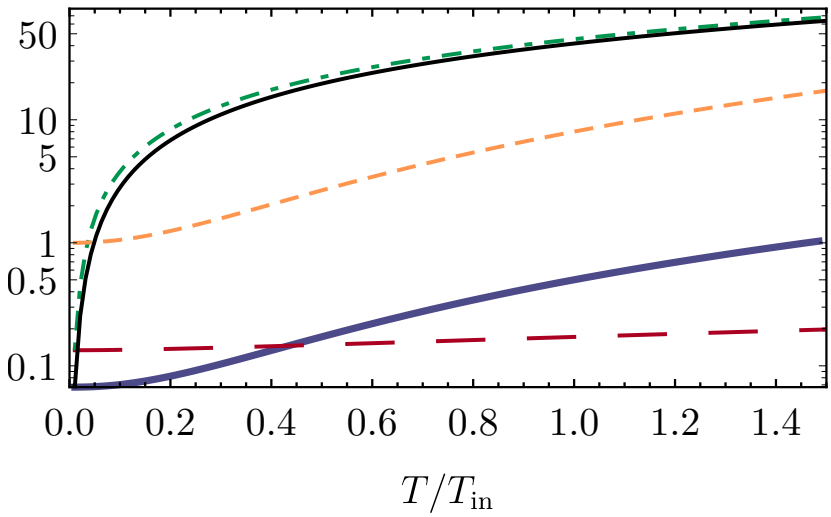

Figure 3.5: Thermodynamic functions of a spherically-symmetric bosonic gas plotted as a function of the temperature T/T_{in}, where $T_{\mathrm{in}} = 35\,\mathrm{nK}$. These curves represent: the specific heat per unit of mass and of atom number $\tilde{c}_v$ (green dot-dashed), the entropy per unit of mass and atom number $\tilde{s}$ (black), the ratio κ_T/κ_S between the isothermal and adiabatic compressibilities (orange dashed), the adimensional chemical potential $\mu/E_{l_\perp}$ (red long-dashed), and the grand potential $\Omega/E_{l_\perp}$ (blue thick). For this plot, we consider a spherically-symmetric gas of ^{87}Rb atoms trapped with the external potential of Eq. (3.1), where we set $M_F = 1$, $\omega_r = 2\pi \times 173\,\mathrm{Hz}$, $\Delta = 2\pi \times 30\,\mathrm{kHz}$, and $\Omega_r = 2\pi \times 3\,\mathrm{kHz}$ [52], and we have $E_{l_\perp} = \hbar^2/(2ml_\perp^2)$, with $l_\perp = 0.4\,\mu\mathrm{m}$ the shell thickness. Moreover, the scattering length is modeled as in Eq. (3.52). From [55].

in which F, the free energy of the system that is determined by fixing T, V, N, is obtained from the grand potential. For this operation, it is necessary to know the chemical potential as a function of T, V, N. To obtain it numerically, we calculate the number of atoms N of Eq. (3.55) for a fixed volume V and on a grid of values of T and μ. After that, we fit and invert numerically the function $N(T, V, \mu)$, obtaining $\mu(T, V, N)$.

Once that the free energy is known, all the other thermodynamic functions can be derived with the usual thermodynamic identities. We show in Fig. 3.5 some relevant thermodynamic functions of a spherically-symmetric Bose gas.

3.2 Bare superfluid density

We derive the superfluid density of a two-dimensional spherical superfluid, by extending the functional integral calculation implemented in section 3.1.1. Inspired

by Landau, i. e. Ref. [12], we suppose that the trapping potential rotates along a fixed axis with a constant angular velocity, so that the superfluid part of the fluid remains unperturbed, while, at the equilibrium, the normal fluid rotates with the trap.

Thus, when a spherical superfluid is rotating, the angular momentum of the system is proportional to the nonclassical moment of inertia and, therefore, it is also proportional to the density of the normal fluid. Given the normal density, it is then possible to derive the superfluid density as the total density minus the normal one. To implement quantitatively these concepts, we impose a rotation of the normal fluid along z, with angular velocity Ω_z, by shifting the imaginary time derivative in Eq. (3.5) as

$$\hbar\partial_\tau \to \hbar\partial_\tau + \Omega_z \hat{L}_z, \tag{3.57}$$

where $\hat{L}_z = -i\hbar\,\partial_\varphi$. Taking into account this modified term, the steps in section 3.1.1 can be essentially repeated up to the Lagrangian of Eq. (3.11), which is shifted as $\mathcal{L}_{\rm g} \to \mathcal{L}_{\rm g} - i\hbar\,\bar{\eta}(\theta,\varphi,\tau)\,\partial_\varphi\eta(\theta,\varphi,\tau)$. Then, besides including a few additional terms, all the other calculations can be done in the same formal order, and the grand potential contribution at Eq. (3.17) reads

$$\Omega_{\rm g}(\mu,\psi_0^2) = \frac{1}{2\beta}\sum_{\omega_n}\sum_{l=1}^{\infty}\sum_{m_l=-l}^{l}\ln\{\beta^2[\hbar^2\omega_n^2 + \xi_l^2(\mu,\psi_0^2)]\}, \tag{3.58}$$

where $\xi_l(\mu,\psi_0^2) = E_l(\mu,\psi_0^2) + m_l\hbar\Omega_z$, with $E_l(\mu,\psi_0^2)$ given by Eq. (3.18). As before, we perform the sum over the Matsubara frequencies with standard techniques (see Ref. [98]), and the total grand potential becomes

$$\begin{aligned}\Omega(\mu,\psi_0^2) =& (4\pi R^2)\bigg(-\mu\psi_0^2 + \frac{g_0}{2}\psi_0^4\bigg) + \frac{1}{2}\sum_{l=1}^{\infty}\sum_{m_l=-l}^{l}E_l(\mu,\psi_0^2)\\ &+ \frac{1}{\beta}\sum_{l=1}^{\infty}\sum_{m_l=-l}^{l}\ln\{1 - e^{-\beta[E_l(\mu,\psi_0^2)+m_l\hbar\Omega_z]}\},\end{aligned} \tag{3.59}$$

where the zero-temperature counterterms, included in the previous Eq. (3.19), are inessential for the derivation of the present section.

Given the grand potential of the rotating fluid, and considering the analogy with a similar calculation done in flat geometries [97], the angular momentum of the normal fluid can be calculated as

$$L_n = -\frac{\partial\Omega(\mu,\psi_0^2)}{\partial\Omega_z}\bigg|_{\psi_0^2=n_0(\mu)} \overset{\Omega_z\sim 0}{\longrightarrow} \beta\sum_{l=1}^{\infty}\sum_{m_l=-l}^{l}\hbar^2 m_l^2\,\frac{e^{\beta E_l^{\rm B}}}{(e^{\beta E_l^{\rm B}}-1)^2}\,\Omega_z, \tag{3.60}$$

where the right-hand side is obtained by expanding the resulting angular momentum for a small angular velocity Ω_z. Taking into account the known identity

$$\sum_{m_l=-l}^{l} m_l^2 = \frac{1}{3}(2l+1)(l^2+l), \tag{3.61}$$

the angular momentum of the normal fluid, which is dragged by the rotating trap, reads

$$L_n = \frac{\beta}{3}\sum_{l=1}^{\infty}(2l+1)\,\hbar^2(l^2+l)\,\frac{e^{\beta E_l^{\mathrm{B}}}}{(e^{\beta E_l^{\mathrm{B}}}-1)^2}\,\Omega_z, \tag{3.62}$$

which results from a microscopic calculation. But the angular momentum can also be expressed as $L_n = I_n\Omega_z$, where

$$I_n = \frac{2}{3}M_nR^2 \tag{3.63}$$

is the moment of inertia of a hollow sphere with mass $M_n = mn_n(4\pi R^2)$, and $n_n^{(0)}$ is the (bare) number density of the normal fluid. A simple comparison of the previous relations yields the bare normal density of the spherical superfluid

$$n_n^{(0)} = \beta\sum_{l=1}^{\infty}\frac{(2l+1)}{4\pi R^2}\,\frac{\hbar^2 l(l+1)}{2mR^2}\,\frac{e^{\beta E_l^{\mathrm{B}}}}{(e^{\beta E_l^{\mathrm{B}}}-1)^2}, \tag{3.64}$$

and, consequently, the bare superfluid density

$$n_s^{(0)} = n - n_n^{(0)}, \tag{3.65}$$

which coincides with the result postulated in Ref. [54].

The superfluid density derived in this section is denoted as *bare*, meaning that it takes into account only the Bogoliubov excitations of the system and that it neglects the vortex-antivortex excitations. In two-dimensional systems, including spherical superfluids, these topological excitations proliferate with the temperature, renormalizing the superfluid density. In the next sections, we will include in our theory the physics of vortices, by modeling explicitly their contribution to the energy of the superfluid.

3.3 Vortices in a spherical superfluid shell

In the calculations of the previous sections we obtained the grand potential Ω of a spherical bosonic gas as a sum of a mean-field part and of a beyond-mean-field

part, the latter obtained at a one-loop level. In particular, the beyond-mean-field terms describe the Bogoliubov excitations of the system on top of the mean-field condensate state. In ultracold bosonic gases, however, the Bogoliubov quasiparticles are not the only excitations that the system may possess. Indeed, even at zero temperature, a superfluid can host quantized vortices, namely, configurations of the macroscopic field in which the fluid rotates around a single point (the core of the vortex) with quantized angular momentum.

In this section, we construct an effective model to calculate the energy of a system of vortices on a spherical superfluid film. For this scope, we suppose that the superfluid at a finite temperature is described by the order parameter

$$\psi(\theta,\varphi) = \left[n_s^{(0)}(T)\right]^{1/2} e^{i\Phi(\theta,\varphi)}, \tag{3.66}$$

where $n_s^{(0)}$ is the uniform (bare) superfluid density given by Eq. (3.65), and where the field $\Phi(\theta,\varphi)$ represents the phase field of the bosonic fluid. The bare superfluid density, which contains only the contribution due to the Bogoliubov excitations vanishes at a temperature T^*, and therefore, when this superfluid transition occurs, the order parameter becomes zero. Actually, it turns out that the vortical configurations of the superfluid can be thermally excited, and renormalize the superfluid density. Since the present section discusses the calculation of the vortex energy, the issue of renormalization will be analyzed in detail in the next section.

We calculate the kinetic energy associated to the order parameter $\psi(\theta,\varphi)$ as

$$E = \int_0^{2\pi} \mathrm{d}\varphi \int_0^{\pi} \mathrm{d}\theta \, \sin\theta \, R^2 \, \psi^*(\theta,\varphi) \left(\frac{\hat{L}^2}{2mR^2}\right) \psi(\theta,\varphi), \tag{3.67}$$

where the energy contributions associated to the radial motion, as in the previous section, are also not included here. After some simple steps, the kinetic energy can be rewritten as

$$E = \frac{1}{2} m n_s^{(0)} \int_0^{2\pi} \mathrm{d}\varphi \int_0^{\pi} \mathrm{d}\theta \, \sin\theta \, \mathbf{v}(\theta,\varphi) \cdot \mathbf{v}(\theta,\varphi), \tag{3.68}$$

in which we define the velocity field $\mathbf{v}(\theta,\varphi)$ as

$$\mathbf{v}(\theta,\varphi) = \frac{\hbar}{mR} \tilde{\nabla}_R \Phi(\theta,\varphi), \tag{3.69}$$

where $\tilde{\nabla}_R = \mathbf{e}_\theta \, \partial_\theta + (\sin\theta)^{-1} \, \mathbf{e}_\varphi \, \partial_\varphi$ is the dimensionless gradient in spherical coordinates for R fixed, with $\mathbf{e}_\theta$ and $\mathbf{e}_\varphi$ the unitary vectors along θ and φ. Due to its definition, the velocity field is irrotational in all the spatial coordinates where the phase field is defined, namely

$$\nabla \times \mathbf{v} = 0, \tag{3.70}$$

which can be verified calculating the curl in spherical coordinates and considering that the velocity field has a zero radial component. However, a superfluid can have some phase defects, namely, point singularities where the phase field is not defined and the curl of the velocity is nonzero. In general, we can express $\mathbf{v}(\theta, \varphi)$ as

$$\mathbf{v}(\theta, \varphi) = \mathbf{v}_0(\theta, \varphi) + \mathbf{v}_{\rm v}(\theta, \varphi), \tag{3.71}$$

decomposing it in an irrotational part $\mathbf{v}_0(\theta, \varphi)$ without phase defects, and in a part with nonzero curl $\mathbf{v}_{\rm v}(\theta, \varphi)$ that describes the velocity field of the vortices. For the vortical part, we write the Feynman-Onsager condition of quantized circulation [130, 131], namely

$$\oint_{\partial\Sigma} \mathbf{v}_{\rm v} \cdot \mathrm{d}\mathbf{l} = 2\pi \frac{\hbar}{m} \sum_i q_i, \tag{3.72}$$

where q_i are the integer charges of the vortices inside the region Σ, with border $\partial\Sigma$.

The fields $\mathbf{v}_0$ and $\mathbf{v}_{\rm v}$ are orthogonal, and the kinetic energy splits into the sum of the kinetic energy of the vortical fluid, and of the kinetic energy of the (everywhere) irrotational fluid. Broadly speaking, the kinetic energy of the part of the fluid without phase defects can be associated to the grand potential derived previously in Eq. (3.22). This analogy is motivated by works on two-dimensional superfluid fermionic systems [132], where the kinetic energy contribution without vortices, in the form of Eq. (3.68), is obtained from a microscopic calculation analogous to our Bogoliubov-Popov theory. To analyze, as stated, the energy of the vortical part of the fluid, here we focus only on the kinetic energy associated to $\mathbf{v}_{\rm v}(\theta, \varphi)$, which reads

$$E^{(\rm vor)} = \frac{1}{2} m n_s^{(0)} \int_0^{2\pi} \mathrm{d}\varphi \int_0^{\pi} \mathrm{d}\theta \, \sin\theta \, R^2 \, \mathbf{v}_{\rm v}(\theta, \varphi) \cdot \mathbf{v}_{\rm v}(\theta, \varphi), \tag{3.73}$$

and, once that the velocity field is known, can be calculated analytically.

To obtain $\mathbf{v}_{\rm v}(\theta, \varphi)$, we consider a system of $M_{\rm v}$ vortices with charges q_i, where $i = 1, ..., M_{\rm v}$. Due to topological constraints, the net vortex charge of a spherical superfluid must be zero. Indeed, a path $\partial\Sigma$ on the sphere corresponds to two complementary spherical caps Σ_1 and Σ_2. If the path $\partial\Sigma$ is chosen in a such a way that Σ_1 does not contain vortices, and that Σ_2 contains all the vortices, one finds that

$$\sum_{i=1}^{M_{\rm v}} q_i = 0 \tag{3.74}$$

by applying to both caps the condition of quantized circulation of Eq. (3.72). We now assume that the flow associated to the vortical velocity field $\mathbf{v}_{\rm v}(\theta, \varphi)$ is incompressible, namely, that $\nabla \cdot \mathbf{v}_{\rm v} = 0$. From this condition, it follows that

$$\mathbf{v}_{\rm v}(\theta, \varphi) = 2\pi \, \frac{\hbar}{mR} \, \mathbf{e}_r \times \big[\tilde{\nabla}_R \, \chi(\theta, \varphi)\big], \tag{3.75}$$

where $\mathbf{e}_r$ is the unitary vector along the radial direction, and where $\chi(\theta,\varphi)$ is the stream function, which is constant along the streamlines of the fluid. For point vortices, the stream function can be calculated analytically, and the velocity field is therefore known. Indeed, introducing the vortex charge density

$$n_{\rm v}(\theta,\varphi) = \sum_{i=1}^{M_{\rm v}} q_i \left[\delta(\cos\theta - \cos\theta_i)\,\delta(\varphi-\varphi_i) - \frac{1}{4\pi}\right], \tag{3.76}$$

where the factor $1/(4\pi)$ is introduced for regularization purposes by using the condition of charge neutrality of Eq. (3.74), the stream function is determined by

$$-\frac{\hat{L}^2}{\hbar^2}\chi(\theta,\varphi) = n_{\rm v}(\theta,\varphi), \tag{3.77}$$

where the angular momentum operator is defined as in Eq. (2.25). The general form of the stream function reads

$$\chi(\theta,\varphi) = \sum_{i=1}^{M_{\rm v}} \chi_i(\theta,\varphi), \tag{3.78}$$

where we define

$$\chi_i(\theta,\varphi) = \frac{q_i}{2\pi}\,\ln\left[\sin\left(\frac{\gamma_i}{2}\right)\right], \tag{3.79}$$

and γ_i is the angular distance between (θ,φ) and (θ_i,φ_i). The detailed steps to solve Eq. (3.77), which is essentially the Green's function of the Laplace equation in spherical coordinates, are shown in the Appendix A. We stress that, by using the bisection formula of the sine and writing explicitly the cosine of the angular distance, one finds

$$\sin(\gamma_i/2) = \sqrt{\frac{1-\cos\theta\cos\theta_i - \sin\theta\sin\theta_i\cos(\varphi-\varphi_i)}{2}}, \tag{3.80}$$

which allows us to determine the single-vortex stream function $\chi_i(\theta,\varphi)$ once that the position of its core (θ_i,φ_i) is fixed.

For a given configuration of the vortices, the velocity field $\mathbf{v}_{\rm v}(\theta,\varphi)$ can be calculated with Eq. (3.75), and the energy of Eq. (3.73) can be expressed as

$$E^{(\rm vor)} = \sum_{i=1}^{M_{\rm v}} E_i^{(\rm vor)} + \sum_{\substack{i,j=1\\ i\neq j}}^{M_{\rm v}} E_{ij}^{(\rm vor)}, \tag{3.81}$$

where the self-energy contribution reads

$$E_i^{(\mathrm{vor})} = \frac{\hbar^2 n_s^{(0)}}{2m} \int_0^{2\pi} \mathrm{d}\varphi \int_\epsilon^\pi \mathrm{d}\theta \sin\theta \left[2\pi \left(\tilde{\nabla}_{\mathrm{R}} \chi_i\right)\right]^2, \tag{3.82}$$

with ϵ a small angular cutoff included to regularize the self-energy, and where

$$E_{ij}^{(\mathrm{vor})} = \frac{\hbar^2 n_s^{(0)}}{2m} \int_0^{2\pi} \mathrm{d}\varphi \int_0^\pi \mathrm{d}\theta \sin\theta \left[2\pi \left(\tilde{\nabla}_{\mathrm{R}} \chi_i\right)\right] \cdot \left[2\pi \left(\tilde{\nabla}_{\mathrm{R}} \chi_j\right)\right] \tag{3.83}$$

is the "interaction"-energy contribution among the vortices. Due to symmetry considerations, the self-energy integrals can be evaluated for $\theta_i = 0$, $\varphi_i = 0$ without loss of generality, leading to

$$E_i^{(\mathrm{vor})} = \frac{\hbar^2 n_s^{(0)}}{m} \pi q_i^2 \left\{ \ln\left[\frac{1}{\sin(\epsilon/2)}\right] - \frac{1+\cos\epsilon}{4} \right\}, \tag{3.84}$$

where we simply integrated $[2\pi\,(\partial_\theta \chi_i)]^2 = [(q_i/2)\cot(\theta/2)]^2$ over the spherical coordinates. The terms $E_{ij}^{(\mathrm{vor})}$ can be calculated integrating Eq. (3.83) by parts and using the property of Eq. (A.1) of the Green's function, obtaining

$$E_{ij}^{(\mathrm{vor})} = -\frac{\hbar^2 n_s^{(0)}}{m} \pi\, q_i q_j \left\{ \ln\left[\sin\left(\frac{\gamma_{ij}}{2}\right)\right] + \frac{1}{2} \right\}, \tag{3.85}$$

where

$$\sin\left(\frac{\gamma_{12}}{2}\right) = \sqrt{\frac{1 - \cos\theta_1\cos\theta_2 - \sin\theta_1 \sin\theta_2 \cos(\varphi_1 - \varphi_2)}{2}} \tag{3.86}$$

is the angular distance between the couple of vortices. Putting everything together, the general expression of $E^{(\mathrm{vor})}$ is given by

$$\begin{aligned} E^{(\mathrm{vor})} = &\sum_{i=1}^{M_{\mathrm{v}}} \frac{\hbar^2 n_s^{(0)}}{m} \pi q_i^2 \left(\ln\left\{\frac{\sin[\xi/(2R)]}{\sin(\epsilon/2)}\right\} + \frac{1-\cos\epsilon}{4} \right) \\ &- \sum_{i,j=1}^{M_{\mathrm{v}}} \frac{\hbar^2 n_s^{(0)}}{m} \pi\, q_i q_j \, \ln\left\{\frac{\sin(\gamma_{ij}/2)}{\sin[\xi/(2R)]}\right\}, \end{aligned} \tag{3.87}$$

where we used the conditions of charge neutrality and the properties of the logarithms to include M_{v} terms of the form of $\ln\{\sin[\xi/(2R)]\}$, where ξ is the healing length of the superfluid.

The kinetic energy of the vorticous superfluid depends on the cutoff ϵ, which, in general, is unknown and arbitrary. In particular, the first line of Eq. (3.87)

represents the energy necessary to create a system of $M_{\rm v}$ vortices with charges q_i, with $i = 1, ..., M_{\rm v}$. We expect that, at least for a sphere with a radius $R \gg \xi$, these self-energy terms coincide with those obtained by Kosterlitz and Thouless in the flat case [71]. Thus, denoting with $2q^2\mu_{\rm v}$ the energy necessary to create a vortex-antivortex dipole with charges $\pm q$ at the minimal distance of $\epsilon \propto \xi/R$, we assume that the vortex chemical potential $\mu_{\rm v}$ is given by

$$\mu_{\rm v} \approx \frac{\hbar^2 n_s^{(0)}}{m}\,\pi\,\ln\left[\frac{(\xi/R)}{\epsilon}\right] = \frac{\hbar^2 n_s^{(0)}}{m}\,\pi\,[\ln(2\sqrt{2}) + \gamma_{\rm E}], \tag{3.88}$$

where the last expression coincides with the value obtained in Ref. [71]. In conclusion, we obtain the kinetic energy of a spherical vorticous superfluid, namely

$$E^{(\rm vor)} = \sum_{i=1}^{M_{\rm v}} q_i^2\mu_{\rm v} - \pi\,\frac{\hbar^2 n_s^{(0)}}{m}\sum_{\substack{i,j=1\\ i\neq j}}^{M_{\rm v}} q_i q_j\,\ln\left[\frac{2R\,\sin(\gamma_{ij}/2)}{\xi}\right], \tag{3.89}$$

which holds in the large-sphere regime. We emphasize that the energy derived here reproduces the known result reported in Ref. [133]. At the same time, we stress that, with this derivation, we can justify the introduction of the chemical potential $\mu_{\rm v}$, on which the calculations of the next section are based.

3.4 Renormalization of the superfluid density

At zero temperature, in a uniform system of weakly-interacting bosons, the superfluid density coincides with the density itself. When the temperature is increased, however, thermal excitations appear spontaneously in the system, decreasing the portion of the fluid which displays superfluid properties. From a microscopic point of view, this "normal" fluid component that appears at finite temperature is composed by two kinds of excitations: the Bogoliubov quasiparticles, and the vortices. Actually, in a nonzero but low temperature regime, the production of free vortices at large distances from each other requires a large amount free energy, and is therefore highly unfavored. In this case, one may assume that the Bogoliubov excitations are the only quasiparticles in the system, and that the Landau superfluid density, obtained in Eq. (3.65), is a good approximation of the real superfluid density $n_{\rm s}$.

Concerning its temperature dependence, the Landau superfluid density $n_{\rm s}^{(0)}$ goes to zero smoothly at a temperature T^*, but, in two-dimensional systems, this simple behavior does not represent what occurs in the experiments. Indeed, while the free vortices have a high free-energy cost at low temperatures, at which they can

only exist as vortex-antivortex dipoles, they actually unbind and exist as thermal excitations when a critical temperature is reached. At this "BKT" transition, which is named after Berezinskii, Kosterlitz and Thouless, the vortices proliferate, and the vortical velocity field disrupts any underlying superfluid flow.

This superfluid transition has been qualitatively and quantitatively analyzed in Refs. [69,71,72], and the specific analysis for two-dimensional superfluid Helium was done by Nelson and Kosterlitz in Ref. [73]. In the infinite-size case, Bose-Einstein condensation cannot occur due to the Hohenberg-Mermin-Wagner theorem [90, 91], but superfluidity, associated to quasi-long-range order and to a power-law decay of the phase correlations, does occur. It was shown that the bare superfluid density $n_s^{(0)}$ is renormalized to n_s by the thermal excitation of vortices, and that n_s jumps abruptly to zero at a temperature given by the Kosterlitz-Nelson criterion [73]

$$\frac{n_s(T_{\mathrm{BKT}}^-)}{T_{\mathrm{BKT}}} = \frac{2}{\pi}\frac{mk_{\mathrm{B}}}{\hbar^2}, \tag{3.90}$$

so that the size of the jump is a universal constant which does not depend on the interatomic interactions. In finite-size two-dimensional superfluids, Bose-Einstein condensation takes place, and the BKT transition typically occurs as a smooth nonuniversal crossover, rather than a universal system-independent jump. The main underlying mechanism is however the same: the unbinding of vortex-antivortex dipoles and the proliferation of free vortices.

In this section we model the BKT transition in bubble-trapped bosonic superfluids. In particular, to employ the analytical relations obtained in the previous sections, we will limit here to the spherically-symmetric case. The Kosterlitz-Thouless analysis is based on the analogy between a system of electric charges in two dimensions, whose interaction scales logarithmically with their distance, and the physics of vortices in a superfluid. In extending this analogy to the spherical case, we consider a vortex-antivortex dipole with quantized unitary charges, whose energy, due to Eq. (3.89), reads

$$\beta U_0(\theta) = 2\beta\mu_{\mathrm{v}} + 2\pi K_0 \ln\left[\frac{2R}{\xi}\sin\left(\frac{\theta}{2}\right)\right], \tag{3.91}$$

where, without loss of generality, we consider $\varphi_1 = \varphi_2 = 0$ and $\theta_1 = \theta$, $\theta_2 = 0$. In the previous equation, we choose the symbol U_0 for the bare interaction energy between the vortices instead of $E^{(\mathrm{vor})}$, and we define the parameter

$$K_0 = \frac{\hbar^2 n_s^{(0)}}{mk_{\mathrm{B}}T}, \tag{3.92}$$

which is essentially the adimensionalized bare superfluid density. Due to the presence of other vortex-antivortex dipoles in the angular interval θ among the

charges, the "Coulomb" force is screened as

$$\frac{\mathrm{d}U}{\mathrm{d}\theta} = \frac{1}{\varepsilon(\theta)} \frac{\mathrm{d}U_0}{\mathrm{d}\theta}, \tag{3.93}$$

and U, the renormalized interaction potential of the vortices, reads

$$\beta U(\theta) = \int_{\xi/R}^{\theta} \mathrm{d}\theta' \, \frac{\pi K(\theta')}{\tan(\theta'/2)} = 2\pi \int_{\ell(\xi/R)}^{\ell(\theta)} K(\theta') \; \mathrm{d}[\ell(\theta')], \tag{3.94}$$

where $\ell(\theta) = \ln[(2R/\xi)\sin(\theta/2)]$, and we define the renormalized parameter

$$K(\theta) = \frac{\hbar^2}{m k_B T} \frac{n_s^{(0)}}{\varepsilon(\theta)}, \tag{3.95}$$

which is essentially the renormalized superfluid density $n_s = n_s^{(0)}/\varepsilon(\theta)$ in an adimensional form. Once that the relative dielectric function $\varepsilon(\theta)$ is known, it is then possible to calculate the renormalized superfluid density, and the renormalized interaction $U(\theta)$.

Let us develop a perturbative calculation of the dielectric function $\varepsilon(\theta)$. We express $\varepsilon(\theta)$ in terms of the electric susceptibility of the dipoles, i. e. $\chi_{\mathrm{e}}(\theta)$, as $\varepsilon(\theta) = 1 + 4\pi\chi_{\mathrm{e}}(\theta)$, and we calculate $\chi_{\mathrm{e}}(\theta)$ as

$$\chi_{\mathrm{e}}(\theta) = \int_{\xi/R}^{\theta} \mathrm{d}\theta' \, n_{\mathrm{d}}(\theta') \, \alpha(\theta'), \tag{3.96}$$

namely, as the product between the polarizability of the superfluid medium $\alpha(\theta')$ and the density of dipoles $n_{\mathrm{d}}(\theta')$ at a distance θ', integrated for all $\theta' < \theta$. In this way, the renormalized superfluid parameter $K(\theta)$ can be expressed as

$$K^{-1}(\theta) = K_0^{-1} + 4\pi K_0^{-1} \int_{\xi/R}^{\theta} \mathrm{d}\theta' \, n_{\mathrm{d}}(\theta') \, \alpha(\theta'), \tag{3.97}$$

as follows from its definition at Eq. (3.95). We now implement a perturbative calculation of $n_{\mathrm{d}}(\theta')$ and of $\alpha(\theta')$. We express the density of dipoles as [134, 135]

$$n_{\mathrm{d}}(\theta') = 2\pi \, \frac{R^2}{\xi^4} \sin\theta' \, y_0^2 \, e^{-\beta U(\theta')} + o(y_0^4), \tag{3.98}$$

namely, as the product between the integral measure $2\pi \sin\theta' (R/\xi)^2$ and the dipole density along θ, which, at the lowest order in the vortex fugacity $y_0 = e^{-\beta\mu_{\mathrm{v}}}$, is proportional to the Boltzmann factor $y_0^2 \, e^{-\beta U(\theta')}$.

To calculate $\alpha(\theta')$, we consider a vortex-antivortex dipole with an angular distance θ' in an external superfluid flow with velocity $v_{\rm ext}$. For small θ', the external flow is practically uniform, and it is the analogous of an "electric" field $|\mathbf{e}| = 2mv_{\rm ext}/\hbar$ that polarizes the medium between the vortex and the antivortex. At a finite temperature, the dipole moment of the vortex antivortex dipole is given by

$$\langle \mathbf{d}(\theta') \rangle = \langle 2R \sin(\theta'/2) \cos\varphi \rangle, \tag{3.99}$$

where we assume that the flow forms and angle φ with the dipole moment, and where the thermal average is performed with the Boltzmann factor

$$\exp\{-[\beta U_0(\theta'') - \pi K_0\, \mathbf{d}(\theta'') \cdot \mathbf{e}]\}, \tag{3.100}$$

and integrating in the annulus $\theta' < \theta'' < \theta' + d\theta$. The polarizability is then given by [71, 135]

$$\alpha(\theta') = \frac{\partial}{\partial |\mathbf{e}|} \langle 2R \sin(\theta'/2) \cos\varphi \rangle \Big|_{|\mathbf{e}|=0}, \tag{3.101}$$

from which we find that

$$\alpha(\theta') = 2\pi K_0\, R^2 \sin^2(\theta'/2). \tag{3.102}$$

Putting Eq. (3.98) and (3.102) inside Eq. (3.97), we can write the inverse of the renormalized superfluid parameter as

$$K^{-1}(\theta) = K_0^{-1} + 4\pi^3 \int_{\ell(\xi/R)}^{\ell(\theta)} y^2(\theta')\ \mathrm{d}[\ell(\theta')], \tag{3.103}$$

where

$$y^2(\theta) = y_0^2\, \frac{\sin^4(\theta/2)}{[\xi/(2R)]^4}\, e^{-\beta U(\theta)} \tag{3.104}$$

is the renormalized fugacity of a spherical superfluid. Considering the different equivalent forms of the renormalized interaction $U(\theta)$ of Eq. (3.94), the renormalized fugacity can also be written as

$$y^2(\theta) = y_0^2\, \exp\left\{ 4\ell(\theta) - 2\pi \int_{\ell(\xi/R)}^{\ell(\theta)} K(\theta')\ \mathrm{d}[\ell(\theta')] \right\}, \tag{3.105}$$

where the dependence from the renormalization group scale $\ell(\theta)$, which contains the vortex-antivortex chordal distance, is made explicit. We emphasize that Eq. (3.105) leads to an expression of $y(\theta)$ in the spherical case which is the analogous of the flat-case one obtained by Young in 1978, and avoids making further approximations [136, 137]. Finally, we derive Eqs. (3.103) and (3.105) with

respect to $\ell(\theta)$, to obtain the renormalization group differential equations of a spherical superfluid, namely

$$\begin{aligned} \frac{\partial K^{-1}(\theta)}{\partial \ell(\theta)} &= 4\pi^3 y^2(\theta), \\ \frac{\partial y(\theta)}{\partial \ell(\theta)} &= [2 - \pi K(\theta)]\, y(\theta), \end{aligned} \tag{3.106}$$

which allow to calculate the renormalized superfluid parameters using the bare ones as initial conditions. Note that this two-step renormalization group procedure yields a renormalized superfluid density which takes into account both the Bogoliubov quasiparticles and the vortices. The validity of this approach has been carefully analyzed in Ref. [138], where the critical temperature obtained through the two-step procedure is found to be in good agreement with that of Quantum Monte Carlo simulations and of functional renormalization group ones.

The numerical solution of the renormalization group equations (3.106) in the interval $\ell(\theta) \in [\ell(\xi/R), \ell(\pi)]$ yields the solutions $\{y(\pi), K(\pi)\}$ as a function of temperature and, therefore, allows to calculate the renormalized superfluid density $n_s = m k_{\mathrm{B}} T K(\pi)/\hbar^2$. In particular, as initial condition at $\ell(\theta) = \ell(\xi/R)$, we consider the bare values of y_0 and of K_0. These parameters, which are calculated numerically according to their definitions, depend on the bare Landau superfluid density $n_s^{(0)}$ of Eq. (3.65). In turn, the calculation of $n_s^{(0)}$ at a fixed temperature, number of atoms, and area, requires the knowledge of the equation of state, i. e. of the chemical potential $\mu(T, V, N)$ discussed in section 3.1.4. By putting all these elements together, it is possible to study how the BKT transition occurs in bubble-trapped superfluids.

Implementing this description for the typical number of atoms, temperature, and interaction regimes, we analyzed the superfluid BKT transition for experimentally relevant configurations in Ref. [55]. Due to the finite size of the system, the renormalization group equations are solved up to the finite scale $\ell(\pi)$, which implies that the superfluid density vanishes smoothly when increasing the temperature. This behavior can be seen in Fig. 3.6(a), where we plot the superfluid fraction as a function of temperature.

We identify the typical temperature at which the finite-size BKT transition occurs with T_{in}, which is the temperature of the inflection point of n_s/n [139]. The width of the transition is instead identified as the temperature interval corresponding to the intersection of the tangent in $n_s(T_{\mathrm{in}})$ with the constants $n_s/n = 0$, $n_s/n = 1$. The other panels show the universal scaling of finite-size BKT physics, depicting in Fig. 3.6(b) the values of $m k_{\mathrm{B}} T_{\mathrm{in}}/[\hbar^2 n_s(T_{\mathrm{in}})]$, and showing in Fig. 3.6(c) how the finite width of the transition vanishes when increasing the system size. These

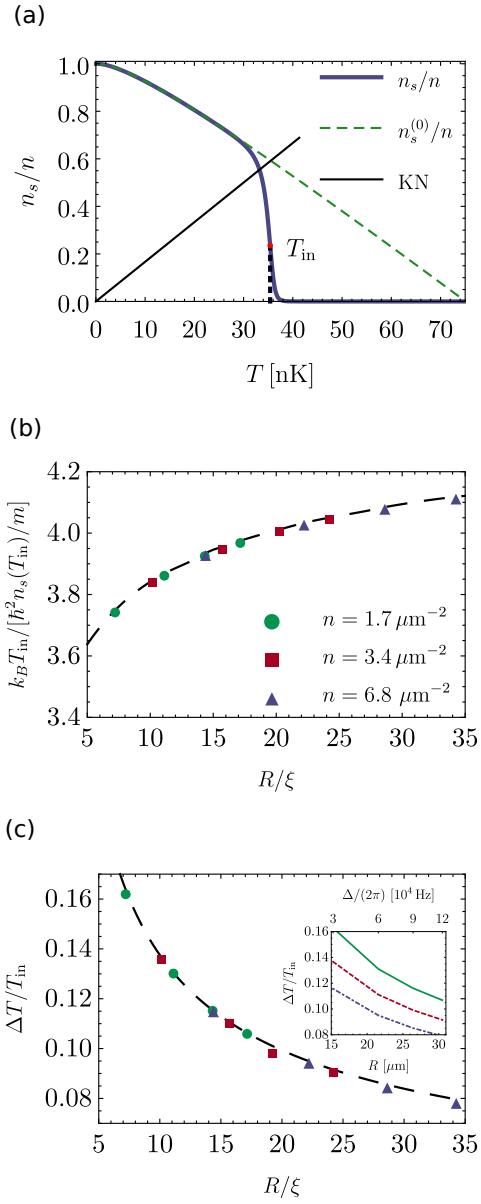

Figure 3.6: Superfluid BKT transition in bubble-trapped condensates. Panel (a) shows the superfluid fraction as a function of temperature, with $T_{\rm in}$ being the inflection point. In panel (b) we plot $mk_{\rm B}T_{\rm in}/[\hbar^2 n_s(T_{\rm in})]$ as a function of R/ξ, showing how, for different values of the two-dimensional density n, all the data collapse on the same line. Panel (c) highlights the logarithmic scaling of the transition width as $\Delta T/T_{\rm in} = 2.1/\ln^2(5R/\xi)$ (see Refs. [140–142]), which is justified by the correlation length of BKT theory [72]. We use for this plot the same parameters adopted for Fig. 3.5. From Ref. [55].

universal, i. e. interaction independent, scalings emerge when the horizontal axis is rescaled as R/ξ, where the vortex core size ξ is identified with the healing length of Eq. (3.50).

3.5 Numerical results for ellipsoidal shells

In the previous sections of this chapter, we analyzed the physics of bubble-trapped condensates, obtaining several analytical results for a spherically-symmetric configuration. Relaxing this symmetry constraint, the study of these systems requires the adoption of numerical techniques, and the phenomenology becomes richer and more involved. In this section, we provide several tests and predictions for prolate axially-symmetric shells, using the typical experimental parameters of the microgravity experiments, illustrated in Refs. [51, 52].

3.5.1 Critical condensation temperature and ground state

To calculate the critical temperature of ellipsoidal shells, we use the Hartree-Fock-Bogoliubov theory developed in Refs. [143,144] limited to the so-called Hartree-Fock approximation. Referencing to these works, we now introduce the essential details of this approach. The general idea is to start from the Heisenberg equation for the field operator $\hat{\psi}(\mathbf{r})$, which evolves under the action of the grand canonical Hamiltonian $\hat{H} - \mu\hat{N}$, with $\hat{H}$ given by Eq. (2.32) and $\hat{N}$ by Eq. (2.33). In particular, the field operator satisfies the equation

$$i\hbar\frac{\partial\hat{\psi}(\mathbf{r},t)}{\partial t} = \left[-\frac{\hbar^2\nabla^2}{2m} + U(\mathbf{r}) - \mu + g_0\,\hat{\psi}^\dagger(\mathbf{r},t)\hat{\psi}(\mathbf{r},t)\right]\hat{\psi}(\mathbf{r},t), \tag{3.107}$$

where we limit ourselves to considering a contact interaction between bosons, i. e. $V(\mathbf{r}-\mathbf{r}') = g_0\,\delta^{(3)}(\mathbf{r}-\mathbf{r}')$. We then decompose the field operator as

$$\hat{\psi}(\mathbf{r},t) = \Phi(\mathbf{r}) + \hat{\eta}(\mathbf{r},t), \tag{3.108}$$

where $\Phi(\mathbf{r}) = \langle\hat{\psi}(\mathbf{r})\rangle$ is the condensate field, with $\langle ...\rangle$ denoting the statistical average, and $\hat{\eta}(\mathbf{r},t)$ is the fluctuations operator, which has zero thermal average $\langle\hat{\eta}(\mathbf{r},t)\rangle = 0$. Inserting this decomposition into Eq. (3.107) and calculating the average, we get [143]

$$\left\{ -\frac{\hbar^2\nabla^2}{2m} + U(\mathbf{r}) - \mu + g_0\left[n_c(\mathbf{r}) + 2\tilde{n}(\mathbf{r})\right]\right\}\Phi(\mathbf{r}) + \tilde{m}(\mathbf{r})\Phi^*(\mathbf{r}) = 0, \tag{3.109}$$

with $n_c(\mathbf{r}) = |\Phi(\mathbf{r})|^2$, and where we define the noncondensed density $\tilde{n}(\mathbf{r}) = \langle\hat{\eta}^\dagger(\mathbf{r},t)\hat{\eta}(\mathbf{r},t)\rangle$, and the anomalous density $\tilde{m}(\mathbf{r}) = \langle\hat{\eta}(\mathbf{r},t)\hat{\eta}(\mathbf{r},t)\rangle$. Note that, to obtain Eq. (3.109), it is necessary to evaluate the average of cubic terms in the fluctuation field within a mean-field approximation [143].

The equation of motion of the fluctuation operator $\hat{\eta}(\mathbf{r},t)$ is obtained subtracting Eq. (3.109) from Eq. (3.107), getting

$$i\hbar\frac{\partial\hat{\eta}(\mathbf{r},t)}{\partial t} = \left\{-\frac{\hbar^2\nabla^2}{2m}+U(\mathbf{r})-\mu+2g_0\left[n_c(\mathbf{r})+\tilde{n}(\mathbf{r})\right]\right\}\hat{\eta}(\mathbf{r},t)+g_0\left[n_c(\mathbf{r})+\tilde{m}(\mathbf{r})\right]\hat{\eta}^\dagger(\mathbf{r},t), \tag{3.110}$$

whose solution can be implemented with different levels of approximation, the most convenient being the Popov approximation [143], where the anomalous density contribution $\tilde{m}(\mathbf{r})$ is neglected. We now decompose $\hat{\eta}(\mathbf{r},t)$ as

$$\hat{\eta}(\mathbf{r},t) = \sum_j \left[u_j(\mathbf{r})e^{-iE_jt/\hbar}\,\hat{a}_j + v_j^*(\mathbf{r})e^{iE_jt/\hbar}\,\hat{a}_j^\dagger\right] \tag{3.111}$$

$$\hat{\eta}^\dagger(\mathbf{r},t) = \sum_j \left[u_j^*(\mathbf{r})e^{iE_jt/\hbar}\,\hat{a}_j^\dagger + v_j(\mathbf{r})e^{-iE_jt/\hbar}\,\hat{a}_j\right], \tag{3.112}$$

where $\hat{a}_j$, $\hat{a}_j^\dagger$ are operators satisfying bosonic commutation rules. The functions $u_j(\mathbf{r})$ and $v_j(\mathbf{r})$ satisfy the relation

$$\int \mathrm{d}\mathbf{r}\left[u_j^*(\mathbf{r})u_k(\mathbf{r}) - v_j^*(\mathbf{r})v_k(\mathbf{r})\right] = \delta_{jk}, \tag{3.113}$$

which ensures their orthonormalization. Substituting this decomposition into the previous Eq. (3.110), we get the Bogoliubov-de Gennes equations

$$\hat{\mathfrak{L}}u_j(\mathbf{r}) - g_0\left[n_c(\mathbf{r}) + \tilde{m}(\mathbf{r})\right]v_j(\mathbf{r}) = E_ju_j(\mathbf{r}), \tag{3.114}$$

$$\hat{\mathfrak{L}}v_j(\mathbf{r}) - g_0\left[n_c(\mathbf{r}) + \tilde{m}^*(\mathbf{r})\right]u_j(\mathbf{r}) = -E_jv_j(\mathbf{r}), \tag{3.115}$$

where we define the differential operator

$$\hat{\mathfrak{L}} = -\frac{\hbar^2\nabla^2}{2m} + U(\mathbf{r}) - \mu + 2g_0\left[n_c(\mathbf{r}) + \tilde{n}(\mathbf{r})\right]. \tag{3.116}$$

The solution of the Bogoliubov-de Gennes equations, for a given external potential $U(\mathrm{r})$, gives the full set of functions $\{u_j(\mathbf{r}), v_j(\mathbf{r})\}$. The total density is then given by [143]

$$n(\mathbf{r}) = n_\mathrm{c}(\mathbf{r}) + \tilde{n}(\mathbf{r}) + \tilde{m}(\mathbf{r}), \tag{3.117}$$

with the noncondensed density written as

$$\tilde{n}(\mathbf{r}) = \sum_j \left\{\left[|u_j(\mathbf{r})|^2 + |v_j(\mathbf{r})|^2\right]\langle\hat{a}_j^\dagger\hat{a}_j\rangle + |v_j(\mathbf{r})|^2\right\}, \tag{3.118}$$

and where the anomalous density reads

$$\tilde{m}(\mathbf{r}) = -\sum_j u_j(\mathbf{r}) v_j^*(\mathbf{r}) \big(2\,\langle \hat{a}_j^\dagger \hat{a}_j \rangle + 1\big), \tag{3.119}$$

in which

$$\langle \hat{a}_j^\dagger \hat{a}_j \rangle = \frac{1}{e^{\beta E_j} - 1} \tag{3.120}$$

is the Bose-Einstein distribution.

We now describe how to calculate the critical temperature of an ellipsoidal bubble-trapped condensate relying on the previous formalism. Within the standard Popov approximation, we neglect the anomalous density $\tilde{m}(\mathbf{r})$ in the previous relations, and we solve the Bogoliubov-de Gennes equations by considering the semiclassical approximation $\nabla = i\mathbf{k}$, where $\mathbf{k}$ is a continuous wave vector for which $\sum_j \to \int \mathrm{d}\mathbf{k}/(2\pi)^3$ [145]. In this case, the energies E_j reduce to the simple Hartree-Fock spectrum

$$E_{\mathrm{HF}}(k, \mathbf{r}) = \frac{\hbar^2 k^2}{2m} + U(\mathbf{r}) - \mu + 2g_0\,[n_c(\mathbf{r}) + \tilde{n}(\mathbf{r})], \tag{3.121}$$

and the functions $u_j(\mathbf{r})$, $v_j(\mathbf{r})$ are given by $u_{\mathbf{k}}^2(\mathbf{r}) = 1$, and $v_{\mathbf{k}}^2(\mathbf{r}) = 0$ [144]. At the critical temperature of Bose-Einstein condensation, i. e. T_{BEC}, the condensate density $n_c(\mathbf{r})$ is zero and the thermal density $\tilde{n}(\mathbf{r})$ coincides with the total density $n(\mathbf{r})$. In this specific case, the density reads

$$n(\mathbf{r}) = \int \frac{\mathrm{d}\mathbf{k}}{(2\pi)^3}\, \frac{1}{e^{E_{\mathrm{HF}}(k,\mathbf{r})/(k_{\mathrm{B}} T_{\mathrm{BEC}})} - 1}, \tag{3.122}$$

where $E_{\mathrm{HF}}(k, \mathbf{r})$ is evaluated at $n_c(\mathbf{r}) = 0$.

In Fig. 3.7, top panel, we plot the critical temperature of bubble-trapped ellipsoidal condensates as a function of the total number of particles, which is fixed by the chemical potential. For this plot, we consider the external potential of Eq. (3.1) where $\omega_x/(2\pi) = 30\,\mathrm{Hz}$, $\omega_y/(2\pi) = \omega_y/(2\pi) = 100\,\mathrm{Hz}$, and $\Omega_{\mathrm{r}}/(2\pi) = 5\,\mathrm{kHz}$. We emphasize that, in order to consider valid the results of the semiclassical approximation, it is necessary to analyze temperature regimes where the thermal energy $k_{\mathrm{B}}T$ is larger than the typical spacing between the quantum levels. As the bottom panel of Fig. 3.7 shows, the critical temperature decreases during the adiabatic expansion of a harmonic trap into a shell-shaped condensate. Since the gas cools down in this process, an initial condensate does not necessarily become a thermal cloud. Nonetheless, the typical temperatures that is necessary to reach in these systems to observe Bose-Einstein condensation are quite low [51, 60]. As a

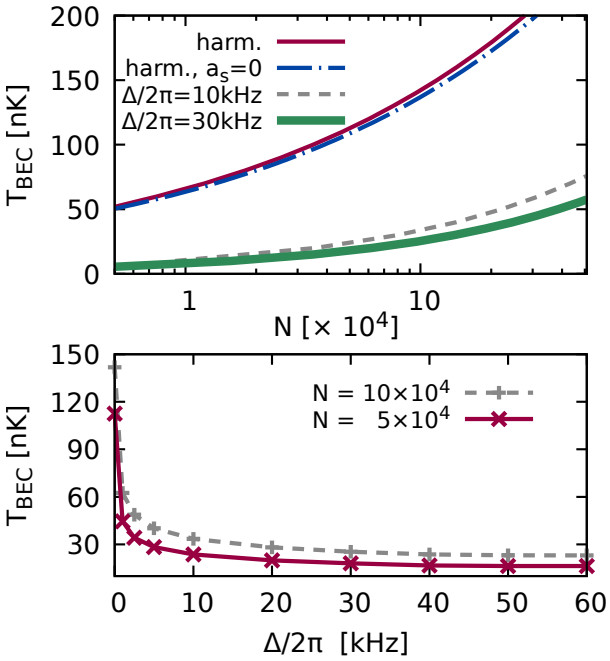

Figure 3.7: Critical temperature of Bose-Einstein condensation in ellipsoidal bubble-trapped condensates. Top: critical temperature as a function of the atom number N, obtained solving Eq. (3.122) self-consistently. For the same number of atoms, the critical temperature is much smaller for bubble-trapped condensates than for harmonically-trapped ones. Bottom: as the detuning Δ is increased, the harmonic trap (corresponding to $\Delta = 0$) becomes a hollow bubble-trapped condensate, and the critical temperature drops quickly. From Ref. [56].

consequence, the theoretical investigation of the finite-temperature properties is particularly relevant for the experiments.

At zero temperature, within the degree of approximation adopted here, all the particles occupy the condensate state. In this case, the condensate density $n_c(\mathbf{r}) = |\Phi(\mathbf{r})|^2$ can be calculated by solving numerically the Gross-Pitaevskii equation [81, 82]

$$\mu\Phi(\mathbf{r}) = \left[-\frac{\hbar^2\nabla^2}{2m} + U(\mathbf{r}) + g_0|\Phi(\mathbf{r})|^2 \right]\Phi(\mathbf{r}), \tag{3.123}$$

where the chemical potential μ determines the total number of particles in the system. In the top panel of Fig. 3.8 we plot the condensate density in the xz plane of a system of $N = 57100$ atoms confined in a trap with the same parameters of Fig. 3.7 and with $\Delta/(2\pi) = 30\,\mathrm{kHz}$. A relevant difference with respect to the spherical case is that the condensate density is not uniform along the shell, but the atoms tend to concentrate on the lobes. This distribution is the consequence of a nonuniform local harmonic trapping, since the external potential can be locally approximated as a harmonic trap with an effective trapping frequency that varies across the shell. Thus, in the lobes of the ellipsoid at $x \sim \pm 100\,\mu\mathrm{m}$, the effective frequency is lower than in the region near $x \sim 0$, and the trap accommodates less atoms in the latter region.

In the bottom panel of Fig. 3.8 we compare the density along the main ellipsoidal axes at zero and at the critical temperature. While the zero-temperature condensate is not uniform, the thermal cloud has a constant density across the whole shell. In the first experiments with Bose-Einstein condensates, which were held in harmonic traps, this different density distribution of the thermal and of the condensate components was also observed, and it was actually considered a proof of the phenomenon of condensation. From the opposite perspective, the uniformity of the density distribution can be used experimentally to estimate the temperature of the shell-shaped condensate.

3.5.2 Free expansion

The total energy a gas of ultracold bosonic atoms can be thought as the sum of three contributions: kinetic, potential, and interaction ones. In single-component quantum gases, usually, the density distribution corresponds to the optimal configuration in which the attractive potential energy is balanced by the repulsive kinetic and interaction contributions. In the absence of any confinement, thus, the system expands freely in space due to the diffusion and to the repulsive interactions between bosons.

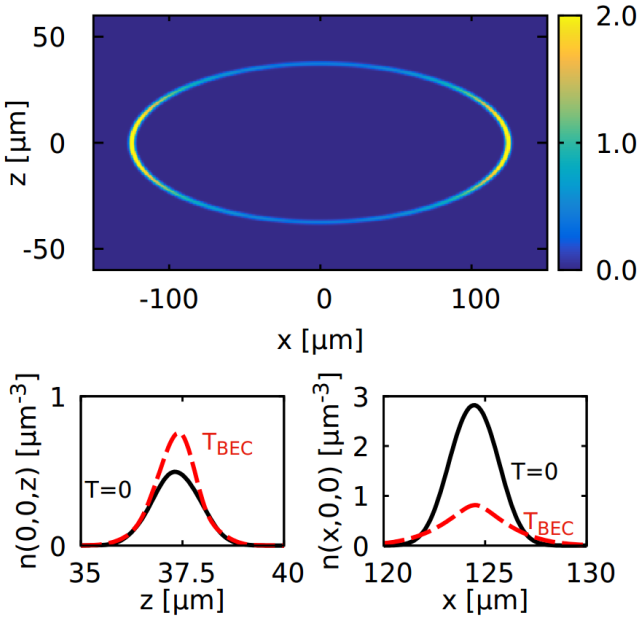

Figure 3.8: Density distribution of a shell-shaped condensate. Top: atomic density at zero temperature, where the colorbox unit is μm^{-3}. Bottom: cuts of the condensate density at $T = 0$, in comparison with the thermal density at T_{BEC}. From Ref. [56].

Connected to these concepts, let us briefly analyze one of the most common destructive experimental techniques: absorption imaging. The basic idea of the technique is to suddenly turn off the external potential and, after some time of free expansion, to flash the gas with a resonant laser light. The projection of the atomic cloud is then recorded on a CCD camera, which yields a larger signal for the low-density regions and a lower signal for denser ones. Thus, a precise quantitative understanding of how a trapped quantum gas expands is fundamental for the comparison with the experiments.

In this section, we analyze theoretically how a bubble-trapped gas freely expands and self-interferes after the sudden turning off of the trapping potential. For this scope, we solve numerically the time-dependent version of the Gross-Pitaevskii equation of Eq. (3.123), namely

$$i\hbar\frac{\partial\Phi(\mathbf{r},t)}{\partial t} = \left[-\frac{\hbar^2\nabla^2}{2m} + U(\mathbf{r}) + g_0|\Phi(\mathbf{r},t)|^2\right]\Phi(\mathbf{r},t), \tag{3.124}$$

which models the dynamics of the macroscopic wave function. Strictly speaking, since bubble-traps confine the atoms in a dressed state that results from the superposition of different hyperfine states $|F, m_F\rangle$, it would be necessary to solve

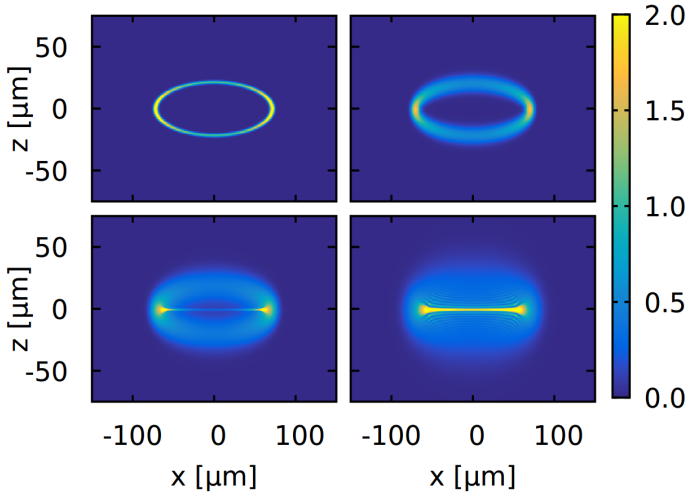

Figure 3.9: Contour plot of the condensate density distribution $n_0(x, 0, z, t)$, cut along the xz plane, of an ellipsoidal shell-shaped condensate. We plot the expansion at increasing times: $\{0, 4.5, 9, 18\}$ ms. The colorbox is in units of μm^{-3}. From Ref. [56].

$2m_F + 1$ coupled Gross-Pitaevskii equations. However, the experiments with shell-shaped condensates are carried on with ^{87}Rb atoms, in which the scattering lengths between the atoms in the different hyperfine states are almost equal, i. e. $\sim 100\, a_0$, with a_0 the Bohr radius. Thus, it is a good approximation to solve a single Gross-Pitaevskii equation.

The theoretical modeling of the free expansion follows these steps: first, we solve the Gross-Pitaevskii equation of Eq. (3.123) in imaginary time, which leads to the ground-state solution for the potential $U(\mathbf{r})$, which we have discussed in the previous section. Then, by using this ground state distribution as the initial condition, we solve numerically Eq. (3.124) in which, during the dynamics, we set $U(\mathbf{r}) = 0$. In Fig. 3.9 we show how the condensate density $n_0(\mathbf{r}, t) = |\Phi(\mathbf{r}, t)|^2$ evolves during the free expansion. From left to right and from top to bottom, the simulation times, measured in ms, are given by: 0, 4.5, 9, 18. Due to the hollow shape of the condensate, the cloud expands both inwards and outwards, self-interfering at the center of the trap. We also emphasize that the direct comparison of these simulations with the experiments would actually require the integration of the condensate density $n_0(x, y, z, t)$ along the direction of the imaging axis y.

4

Hydrodynamic excitations of atomic superfluids

Hydrodynamic excitations, i. e. long-wavelength excitations of a quantum liquid at zero and at finite temperature, constitute one of the main probes of superfluid hydrodynamics in atomic condensates. In these systems, modeled as a mixture of a normal part and of a superfluid part, two branches of hydrodynamic excitations can coexist. In flat superfluids, these excitations propagate as sound waves, with a linear relation between the wave vector and the frequency. In spherically-symmetric superfluids, the hydrodynamic excitations are complex surface modes that can be decomposed in the basis of the spherical harmonics. We will analyze these setups in detail in the next sections.

4.1 Sound propagation in 2D Fermi gases

In this section, we analyze sound propagation in systems of uniform two-dimensional fermions. In particular we calculate the velocities of first and second sound by implementing the Landau two-fluid model, which is a general phenomenological description of a quantum fluid, independent of the underlying quantum statistics. In particular, following Ref. [146], we will derive the thermodynamics of two-dimensional uniform fermions across the BCS-BEC crossover and, calculating also the superfluid density, we will obtain the sound speeds and compare them with a recent experiment [77].

4.1.1 Thermodynamics along the 2D BCS-BEC crossover

To obtain the thermodynamics of the system, we need to calculate first the grand canonical partition function $\mathcal{Z}$. Our starting point is Eq. (2.48), in which $\mathcal{Z}$ is expressed as a functional integral over two fields: the fermionic Grassmann field $\psi_\sigma(\mathbf{r},\tau)$, and the bosonic pairing field $\Delta(\mathbf{r},\tau)$. At a mean-field level, the gap can be assumed to be uniform and constant, namely

$$\Delta(\mathbf{r},\tau) = \Delta_0, \tag{4.1}$$

and, substituting this expression into Eq. (2.48), we need to perform the functional integration over the fermionic field only. Explicitly, to diagonalize the fermionic inverse propagator, and to calculate the Gaussian integral, we first need to expand the fermionic field in the basis of plane waves, labelled by the two-dimensional wave vector $\mathbf{k} = (2\pi/L)(n_x, n_y)$, with $n_x, n_y \in \mathbb{Z}$. After doing so, we calculate the grand canonical partition function at the mean-field level $\mathcal{Z}_{\rm mf}$ (see Ref. [147] for additional details), which immediately yields the mean-field grand potential, given by

$$\Omega_{\rm mf} = -L^2\frac{\Delta_0^2}{g} - \sum_{\mathbf{k}}(E_k^{\rm sp} - \xi_k) - \frac{2}{\beta}\sum_{\mathbf{k}}\ln(1+e^{-\beta E_k^{\rm sp}}), \tag{4.2}$$

where we define the single particle excitation spectrum $E_k^{\rm sp}$ as

$$E_k^{\rm sp} = \sqrt{\xi_k^2 + \Delta_0^2}, \tag{4.3}$$

and where $\xi_k = \hbar^2k^2/(2m) - \mu$. Note that, to obtain the thermodynamic potential, we have also performed the sum over the fermionic Matsubara frequencies [147]. The mean-field grand potential can be calculated analytically in the regime of zero temperature, in which the third term at the right-hand side of Eq. (4.2) is zero. In particular, we regularize the divergent sum through the equation [117]

$$-\frac{1}{g} = \frac{1}{2L^2}\sum_{\mathbf{k}}\frac{1}{\hbar^2k^2/(2m) + \epsilon_{\rm B}/2}, \tag{4.4}$$

where $\epsilon_{\rm B}$ is the binding energy, and, performing the sum as an integral, we obtain

$$\frac{\Omega_{\rm mf}(T=0)}{L^2} = -\frac{m}{4\pi\hbar^2}\left[\frac{\Delta_0^2}{2} + \mu^2 + \mu\sqrt{\mu^2+\Delta_0^2} + \Delta_0^2\ln\left(\frac{\sqrt{\mu^2+\Delta_0^2}-\mu}{\epsilon_{\rm B}}\right)\right], \tag{4.5}$$

which is the mean-field zero-temperature grand potential per unit of area.

To implement a beyond-mean-field Gaussian description, we include higher order terms in the expansion of the pairing field around the uniform configuration, by writing

$$\Delta(\mathbf{r},\tau) = \Delta_0 + \eta(\mathbf{r},\tau), \tag{4.6}$$

where $\eta(\mathbf{r},\tau)$ represents the small fluctuation of the pairing gap with respect to its uniform configuration. Substituting this expansion into Eq. (2.48), we neglect the terms in the field η whose order is higher than quadratic, and again, we move to Fourier space and we integrate the fermionic field. While the lowest-order terms reproduce the previous results obtained with the simple mean-field approximation, the beyond-mean-field terms can be rearranged to write the partition function as

$$\mathcal{Z} = \mathcal{Z}_{\rm mf} \int \mathcal{D}[\bar{\eta},\eta]\, \mathrm{e}^{-\frac{S_{\rm g}(\bar{\eta},\eta)}{\hbar}}, \tag{4.7}$$

where the Gaussian action is written as

$$S_g(\eta,\bar{\eta}) = \frac{1}{2}\sum_{\Omega_n}\sum_{\mathbf{q}} \begin{bmatrix}\eta(\Omega_n,\mathbf{q}) & \bar{\eta}(-\Omega_n,-\mathbf{q})\end{bmatrix} \mathbf{M}(\Omega_n,\mathbf{q}) \begin{bmatrix}\eta(\Omega_n,\mathbf{q}) \\ \bar{\eta}(-\Omega_n,-\mathbf{q})\end{bmatrix}, \tag{4.8}$$

where $\mathbf{q}$ is the bosonic wave vector, and Ω_n are the bosonic Matsubara frequencies of the pairing fluctuation field. The elements of the matrix $\mathbf{M}(\Omega_n,\mathbf{q})$ have involved expressions that are reported in detail in Refs. [103, 148]. Here we simply show the final results for the grand potential at a beyond-mean-field level, which is given by

$$\Omega(\mu,T,L^2,\Delta_0) = \Omega_{\rm mf}(\mu,T,L^2,\Delta_0) + \Omega_{\rm g}(\mu,T,L^2,\Delta_0) \tag{4.9}$$

where $\Omega_{\rm mf}$ is defined in Eq. (4.2), while

$$\Omega_{\rm g} = \frac{1}{2\beta}\sum_{\Omega_n}\sum_{\mathbf{q}} \ln\det \mathbf{M}(\Omega_n,\mathbf{q}) \tag{4.10}$$

is the beyond-mean-field contribution to the grand potential. Clearly, the explicit evaluation of the last term requires the determination of the spectrum of the bosonic collective excitations,

$$E^{\rm col}_{\mathbf{q}} = \hbar\omega^{\rm col}_{\mathbf{q}}, \tag{4.11}$$

where the frequencies $\omega^{\rm col}_{\mathbf{q}}$ correspond to the poles of the inverse of the bosonic propagator, and are determined by the equation $\det \mathbf{M}(\omega,\mathbf{q}) = 0$ for the variable ω.

Since we are considering a uniform system, the grand potential of Eq. (4.9) is an extensive quantity and, thus, scales linearly with the area L^2. Therefore, neglecting any finite-size correction, the grand potential per unit of area reads

$$\frac{\Omega}{L^2} = \frac{\Omega_{\rm mf}(T=0)}{L^2} - \frac{2}{\beta}\int \frac{\mathrm{d}\mathbf{k}}{(2\pi)^2} \ln(1+e^{-\beta E^{\rm sp}_k}) + \frac{1}{2\beta}\sum_{\Omega_n}\int \frac{\mathrm{d}\mathbf{q}}{(2\pi)^2} \ln\det \mathbf{M}(\Omega_n,\mathbf{q}), \tag{4.12}$$

where we have substituted the summations over the wave vectors with integrals, and where the right-hand side is a function of intensive thermodynamics quantities only: μ, T, and Δ_0. But to compare the theoretical results with the experiments, μ and Δ_0 should be expressed as functions of controllable parameters as the number density n and the temperature T. This is achieved by solving simultaneously the number equation

$$n = -\frac{1}{L^2}\left(\frac{\partial\Omega}{\partial\mu}\right)_T, \tag{4.13}$$

and the gap equation

$$\left(\frac{\partial\Omega_{\rm mf}}{\partial\Delta_0}\right)_{\mu,T} = 0. \tag{4.14}$$

At zero temperature, the gap equation yields a simple analytical result:

$$\Delta_0 = \sqrt{\epsilon_{\rm B}^2 + 2\mu\epsilon_{\rm B}}, \tag{4.15}$$

which can be verified by deriving the mean-field grand potential $\Omega_{\rm mf}$ of Eq. (4.5). Concerning the number equation, the situation is more complicated. The results of this section rely on Ref. [149], where Eqs. (4.13) and (4.14) were solved at zero temperature and at a beyond-mean-field level, obtaining $\mu/\epsilon_{\rm F}$ and $\Delta_0/\epsilon_{\rm F}$ as a function of the crossover parameter $\ln(\epsilon_{\rm B}/\epsilon_{\rm F})$, where $\epsilon_{\rm F} = \hbar^2\pi n/m$ is the Fermi energy. Given these functions, the single-particle excitation spectrum $E_k^{\rm sp}$ can be immediately calculated as a function of $\ln(\epsilon_{\rm B}/\epsilon_{\rm F})$, and also the zero-temperature spectrum of the bosonic excitations $E_{\mathbf{q}}^{\rm col}$ was determined in Ref. [149]. This modeling provides, therefore, the knowledge of the beyond-mean-field grand potential at zero temperature as a function of the crossover parameter $\ln(\epsilon_{\rm B}/\epsilon_{\rm F})$. The extension at finite-temperature is not trivial, as it requires the evaluation and the regularization of multiple wave vector and Matsubara frequency summations for solving the gap and the number equations. Since the temperature dependence of μ and of Δ_0 is expected to be weak, we now develop a calculation which includes the finite-temperature effects only through the factor β. This simplified description works well and is justified in the cases in which the equation of state depends marginally on temperature.

We calculate the effective low-temperature free energy of the system, which includes both fermionic single-particle excitations and bosonic collective ones, as [150]

$$F = \mu N + \Omega_{\rm mf}(T=0) - \frac{2}{\beta}\sum_{\mathbf{k}}\ln(1+e^{-\beta E_k^{\rm sp}}) + \frac{1}{\beta}\sum_{\mathbf{q}}\ln(1-e^{-\beta E_{\mathbf{q}}^{\rm col}}), \tag{4.16}$$

where $\Omega_{\rm mf}(T=0)$ is given by Eq. (4.5). This formulation is particularly convenient since the ratio $F/\epsilon_{\rm F}$ depends only on the reduced temperature $T/T_{\rm F}$, where $T_{\rm F} =$

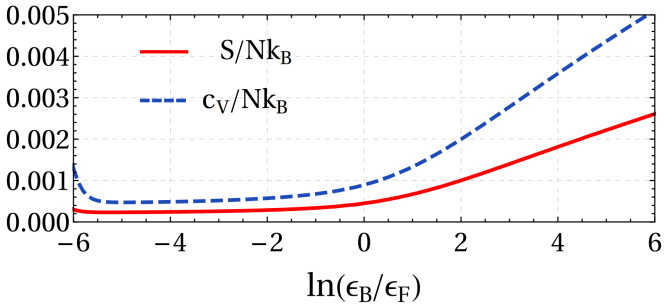

Figure 4.1: Dimensionless entropy, $S/(Nk_{\rm B})$, and dimensionless specific heat at constant volume, $c_V/(Nk_{\rm B})$, of a two-dimensional Fermi gas along the BCS-BEC crossover. From Ref. [146].

$\epsilon_{\rm F}/k_{\rm B}$ is the Fermi temperature [150]. Given F, we then evaluate numerically all the other thermodynamic functions. For instance, in Fig. 4.1, we plot the entropy and the specific heat calculated within our theory, which we rescale with $Nk_{\rm B}$, and which are shown as a function of the crossover parameter $\ln(\epsilon_{\rm B}/\epsilon_{\rm F})$. We also derive the pressure and the derivatives of the pressure with respect to density, both at constant temperature, and, at constant entropy, using the relation [151]

$$\left(\frac{\partial P}{\partial \rho}\right)_S = \left(\frac{\partial P}{\partial \rho}\right)_T + \frac{mNT}{\rho^2 c_V}\left[\left(\frac{\partial P}{\partial T}\right)_\rho\right]^2, \tag{4.17}$$

which completes the set of thermodynamic functions needed to calculate the velocities of the first and second sound.

4.1.2 Sound modes and comparison with the experiments

To calculate the sound modes, we need two different theoretical inputs: on the one hand the thermodynamic functions that we have obtained, as the entropy, the specific heat, and the derivatives of the pressure; on the other hand the superfluid density of the system. In a two-dimensional Fermi gas, the Berezinskii-Kosterlitz-Thouless transition drives the superfluid density to zero at the BKT temperature $T_{\rm BKT}$, over which the proliferation of vortices is energetically convenient. Thus, before discussing sound propagation, we briefly model this transition, adopting the same procedure developed in bubble-trapped condensates. Specifically, we calculate the renormalized superfluid density by solving the renormalization group equations, whose initial conditions are expressed in terms of the bare superfluid density

$$n_s^{(0)} = n - \beta \int \frac{{\rm d}\mathbf{k}}{(2\pi)^2}\frac{\hbar^2 k^2}{m}\frac{e^{\beta E_k^{\rm sp}}}{(e^{\beta E_k^{\rm sp}}+1)^2} - \frac{\beta}{2}\int \frac{{\rm d}\mathbf{q}}{(2\pi)^2}\frac{\hbar^2 q^2}{m}\frac{e^{\beta E_{\mathbf{q}}^{\rm col}}}{(e^{\beta E_{\mathbf{q}}^{\rm col}}-1)^2}, \tag{4.18}$$

which can be derived from the momentum current of the elementary excitations, following the classic Landau argument [12]. The Kosterlitz-Nelson renormalization group equations, written in terms of the adimensional parameters $K(\ell)$ and $y(\ell)$, read

$$\begin{aligned} \frac{\mathrm{d}K^{-1}(\ell)}{\mathrm{d}\ell} &= -4\pi^3 y(\ell)^2, \\ \frac{\mathrm{d}y(\ell)}{\mathrm{d}\ell} &= \left[2 - \pi K(\ell)\right] y(\ell), \end{aligned} \tag{4.19}$$

where, in the context of two-dimensional superfluid fermions, we define

$$K(\ell) = \frac{\hbar^2 n_s}{4mk_{\mathrm{B}}T}, \tag{4.20}$$

with n_s the renormalized superfluid density we aim to calculate, while $y(\ell)$ is the renormalized fugacity. As initial conditions of Eq. (4.19), we adopt here

$$K(\ell = 0) = \frac{\hbar^2 n_s^{(0)}}{4mk_{\mathrm{B}}T}, \qquad y(\ell = 0) = e^{-\beta\mu_{\mathrm{v}}}, \tag{4.21}$$

and, as the chemical potential of the vortices, we choose the value [152]

$$\mu_{\mathrm{v}} = \frac{\pi^2}{4}\frac{\hbar^2 n_s^{(0)}}{4mk_{\mathrm{B}}T}, \tag{4.22}$$

which is the best estimate for modeling correctly BKT physics in superconductors.

We are now ready to calculate and analyze the sound modes. First, we obtain the thermodynamics of the system, by finding numerically the necessary derivatives (with respect to temperature, volume, density) of Eq. (4.16), and then, we solve Eq. (4.19) to get the renormalized superfluid density. Given these quantities as a function of the crossover parameter $\ln(\epsilon_{\mathrm{B}}/\epsilon_{\mathrm{F}})$, we calculate the first and second sound velocities through their general expression of Eq. (2.74). Our results for the sound modes across the whole BCS-BEC crossover are shown in Fig. 4.2, and are obtained at the fixed temperature of $T/T_{\mathrm{F}} = 0.01$. The green diamonds represent the experimental measurements of Ref. [77], where a single sound wave was observed by exciting the Fermi gas with a density perturbation. In the following, we justify why these data points can be identified with the first sound, and we note, indeed, that as Fig. 4.2 shows, there is a good agreement between the experiment and our result for c_1.

A density perturbation $\delta\rho(\mathbf{r}, t)$, induced in the experiment via a phase shift in a fermionic Josephson junction [153], can excite both sound velocities, and can be expressed as [154]

$$\delta\rho(\mathbf{r}, t) = W_1\, \delta\rho_1(\mathbf{r} \pm c_1 t, t) + W_2\, \delta\rho_2(\mathbf{r} \pm c_2 t, t), \tag{4.23}$$

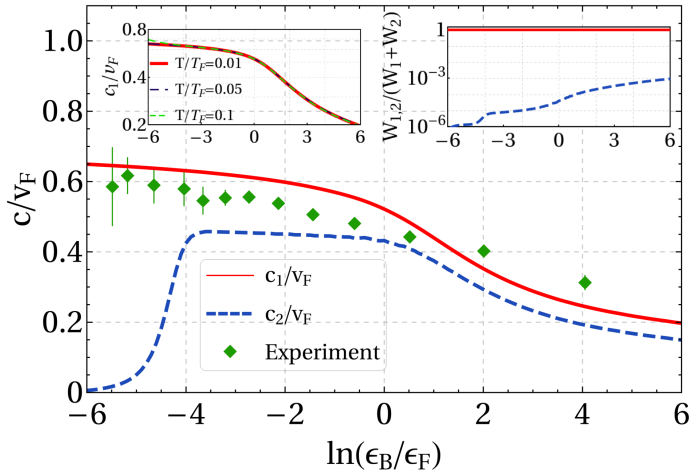

Figure 4.2: Velocities of the first sound c_1 and of the second sound c_2, rescaled with the Fermi velocity $v_{\rm F} = \sqrt{2\epsilon_{\rm F}/m}$, and plotted as a function of $\ln(\epsilon_B/\epsilon_F)$, which parametrizes the crossover from the BCS regime ($\ln(\epsilon_B/\epsilon_F) \ll 0$) to the BEC regime ($\ln(\epsilon_B/\epsilon_F) \gg 0$). In this plot, we fix the temperature at $T/T_{\rm F} = 0.01$ and, since the first sound has a very weak temperature dependence (see the left inset), we can compare our results with the first-sound measurements of Ref. [77], obtained at $T/T_{\rm F} \lesssim 0.1$. From Ref. [146].

where W_1 weights the density response of the first sound wavepacket, $\delta\rho_1(\mathbf{r} \pm c_1 t, t)$, and W_2 weights the response of the second one $\delta\rho_2(\mathbf{r} \pm c_2 t, t)$. These amplitudes are actually related to the velocities themselves, since [155, 156]

$$\frac{W_1}{W_1+W_2} = \frac{(c_1^2 - v_L^2)\, c_2^2}{(c_1^2 - c_2^2)\, v_L^2}, \qquad \frac{W_2}{W_1+W_2} = \frac{(v_L^2 - c_2^2)\, u_1^2}{(c_1^2 - c_2^2)\, v_L^2} \tag{4.24}$$

are their relative weights. In the temperature and interaction regimes considered in Fig. 4.2, we find that $c_2 \approx v_L$ (see also Fig. 4.3), and that, therefore, the density perturbation adopted in Ref. [77] excites mainly the first sound. This consideration

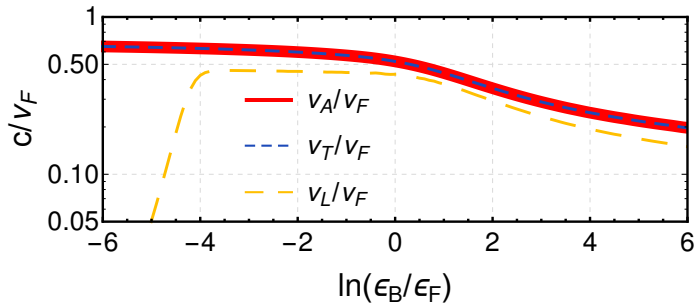

Figure 4.3: Adiabatic velocity v_A, isothermal one v_T, and Landau velocity v_L as a function of the crossover parameter at a fixed temperature of $T/T_{\rm F} = 0.01$. From Ref. [146].

finds a clear quantitative verification in the right panel of Fig. 4.2, where we plot the relative weights of the first and second sound. Conversely, we expect that a heat perturbation excites mainly the second sound [157], which is still unobserved in uniform 2D Fermi gases.

While the temperature influences weakly the behavior of the first sound, the second sound must show a discontinuity at the BKT transition temperature and across the whole BCS-BEC crossover. Indeed, we analyze the temperature behavior of the sound modes in detail in Fig. 4.4, which highlights the stronger temperature dependence of the second sound velocity with respect to the first one. In particular, we predict the jump of the second sound velocity to be an excellent probe of the superfluid BKT transition in uniform 2D Fermi gases. We also evaluate the weights $W_{1,2}$, and, in a similar way with respect to what happens at low temperatures, we find that $W_1 \gg W_2$, besides in the deep BEC regime and near T_{BKT}. As before, this observation confirms that a slight heating of the superfluid will mainly excite the second sound.

4.2 Sound propagation in 2D Bose gases

Let us analyze the propagation of sound waves in uniform two-dimensional Bose gases, by following and contextualizing the results obtained in Ref. [158]. As in the previous section, we need on the one hand to derive the thermodynamics of the system, on the other hand to describe the superfluid BKT transition. This analysis will be carried on in the next subsections.

4.2.1 Thermodynamics of box-trapped 2D bosons

To analyze the thermodynamics of the system, we implement a beyond-mean-field Gaussian calculation of the grand canonical partition function, see Eq. (2.35). We suppose, in particular, that the bosons are confined in a square box of size L, and interact with the contact interaction $V(\mathbf{r}-\mathbf{r}') = g_0\,\delta^{(2)}(\mathbf{r}-\mathbf{r}')$.

We shift the bosonic field as $\psi(\mathbf{r},\tau) = \psi_0 + \eta(\mathbf{r},\tau)$, where ψ_0 is the uniform mean-field configuration of Bose gas, and $\eta(\mathbf{r},\tau)$ is the complex fluctuation field around ψ_0. Substituting this decomposition into the Lagrangian of Eq. (2.37), and neglecting the terms of third and fourth order in η, the partition function can be calculated as a Gaussian functional integral in the fluctuation field η. Since we are describing a box-trapped gas, confined by repulsive walls into a square of side L, we impose reflecting boundary conditions on $\eta(\mathbf{r},\tau)$, expanding it in a series of

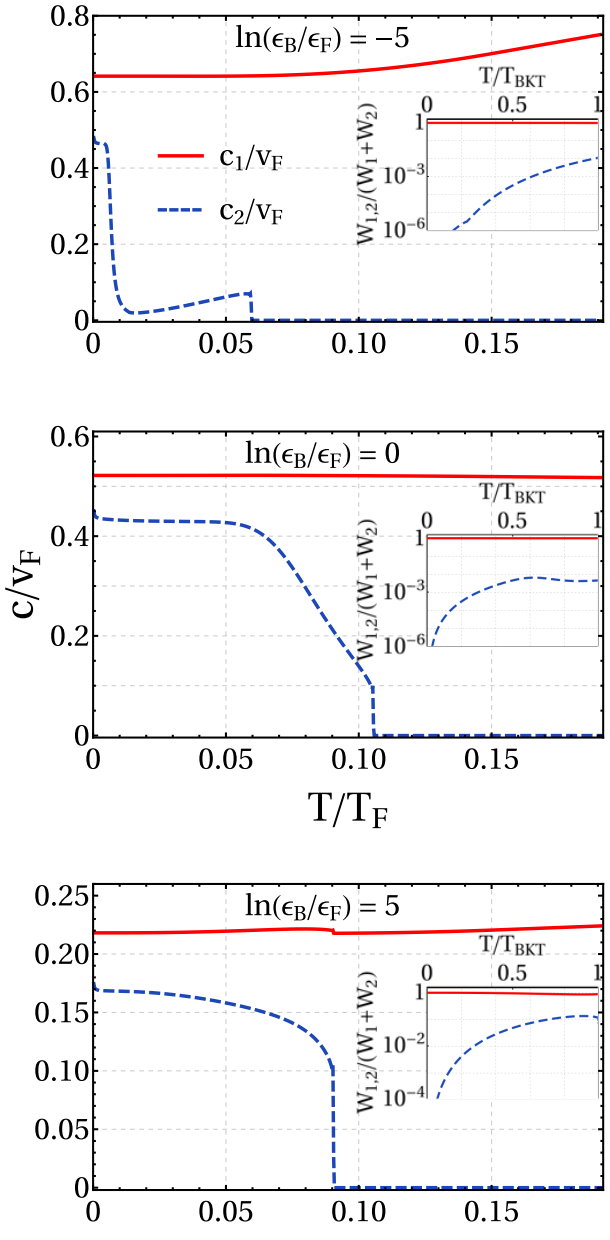

Figure 4.4: First and second sound velocities shown, for fixed values of the crossover parameter, as a function of the adimensional temperature T/T_{F}. From Ref. [146].

cosines as

$$\eta(\mathbf{r},\tau) = \frac{2}{L}\sum_{\omega_n}\sum_{k_{x,y}>0} e^{-i\omega_n\tau}\,\cos(k_x x)\cos(k_y y)\,\eta(\mathbf{k},\omega_n), \tag{4.25}$$

and similarly for its complex conjugate $\bar{\eta}(\mathbf{r},\tau)$. Due to the boundary conditions, the two-dimensional wave vector can assume only the discrete values $\mathbf{k} = (k_x, k_y) = (\pi/L)(n_x, n_y)$, with $n_{x,y}$ positive integers. Also note that the basis of cosines is orthonormal, so that

$$\delta_{n_x n_x'} = \frac{2}{L}\int_0^L \mathrm{d}x\,\cos\left(\frac{n_x\pi x}{L}\right)\cos\left(\frac{n_x'\pi x}{L}\right), \tag{4.26}$$

and similarly for $\delta_{n_y n_y'}$. Expanding the fluctuation field as in Eq. (4.25), the action of Eq. (2.36) can be written, at a Gaussian level, as

$$S = S_0 + \frac{\beta\hbar}{2}\sum_{\omega_n}\sum_{k_{x,y}>0}\begin{bmatrix}\bar{\eta}(\mathbf{k},\omega_n) & \eta(\mathbf{k},-\omega_n)\end{bmatrix}\mathbf{M}\begin{bmatrix}\eta(\mathbf{k},\omega_n)\\ \bar{\eta}(\mathbf{k},-\omega_n)\end{bmatrix} \tag{4.27}$$

where the mean-field action reads $S_0 = \beta\hbar L^D(-\mu\psi_0^2 + g\psi_0^4/2)$, and where the matrix elements of $\mathbf{M}$ are given by

$$\begin{aligned}\mathbf{M}_{jj} &= (-1)^j\, i\hbar\omega_n + \epsilon_k - \mu + 2g_0\psi_0^2,\\ \mathbf{M}_{12} &= \mathbf{M}_{21} = g_0\psi_0^2,\end{aligned} \tag{4.28}$$

with $\epsilon_k = \hbar^2k^2/(2m)$. Performing the Gaussian functional integral and calculating the sum over the Matsubara frequencies [98], we obtain, in analogy to previous calculations done in this thesis, the grand canonical partition function and the grand potential Ω. In particular, we get

$$\begin{aligned}\Omega(\mu,\psi_0^2) = L^2\big(-\mu\psi_0^2 + g_0\psi_0^4/2\big) &+ \frac{1}{2}\sum_{k_{x,y}>0}\left[E_k(\mu,\psi_0^2) - \epsilon_k - \mu\right]\\ &+ \frac{1}{\beta}\sum_{k_{x,y}>0}\ln\left[1 - e^{-\beta E_k(\mu,\psi_0^2)}\right],\end{aligned} \tag{4.29}$$

where the counterterm $-\epsilon_k - \mu$ in the zero point energy appears with the convergence factor regularization [117], and where we define the quasiparticle energies as

$$E_k(\mu,\psi_0^2) = \sqrt{(\epsilon_k - \mu + 2g_0\psi_0^2)^2 - (g_0\psi_0^2)^2}. \tag{4.30}$$

As in section 3.1.1, we impose the saddle-point condition, i. e. $\partial\Omega/\partial\psi_0 = 0$, which determines the condensate density $\psi_0^2 = n_0(\mu)$, and substituting it into the grand potential, we write

$$\Omega[\mu, n_0(\mu)] = -L^2\,\frac{\mu^2}{2g_0} + \frac{1}{2}\sum_{k_{x,y}>0}(E_k^{\mathrm{B}} - \epsilon_k - \mu) + \frac{1}{\beta}\sum_{k_{x,y}>0}\ln(1 - e^{-\beta E_k^{\mathrm{B}}}), \tag{4.31}$$

where we obtain perturbatively the Bogoliubov-Popov excitation spectrum

$$E_k^{\mathrm{B}} = \sqrt{\epsilon_k(\epsilon_k + 2\mu)}, \tag{4.32}$$

and where the Gaussian corrections in $n_0(\mu)$ are treated as perturbations with respect to the mean-field term.

The zero-point energy in the grand potential of Eq. (4.31) is ultraviolet divergent, and needs to be regularized. We follow the same procedure implemented in section 3.1.3, by including a momentum cutoff Λ in the second sum of Eq. (4.31), which we calculate as an integral over wave vectors. Then, we express the contact interaction strength as a function of Λ and of the two-dimensional s-wave scattering length $a_{2\mathrm{D}}$ as [125]

$$g_0 = -\frac{2\pi\hbar^2}{m}\frac{1}{\ln\left(a_{2\mathrm{D}}\,\Lambda\,e^{\gamma}/2\right)}, \tag{4.33}$$

whose logarithmic divergence in Λ balances the opposite and equal contribution in the zero-point energy. As a final result, we obtain

$$\frac{\Omega}{L^2} = -\frac{m\mu^2}{8\pi\hbar^2}\ln\left[\frac{\hbar^2}{m\mu\,a_{2\mathrm{D}}^2 e^{2\gamma+1}}\right] + \frac{1}{\beta}\int\frac{\mathrm{d}\mathbf{k}}{(2\pi)^2}\,\ln(1-e^{-\beta E_k^{\mathrm{B}}}), \tag{4.34}$$

where we have neglected the finite-size corrections which appear due to the lower bound of the integrals over the wave vectors. These finite-size effects in Ω are actually important for small condensates in weakly-interacting regimes, but are not quantitatively relevant for the following analysis.

We emphasize that the grand potential obtained in Eq. (4.34) is a function of μ, T, and L^2, and that the description of a system with a fixed number of particles is more convenient in terms of the Helmholtz free energy F. The latter quantity is obtained from Ω with a Legendre transformation, i. e. $F = \mu N + \Omega$, and requires the determination of the function $\mu = \mu(T, L^2, N)$. In Ref. [158], we have actually calculated $\mu(T, L^2, N)$ numerically to describe precisely the superfluid properties of the system, while the thermodynamics is obtained from an effective simplified calculation of the free energy F. Thus, to avoid implementing a heavy numerical calculation of the thermodynamics, and to obtain analytical results in the low-temperature regime, we have considered the following expression of the free energy

$$\frac{F}{L^2} = \frac{1}{2}\,g_0 n^2 - \frac{m\mu^2}{8\pi\hbar^2}\ln\left[\frac{\hbar^2}{m g_0 n\,a_{2\mathrm{D}}^2 e^{2\gamma+1}}\right] + \frac{1}{\beta}\int\frac{\mathrm{d}\mathbf{k}}{(2\pi)^2}\,\ln(1-e^{-\beta E_k}), \tag{4.35}$$

where $E_k = \sqrt{\epsilon_k(\epsilon_k + 2g_0 n)}$, and which can be obtained from the microscopic expression of the grand potential by setting $\mu = g_0 n$. For a fixed area L^2, for

a fixed number of particles in the system N, and of the scattering length a_{2D}, the free energy is a known function of the temperature. Given F, implementing basic thermodynamic relations, see for instance the end of section 2.1, one can calculate numerically the wave vector integrals and obtain all the inputs for the determination of the sound velocities of Eq. (2.74).

4.2.2 Sound modes and comparison with the experiments

In parallel with the analysis implemented in the fermionic case, we briefly describe our calculation of the renormalized superfluid density of a box-trapped bosonic gas, and we then obtain the sound velocities.

Implementing in two dimensions a standard result of Landau [12], we calculate the bare superfluid density as

$$n_s^{(0)} = n - \beta \int \frac{\mathrm{d}\mathbf{k}}{(2\pi)^2} \frac{\hbar^2 k^2}{2m} \frac{e^{\beta E_k^{\mathrm{B}}}}{(e^{\beta E_k^{\mathrm{B}}} - 1)^2}, \tag{4.36}$$

where the Bogoliubov spectrum is given by Eq. (4.32). We then solve the Kosterlitz-Nelson renormalization group equations, which are formally the same of those at Eq. (4.19), in the interval $[0, \ell_{\max}]$ of the renormalization group scale ℓ. As the initial conditions at the scale $\ell = 0$, we consider the bare parameters $K_0 = K(\ell = 0) = \hbar^2 n_s^{(0)}/(m k_{\mathrm{B}} T)$, and $y_0 = y(\ell = 0) = \exp(-\beta \mu_{\mathrm{v}})$, with the chemical potential of the vortices given by $\beta \mu_{\mathrm{v}} = (\pi^2/2) K_0$ [100]. The cutoff $\ell_{\max}$, at which we interrupt the flow of the renormalization group equations, is given by $\ell_{\max} = \ln(L^2/\xi^2)$, with $\xi = \sqrt{\hbar^2/(m g_0 n)}$ the healing length of the superfluid. The renormalized superfluid density n_s is then calculated as $n_s = (m k_{\mathrm{B}} T/\hbar^2) K(\ell_{\max})$, since $K(\ell) = \hbar^2 n_s(\ell)/(m k_{\mathrm{B}} T)$.

In Fig. 4.5, we compare our results for the superfluid fraction n_s/n with the experimental data of Refs. [76, 159]. Our theory, which is crucially based on the calculation of the Bogoliubov-Popov excitation spectrum of Eq. (4.32), agrees with all the experimental data points. This suggests that, concerning at least the determination of the superfluid properties, the Bogoliubov-Popov scheme provides a reliable description of the superfluid density up to the critical temperature of the BKT transition. Note that, to implement the calculation of the bare superfluid density, we have determined the equation of state $\mu(T, L^2, N)$ numerically by deriving the grand potential of Eq. (4.34). In particular, we model the two-dimensional scattering length as $a_{2D} = 2.092\, l_\perp \ln[-\sqrt{\pi/2}\,(l_\perp/a_{3D})]$ [160], with a_{3D} the three-dimensional s-wave scattering length, and $l_\perp = \sqrt{\hbar/(m\omega_\perp)}$ the characteristic length of the transverse harmonic confinement of frequency $\omega_\perp$.

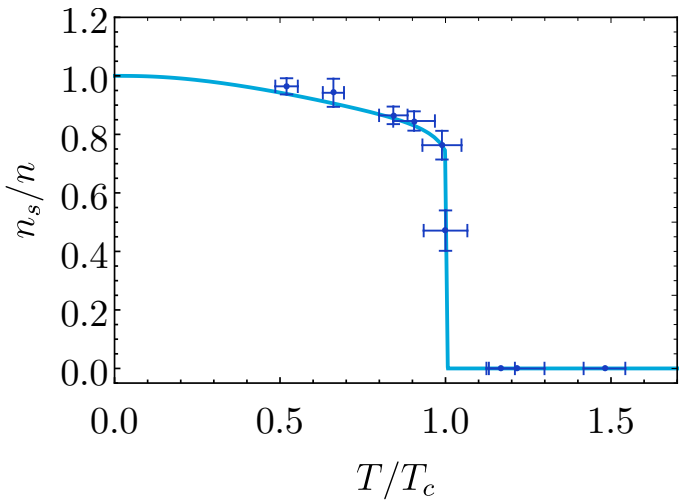

Figure 4.5: Superfluid density of a box-trapped two-dimensional Bose gas, obtained by solving the renormalization group Eqs. (4.19). For their solution, we use in input the bare superfluid density of Eq. (4.36), and consider the following parameters of the experiment in Ref. [76]: density $n = 3\,\mu\text{m}^{-2}$, area $L^2 \approx 33 \times 22\,\mu\text{m}^2$, scattering length $a_{3\text{D}} = 522 a_0$, with a_0 the Bohr radius, frequency of the transverse confinement $\omega_\perp = 2\pi \times 5500\,\text{Hz}$. Here T_c denotes the Berezinskii-Kosterlitz-Thouless critical temperature.

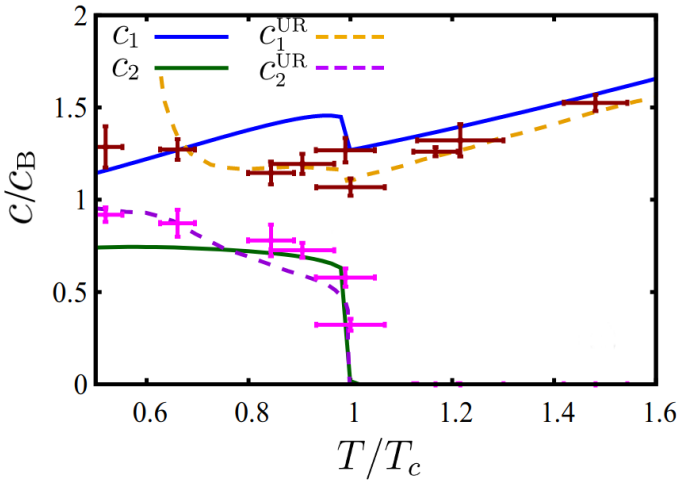

Figure 4.6: Sound velocities of box-trapped uniform bosons across the Berezinskii-Kosterlitz-Thouless transition. Our results, plotted as continuous lines, show a good agreement between our theory and the experimental data. The dashed lines represent the sound velocities obtained from the scale-invariant theory of Ref. [161], which works around the superfluid transition. From Ref. [158].

Let us compare our predictions for the sound velocities, obtained from the solutions of Eq. (2.74) of the Landau biquadratic equation, with the experimental results of Ref. [76]. As can be seen from Fig. 4.6, there is a good qualitative agreement between our theory and the experimental results. To assess the origin of the quantitative differences, we first remark that our theoretical scheme yields a solid estimate of the superfluid fraction, which is obtained in Ref. [159] from the measurements of the sound velocities and from the thermodynamics based on the theory of Ref. [161]. This agreement suggests that, within the experimental error, the superfluid density is not strongly sensitive to the specific finite-temperature behavior of the equation of state. Thus, we can mainly attribute the quantitative discrepancies to a simplified dependence on the temperature, density, and interactions of our thermodynamic functions. In the transition region, indeed, the sound modes are very sensitive to the values of the grand potential and of its derivatives, and their precise determination, beyond the effective calculation based on Eq. (4.35), can lead to a better quantitative agreement.

4.3 Hydrodynamic excitations in 2D superfluid shells

We briefly discuss, in this section, how the two-fluid model can be extended to describe a two-dimensional shell-shaped spherical superfluid. Actually, most of the equations of section 2.4 can be rederived in a straightforward manner, and their analysis will elucidate how the hydrodynamic modes propagate in a spherically symmetric superfluid. The linearized Eqs. (2.55)-(2.58) of a flat two-fluid system can be written in the spherical case as

$$\frac{\partial \rho}{\partial t} + \nabla_R \cdot \mathbf{j} = 0, \tag{4.37}$$

$$\frac{\partial \rho \tilde{s}}{\partial t} + \rho \tilde{s}\, \nabla_R \cdot \mathbf{v}_n = 0, \tag{4.38}$$

$$\frac{\partial \mathbf{j}}{\partial t} + \nabla_R P = 0, \tag{4.39}$$

$$\frac{\partial \mathbf{v}_s}{\partial t} + \nabla_R \left(\frac{G_0}{M} \right) = 0, \tag{4.40}$$

where we define

$$\nabla_R = \frac{\mathbf{e}_\theta}{R}\, \partial_\theta + \frac{\mathbf{e}_\varphi}{R \sin\theta}\, \partial_\varphi \tag{4.41}$$

as the gradient in spherical coordinates for a system with a radius R fixed. With this expression of ∇_R, we are supposing that the vectorial quantities of the model

do not have a radial component, and thus, that the dynamics is constrained to occur only along the surface of the sphere.

Starting from Eqs. (4.37)-(4.40), we perform the same calculations that we have implemented in the flat case, see in particular Eqs. (2.59)-(2.64). In this context, we obtain the following "wave" equations

$$\frac{\partial^2 \rho}{\partial t^2} = -\frac{\hat{L}^2}{\hbar^2 R^2} P, \tag{4.42}$$

$$\frac{\partial^2 \tilde{s}}{\partial t^2} = -\tilde{s}^2 \frac{n_s}{n_n} \frac{\hat{L}^2}{\hbar^2 R^2} T, \tag{4.43}$$

where the Laplacian is simply substituted by the angular momentum operator in spherical coordinates, i. e. $\hat{L}^2$. As in section 2.4.1, it is possible to expand the thermodynamic functions around their equilibrium configuration and to express the density and entropy fluctuations in terms of temperature and pressure ones [see Eqs. (2.65), (2.66)]. However, in the spherical geometry, the standard sound waves are not the correct basis to analyze Eqs. (4.42) and (4.43), which are instead solved in the basis of spherical harmonics. Therefore, we expand the fluctuation fields as

$$P'(t,\theta,\varphi) = \int_{-\infty}^{+\infty} \mathrm{d}\omega \sum_{l=1}^{\infty} \sum_{m_l}^{l} e^{i\omega t}\, \mathcal{Y}_l^{m_l}(\theta,\varphi)\, P(\omega, l, m_l), \tag{4.44}$$

$$T'(t,\theta,\varphi) = \int_{-\infty}^{+\infty} \mathrm{d}\omega \sum_{l=1}^{\infty} \sum_{m_l}^{l} e^{i\omega t}\, \mathcal{Y}_l^{m_l}(\theta,\varphi)\, T(\omega, l, m_l), \tag{4.45}$$

where ω is the frequency of these hydrodynamic low-energy modes and l, m_l are their quantum numbers. With the same previous steps, we obtain

$$\omega^4 - \omega^2 \left[\left(\frac{\partial P}{\partial \rho} \right)_{\tilde{s}} + \frac{T \tilde{s}^2 \rho_s}{\tilde{c}_V \rho_n} \right] \left[\frac{l(l+1)}{R^2} \right] + \frac{\rho_s T \tilde{s}^2}{\rho_n \tilde{c}_V} \left(\frac{\partial P}{\partial \rho} \right)_T \left[\frac{l(l+1)}{R^2} \right]^2 = 0, \tag{4.46}$$

which is the Landau biquadratic equation extended to a spherical superfluid. As this equation shows, there is not a linear relation between the frequency of the wave and the quantum number l which labels the different excitations. Therefore, we cannot actually define and calculate a sound speed, but only the frequencies ω of the hydrodynamic excitations for a given quantum number l. We also stress that the flat-case velocity is obtained only in the limit of a very large radius R, in which $l(l+1)/R^2 \approx l^2/R^2$ and a sound velocity can be approximately defined as $c \approx R\omega/l$.

The previous considerations do not prevent to express, at least formally, the frequencies of the hydrodynamic modes in terms of the adiabatic, isothermal and

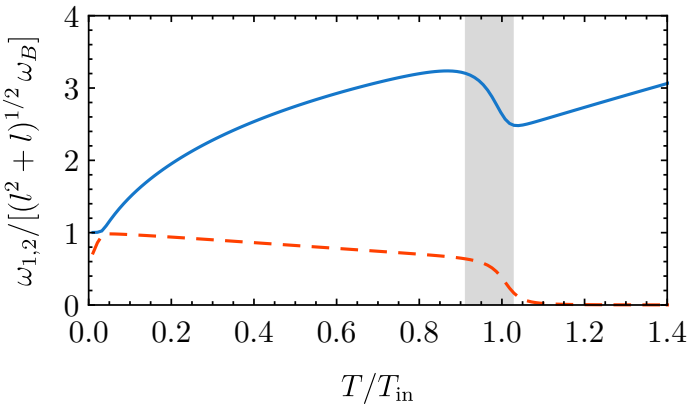

Figure 4.7: Frequencies of the hydrodynamic excitations rescaled with the Bogoliubov frequency $\omega_B = \sqrt{\mu/(mR^2)}$, and where l is the main quantum number of the angular momentum. The gray region, where the hydrodynamic modes are non monotonic, is where the BKT transition occurs. For this figure, we use the same parameters adopted to calculate the thermodynamic functions and the renormalized superfluid density in the previous chapter. From Ref. [55].

Landau velocities defined in Eq. (2.72). In this way, we write the solutions of Eq. (4.46) as

$$\omega_{1,2}^2 = \left[\frac{l(l+1)}{R^2}\right]\left[\frac{v_A^2+v_L^2}{2} \pm \sqrt{\left(\frac{v_A^2+v_L^2}{2}\right)^2 - v_L^2 v_T^2}\right], \tag{4.47}$$

which are the frequencies of the "first" and "second" hydrodynamic excitations of a spherical superfluid. We plot the hydrodynamic frequencies of a spherical bubble-trapped gas in Fig. 4.7, showing their behavior as a function of temperature at a fixed number of particles and for fixed interactions and trap parameters. To calculate $\omega_{1,2}$, we have adopted the thermodynamic description and BKT analysis for shell-shaped condensates developed in chapter 3. It is important to highlight that measuring $\omega_{1,2}$, and in particular their discontinuity as a function of temperature, would prove that the BKT transition occurs also in bubble-trapped superfluids. Indeed, considering that other curved and compact surfaces, as cylinders and large tori, could not display BKT physics [162], the experimental investigation of this phenomenon is of fundamental importance.

5

Static and dynamic properties of one-dimensional atomic gases

The high degree of tunability of ultracold atoms offers countless possibilities to probe and explore the properties of one-dimensional quantum systems. Remarkably, the low spatial dimensionality does not reduce the relevant physical phenomena to a subset of those occurring in three-dimensional systems, but it leads to the emergence of new physics. In this chapter, we will focus on two specific one-dimensional configurations: Bose-Bose mixtures in one dimension, and a couple of parallel tunneling quasicondensates made of bosonic atoms.

5.1 Bright solitons in 1D Bose-Bose mixtures

In this section, we analyze the static and dynamic properties of bright solitons in a one-dimensional mixture of bosonic atoms. Before discussing our new results explicitly, which have been published in Ref. [163], we briefly review the main properties of Bose-Bose mixtures.

5.1.1 An overview of Bose-Bose mixtures

Ultracold quantum gases are typically studied by confining specific hyperfine states of ultracold atomic gases in optical or magnetic traps. In the absence of degeneracy, atoms in different hyperfine states are distinguishable, and cannot be considered as identical particles. An ensemble of atoms in different hyperfine states is usually called "quantum mixture". In these systems, as shown by D. S. Petrov a few years

ago [83, 84], the beyond-mean-field effects do not represent simply perturbative corrections to the mean-field picture, but play a fundamental role in the stabilization of the atomic cloud.

Let us consider, for instance, a mixture of bosonic atoms in two different hyperfine states, or species, and let us suppose that the atoms interact with intra-species contact interactions g_{11}, g_{22}, while the inter-species contact interaction is g_{12}. In the absence of inter-species interactions, i. e. for $g_{12} = 0$, the system is stable and uniform if $g_{11} > 0$, $g_{22} > 0$. These conditions ensure that, in this case, the bosonic species are individually stable against the collapse that occurs for attractive intra-species interactions. Then, in the presence of inter-species interactions, i. e. for $g_{12} \neq 0$, the mean-field theory imposes a more general condition to have a uniform system in which both species coexist, namely [164]

$$g_{12} < \sqrt{g_{11} g_{22}}, \tag{5.1}$$

since, in the opposite case of $g_{12} > \sqrt{g_{11} g_{22}}$, the system forms a phase-separated configuration. Actually, imposing also that the uniform system does not develop density fluctuations, one obtains a stricter condition [164]:

$$|g_{12}| < \sqrt{g_{11} g_{22}}, \tag{5.2}$$

which ensures that the mean-field configuration is dynamically stable. In the following, considering weakly-attractive intraspecies interactions, i. e. $g_{12} < 0$, we define the parameter

$$\delta g = g_{12} + \sqrt{g_{11} g_{22}}, \tag{5.3}$$

and note that, from a mean-field point of view, the system is stable if $\delta g > 0$, while it is unstable for $\delta g < 0$.

At a beyond-mean-field level, the stability condition becomes more complicated than the simple criterion $\delta g > 0$, and the many-body phases displayed by the system must be analyzed more carefully. Interestingly, while the mean-field picture is valid in any spatial dimension, the beyond-mean-field analysis yields different results in different dimensions.

In three-dimensional quantum mixtures, as shown in Ref. [83], the beyond-mean-field energy contributions are responsible for the stabilization of the "unstable" (from a mean-field point of view) regime in which $\delta g < 0$, with $|\delta g| \ll \sqrt{g_{11} g_{22}}$. In this case, even in the absence of a trapping potential, the collapse is therefore avoided by the Lee-Huang-Yang pressure term, which scales with a higher power of the density with respect to the mean-field term. Thus, a liquid droplet, whose name is due to the fact that the internal density is constant, forms spontaneously [165,166].

We now analyze low-dimensional quantum mixtures, by briefly discussing the different results pertaining the two- and the one-dimensional case. In two dimensions, the liquid phase of the system occurs whenever the interspecies interaction is weakly attractive and the intraspecies interactions are repulsive. Thus, while the observation of the liquid phase requires $\delta g < 0$ in three dimensions, which corresponds to an inter-species attraction higher than a critical value, in two-dimensions the system is liquid even for weak inter-species interactions [84]. Finally, the configuration which will be analyzed in detail in this section: one-dimensional quantum mixtures. In this case, for interaction regimes such that $0 < \delta g \ll \sqrt{g_{11}g_{22}}$, the beyond-mean-field energy contribution is attractive, and it is responsible for the self-trapping of the system into a droplet. Thus, in the absence of an external potential (besides the confinement in the transverse direction) the system forms self-bound states rather than expanding as a gas in the longitudinal direction.

5.1.2 Quantum bright solitons: static properties

To analyze the physics of bright solitons in one-dimensional ultracold mixtures, we limit ourselves to considering homonuclear mixtures in which the intra-species scattering lengths are coincident, namely, $g_{11} = g_{22} = g > 0$. In the uniform case, the energy of the system at a beyond-mean-field level is given by [84]

$$E_{1\mathrm{D}}(n_1, n_2) = \frac{g}{2}(n_1 - n_2)^2 + \frac{\delta g}{4}(n_1 + n_2)^2 - \frac{2\sqrt{m}}{3\pi\hbar} g^{3/2}(n_1 + n_2)^{3/2}, \tag{5.4}$$

where n_1 and n_2 are the uniform densities. In the spirit of the density functional theory, we substitute n_1 and n_2 with the local density of the bosonic species given, respectively, by the macroscopic fields $|\psi_1|^2$ and $|\psi_2|^2$. We thus construct an effective field-theory description of the Bose-Bose mixture at zero temperature, considering the Lagrangian density

$$\begin{aligned}\mathcal{L}_{1\mathrm{D}} = \sum_{j=1,2} \frac{i\hbar}{2}(\psi_j^* \partial_t \psi_j - \psi_j \partial_t \psi_j^*) - \Bigg\{ & E_{1D}(|\psi_1|^2, |\psi_2|^2) \\ & + \sum_{j=1,2} \left[\frac{\hbar^2}{2m} |\partial_x \psi_j|^2 - (-1)^j i\gamma \psi_j^* \partial_x \psi_j - \Gamma \psi_j^* \psi_{3-j} \right] \Bigg\},\end{aligned} \tag{5.5}$$

and the effective action of the system is simply given by

$$S = \int \mathrm{d}t \int \mathrm{d}x \, \mathcal{L}_{1\mathrm{D}}. \tag{5.6}$$

Note that we included in $\mathcal{L}_{1\mathrm{D}}$ a kinetic energy contribution of the mixture, and two additional energy terms which describe the tunneling with energy Γ among

the species and an artificial spin-orbit coupling with strength γ. These additional couplings can be engineered by dressing the bare hyperfine states with a couple of lasers with equal Rashba and Dresselhaus strengths [167, 168].

The functional minimization of the action of Eq. (5.6) leads to the Euler-Lagrange equations of $\mathcal{L}_{1D}$, which are the following coupled Gross-Pitaevskii equations

$$\begin{aligned} i\hbar\frac{\partial\psi_j}{\partial t} = \Bigg[& -\frac{\hbar^2}{2m}\partial_x^2 + \frac{\delta g}{2}(|\psi_1|^2+|\psi_2|^2) - (-1)^j g(|\psi_1|^2-|\psi_2|^2) \\ & - \frac{\sqrt{m}}{\pi\hbar}g^{3/2}(|\psi_1|^2+|\psi_2|^2)^{1/2} - (-1)^j i\gamma\partial_x\Bigg]\psi_j - \Gamma\psi_{3-j}, \end{aligned} \tag{5.7}$$

where $j = 1, 2$ labels the species. The general solution of these equations is not known analytically, and it is necessary to implement a numerical method for the solution of partial differential equations. Before entering into the discussion of the numerical solution, we consider the simplified problem discussed in Ref. [163], which can be solved analytically. We initially consider the case in which $\Gamma = 0$ and $\gamma = 0$ and we note that, in the absence of Rabi coupling between the species, the number of bosons N_1 and N_2 are separately conserved. Moreover, we set to zero the interaction strength $\delta g = 0$ and, having considered the homonuclear symmetric case in which $g_{11} = g_{22} = g$, it is meaningful to suppose that

$$\psi_1(x,t) = e^{-i\frac{\mu t}{\hbar}}\sqrt{N}\phi(x), \qquad \psi_2(x,t) = e^{-i\frac{\mu t}{\hbar}}\sqrt{N}\phi^*(x), \tag{5.8}$$

where N is the number of atoms in each species. We thus obtain a single Gross-Pitaevskii equation for ϕ, which reads

$$\mu\phi = \left(-\frac{\hbar^2}{2m}\partial_x^2 - \frac{\sqrt{2m}}{\pi\hbar}g^{3/2}N^{1/2}|\phi|\right)\phi, \tag{5.9}$$

where μ is the chemical potential that fixes the number of atoms in each species. Note that the assumption of having the same N for both species is meaningful due to $\delta g = 0$, and since we are now interested in finding the ground-state solution.

To solve Eq. (5.9), we note that it can be formally rewritten as

$$\ddot{\phi} = -\frac{\partial W}{\partial\phi}, \tag{5.10}$$

namely, as the Newton equation of a particle with "coordinate" ϕ and "time" x, moving in the external potential

$$W(\phi) = -\alpha\,\phi^2 + \beta\,\phi^3, \tag{5.11}$$

where we define the coefficients

$$\alpha = \frac{1}{2}\left(\frac{2m}{\hbar^2}\right)|\mu|, \qquad \beta = \frac{1}{3}\left(\frac{2m}{\hbar^2}\right)\frac{\sqrt{2m}}{\pi\hbar}g^{3/2}N^{1/2}\,. \tag{5.12}$$

The Newton equation has the constant of motion

$$K(\phi) = \frac{(\dot{\phi})^2}{2} + W(\phi), \tag{5.13}$$

which, imposing the vanishing boundary conditions $\phi(\infty) = 0$ and $\dot{\phi}(\infty) = 0$ is actually equal to the constant value $K(\phi) = 0$ at any "time" x of the dynamics. As a consequence, we get

$$\frac{\mathrm{d}\phi}{\mathrm{d}x} = \sqrt{-2W(\phi)}, \tag{5.14}$$

which can be integrated by separation of variables. Specifically, we search for a solution with $\dot{\phi}(0) = 0$, which fixes the value of the wave function in $x = 0$ to $\phi(0) = \alpha/\beta$ and, integrating the previous equation between 0 and x, we find that

$$\phi(x) = \frac{\alpha}{\beta}\,\mathrm{sech}^2\left(\sqrt{\frac{\alpha}{2}}\,x\right), \tag{5.15}$$

which is the analytical form of a fully-quantum bright soliton in a Bose-Bose mixture. Note that, imposing that the wave function is normalized to 1, one obtains the chemical potential of the solution, namely,

$$\mu = \left(\frac{2}{9\pi^4}\right)^{1/3}\frac{mg^2}{\hbar^2}N^{2/3}, \tag{5.16}$$

in terms of the interaction strength and of the total number of atoms. We also emphasize that our solution of Eq. (5.9), which contains a quadratic nonlinearity, is the classical Korteweg-de Vries soliton [169], proportional to sech^2. The analogous equation with a cubic nonlinearity, which would be obtained by considering mean-field terms only, gives a solution $\propto$ sech [170].

Moving to the discussion of the general case, the ground-state solution for nonzero spin-orbit and Rabi couplings is obtained evolving numerically the Eq. (5.7) in imaginary time. In particular, due to the nonzero Γ, only the total number of bosons $N = N_1 + N_2$ is fixed by a single chemical potential μ. Moreover, for the numerical solution we rescale the equation in terms of the characteristic length $l_\perp$ of the transverse harmonic confinement with frequency $\omega_\perp$ and energy $E_\perp = \hbar\omega_\perp$.

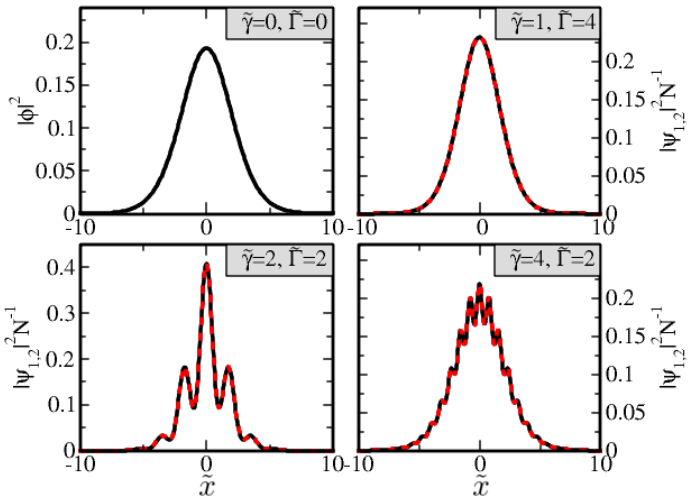

Figure 5.1: Ground-state solution of a 1D Bose-Bose mixture. In the absence of spin-orbit γ and Rabi Γ couplings (top-left plot), the analytical ground state is given by Eq. (5.15). In the other cases, the numerical solution of Eqs. (5.7), rescaled as Eq. (5.17), shows that the components coincide and have either a single-peak shape (top-right plot), or a striped solution (bottom plots). From Ref. [163].

Thus, we solve the following coupled equations for the fields $\tilde{\psi}_j/\sqrt{N}$:

$$\tilde{\mu}\frac{\tilde{\psi}_j}{\sqrt{N}} = \Bigg[-\partial_{\tilde{x}}^2 - (-1)^j(\tilde{g}N)\left(\frac{|\tilde{\psi}_1|^2}{N} - \frac{|\tilde{\psi}_2|^2}{N}\right) - \frac{\tilde{g}^{3/2}N^{1/2}}{\pi}\left(\frac{|\tilde{\psi}_1|^2}{N} + \frac{|\tilde{\psi}_2|^2}{N}\right)^{1/2} - (-1)^j i\tilde{\gamma}\partial_{\tilde{x}}\Bigg]\frac{\tilde{\psi}_j}{\sqrt{N}} - \tilde{\Gamma}\frac{\tilde{\psi}_{3-j}}{\sqrt{N}}, \tag{5.17}$$

where we define the rescaled quantities

$$\tilde{x} = \frac{x}{l_\perp}, \quad \tilde{\psi}_j = \psi_j\, l_\perp^{1/2}, \quad \tilde{\mu} = \frac{\mu}{E_\perp}, \quad \tilde{g} = \frac{g}{E_\perp l_\perp}, \quad \tilde{\Gamma} = \frac{\Gamma}{E_\perp}, \quad \tilde{\gamma} = \frac{\gamma}{E_\perp l_\perp}. \tag{5.18}$$

We show some representative solutions of these coupled equations in Fig. 5.1, where the red-dashed and the black lines represent the (everywhere coincident) density of the species. In these plots, we fix the parameter $\tilde{g}N^{1/3} = 1$ and we change the values of γ and Γ, finding both single-peak wave functions and multi-peak striped solitonic solutions.

Then, repeating our simulations for a fine mesh of the parameters γ and Γ, we plot in Fig. 5.2 a diagram showing the ground-state solutions of the system. This quantum phase transition, in which the ground state of the system develops a

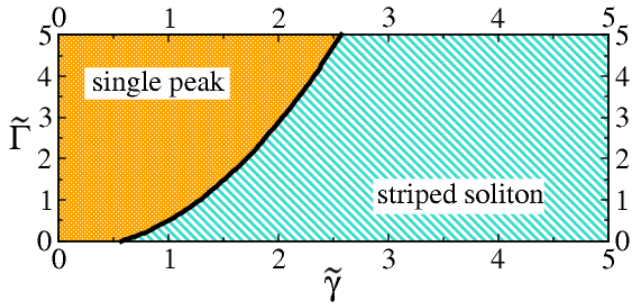

Figure 5.2: Phase diagram of the two possible ground-state solutions, illustrated in Fig. 5.1, of a Bose-Bose mixture with zero mean-field interaction, i. e. $\delta g = 0$. These solutions of Eq. (5.7) are analyzed for the fixed interaction strength $\tilde{g}N^{1/3} = 1$, and changing the spin-orbit and Rabi couplings. From Ref. [163].

density modulation, is driven only by the interplay of the spin-orbit coupling and of beyond-mean-field effects.

We finally emphasize that the Gross-Pitaevskii equations of the Bose-Bose mixture depend separately on N and on $\tilde{g}$, and it should not be possible to simply fix the parameter $\tilde{g}N^{1/3}$. However, since the densities of the two species are always coincident due to the mean-field term $\sim (n_1 - n_2)$, the only relevant dependence in Eq. (5.17) is the one of the beyond-mean-field term, scaling exactly as $(\tilde{g}N^{1/3})^{3/2}$.

5.1.3 Quantum bright solitons: dynamic properties

We now analyze the dynamics of bright solitons with spin-orbit coupling. Specifically, we want to calculate analytically and numerically the breathing-mode frequency $\omega_{\rm b}$ of the condensate, namely, the frequency of the lowest-energy mode that is excited by a small perturbation of the ground-state configuration. As for study of the static properties, we will focus our analysis on describing a fully-quantum soliton, i. e. $\delta g = 0$, for which the dynamics of the bosonic species with equal intra-species interactions is expected to be coincident. Moreover, the analytical calculation of ω_b can be done only in the case of $\gamma = 0$ and $\Gamma = 0$, which is the case that we will initially analyze.

To calculate the breathing-mode frequency, we implement a time-dependent Gaussian variational ansatz for the wave functions of the system. Thus, we consider the following variational expressions [171–173]

$$\psi_1(x,t) = \psi_2(x,t) = \frac{N^{1/2}}{\pi^{1/4}\sigma^{1/2}(t)} \exp\left[-\frac{x^2}{2\sigma^2(t)} + ib(t)x^2 \right], \tag{5.19}$$

where $\sigma(t)$ and $b(t)$ are time-dependent parameters whose dynamics is determined by a variational principle. Indeed, we substitute these equations in the Lagrangian density of Eq. (5.5). Then, we integrate over the spatial coordinate x, obtaining, for $\gamma = \Gamma = 0$, the Lagrangian

$$\frac{L_{1D}}{N} = -\frac{\hbar^2}{2m\sigma^2} - \hbar\sigma^2\dot{b} - 2\frac{\hbar^2}{m}\sigma^2 b^2 + \frac{8}{3^{3/2}\pi^{5/4}}\frac{\sqrt{m}}{\hbar}\frac{g^{3/2}N^{1/2}}{\sigma^{1/2}}, \tag{5.20}$$

which depends only on the variational parameters. A simple analytical solution for ω_b can be found writing the Euler-Lagrange equation for the time-dependent parameter $b(t)$, which reads $b = m\dot{\sigma}/(2\hbar\sigma)$, and substituting it into the Lagrangian, we get

$$\frac{L_{1D}}{N} = -\frac{\hbar^2}{2m\sigma^2} + \frac{m}{2}\dot{\sigma}^2 + \frac{8}{3^{3/2}\pi^{5/4}}\frac{\sqrt{m}}{\hbar}\frac{g^{3/2}N^{1/2}}{\sigma^{1/2}}, \tag{5.21}$$

which is the effective Lagrangian for the width of the wave function. The Euler-Lagrange equation for σ reads

$$\ddot{\sigma} = \frac{\hbar^2}{m^2\sigma^3} - \frac{4}{3^{3/2}\pi^{5/4}}\frac{1}{\sqrt{m}\hbar}\frac{g^{3/2}N^{1/2}}{\sigma^{3/2}}, \tag{5.22}$$

whose general solution is in the form of

$$\sigma(t) = \sigma_{st} + A\cos(\omega_b t + \phi_0), \tag{5.23}$$

where

$$\sigma_{st} = \frac{3\pi^{5/6}\hbar^2}{2^{4/3}mgN^{1/3}} \tag{5.24}$$

is the stationary solution, and where

$$\omega_b = \frac{2^{13/6}}{3^{3/2}\pi^{5/3}}\frac{m}{\hbar^3}\,g^2N^{2/3} \tag{5.25}$$

is the frequency of the breathing-mode oscillations around σ_{st}, with amplitude A and initial phase ϕ_0.

Since the ground-state solution is not Gaussian, but it is proportional to the square of the hyperbolic secant [see Eq. (5.15)], we perform the previous calculations considering also the following variational ansatz:

$$\psi_1(x,t) = \psi_2(x,t) \propto \mathrm{sech}^2\left(\sqrt{\frac{\alpha}{2}}\,x\right)\mathrm{e}^{ib(t)\,x^2}, \tag{5.26}$$

whose prefactor is determined by imposing the normalization of the wave functions to N. We obtain the breathing-mode frequency ω_b', where

$$\omega_b' = c\,\omega_b, \qquad c = \frac{3^{11/6}\,\pi^{1/3}}{2^{5/6}\,5^{1/2}\,(\pi^2-6)^{1/2}} \approx 1.4, \tag{5.27}$$

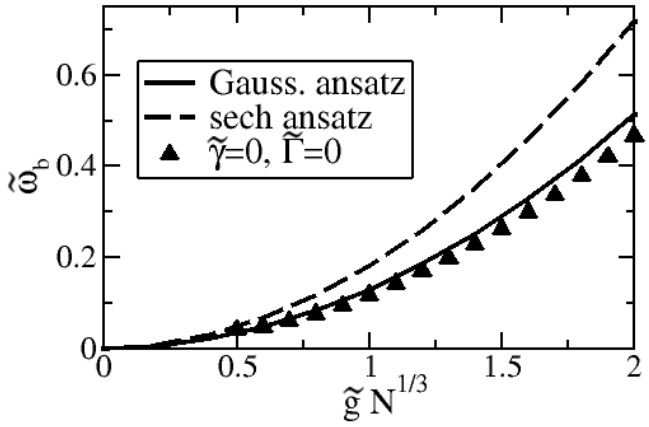

Figure 5.3: Breathing-mode frequency as a function of the parameter $\tilde{g}N^{1/3}$, for a quantum bright soliton, i. e. for $\delta g = 0$, with $\tilde{\gamma} = \tilde{\Gamma} = 0$. The frequencies are obtained either analytically in Eqs. (5.25) and (5.27) with a variational ansatz [171–173], or numerically, by analyzing the time evolution of the average width $\langle x^2 \rangle$ after a small change of the ground state norm. Even if the solution has the hyperbolic secant dependence of Eq. (5.15), the Gaussian ansatz provides a better agreement with the simulation. From Ref. [163].

with $\omega_{\rm b}$ given by Eq. (5.25).

In Fig. 5.3, we plot the breathing-mode frequency of the quantum bright soliton as a function of $\tilde{g}N^{1/3}$. In particular, we compare the numerical results, obtained by solving Eqs. (5.7), with those given by the analytical expressions derived with the Gaussian and sech variational ansätze. Note that, even if the ground-state solution is in the form of a sech^2, the Gaussian variational ansatz leads to a better prediction for the breathing-mode frequency, showing that the Gaussian wave function is able to capture more efficiently the dynamics of the system.

We also performed the numerical calculation of the breathing-mode frequency for nonzero spin-orbit and Rabi couplings. Our results are shown in Fig. 5.4, where we fix different values of Γ and we plot $\omega_{\rm b}$ as a function of γ. First of all, we note that for $\Gamma = 0$ the breathing-mode frequency is not sensitive to the value of γ and coincides with the prediction of Fig. 5.3. We also note that, for a nonzero value of Γ, the breathing-mode frequency displays a peak around the values of γ at which the transition from a striped soliton to a single-peak soliton occurs. Indeed, this consideration can be readily verified from the phase diagram in Fig. 5.2.

To conclude, we analyze the dynamical evolution of a quantum bright soliton following a kick of momentum $\tilde{k} = 2\pi/60$. Numerically, the kick is imposed via a phase shift of the ground-state solutions, which become $e^{ikx}\psi_1$ and $e^{ikx}\psi_2$,

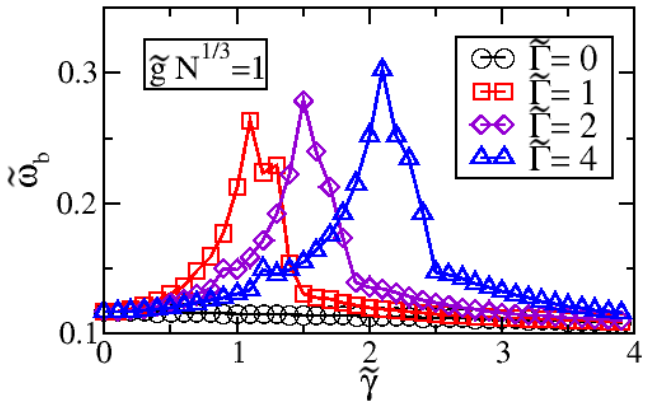

Figure 5.4: Breathing-mode frequency of a quantum bright soliton, obtained through the numerical solution of Eqs. (5.7), and shown as a function of the parameter $\tilde{\gamma}$. As can be seen comparing this plot with the phase diagram of Fig. 5.2, the frequency peak occurs at the transition between the single-peak and the striped soliton. From Ref. [163].

and then performing their time evolution. As shown in Fig. 5.5, the single-peak solution preserves its shape during the propagation. On the contrary, the striped "soliton" changes its shape during the propagation. This dynamical phenomenon is a consequence of the absence of Galilean invariance in spin-orbit coupled Bose-Einstein condensates in the striped phase.

5.2 Phase dynamics of tunneling condensates

The quantum mechanical description of nature, including the emerging equilibrium and nonequilibrium properties of quantum many-body systems, is based on the wave-particle duality. As a broad consequence, quantum mechanics is formulated in terms of complex mathematical entities which, both in operatorial and in field-theory formulations, can be expressed in terms of a phase and of an amplitude. On one hand, the theoretical understanding of the phase properties of a quantum many-body system is a fundamental physical problem: Bose-Einstein condensation, superfluidity, and the Josephson effect [174] are, for instance, emerging phenomena of a macroscopic phase-coherent system. On the other hand, controlling and preserving the phase coherence in quantum technologies and devices is fundamental for technological applications [175]. From this perspective, even if quantum mechanics is an established paradigm, there is still room to make fundamental discoveries and to build new points of view on the old concepts.

A paradigmatic one-dimensional system, whose study led to many fundamental

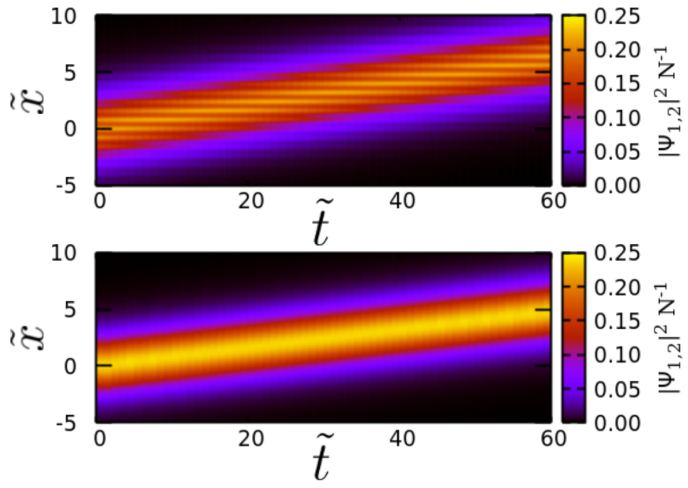

Figure 5.5: Propagation of a quantum bright soliton, either in the striped phase (top panel), or in the single-peak phase (bottom panel), due to a momentum kick of wave vector $\tilde{k} = 2\pi/60$. From Ref. [163].

advances, is the matter-wave interferometer consisting of two coupled quasicondensates [176]. Experiments on this configuration allowed to study the dephasing of split condensates [177], their rephasing dynamics [178], the prethermalization [179], and several other applications. Inspired by this line of research, we studied in Ref. [85] the time evolution of a system of two parallel quasicondensates, analyzing how their coherence evolves after a rapid quench of their tunneling amplitude. Let us now consider a system of parallel bosonic tubes, either in a side-by-side configuration, see Fig. 5.6a, or in a head-to-tail configuration, see Fig. 5.6b. Specifically, we develop a semiclassical effective description of the relative phase which allows us to calculate the time evolution of the coherence factor.

5.2.1 Effective description of the relative phase

We model a system of two one-dimensional parallel quasicondensates of length L with the Lagrangian

$$\mathfrak{L} = \int_0^L \mathrm{d}x\, \mathcal{L}, \qquad \mathcal{L} = \mathcal{L}_{\mathrm{tun}} + \sum_{j=1,2} \mathcal{L}_{0,j}, \tag{5.28}$$

where the Lagrangian density $\mathcal{L}$ is expressed as the sum of two contributions. In particular,

$$\mathcal{L}_{0,j} = i\hbar\psi_j^* \partial_t \psi_j - \frac{\hbar^2}{2m}|\partial_x \psi_j|^2 - \frac{g}{2}|\psi_j|^4 \tag{5.29}$$

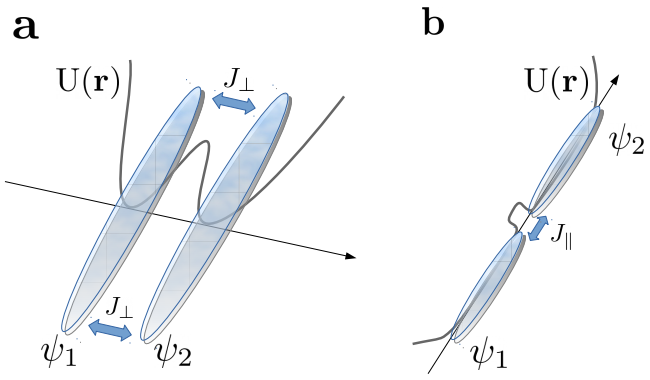

Figure 5.6: We analyze two one-dimensional parallel quasicondensates, either split in the longitudinal direction (side-by-side configuration), or in the midpoint (head-to-tail configuration). These configurations are obtained by engineering the external potential $U(\mathbf{r})$ to trap the atoms in radiofrequency-induced adiabatic potentials (see also Ref. [108]), which are analogous to those on which bubble traps are based [43]. From Ref. [85].

is the Lagrangian density of the parallel tubes, where g represents in this section the one-dimensional contact interaction strength, while we model the tunneling Lagrangian density as

$$\mathcal{L}_{\rm tun} = \frac{J}{2}(\psi_1^*\psi_2 + \psi_2^*\psi_1), \tag{5.30}$$

where J is the tunneling amplitude. Within this formalism, we are able to describe in a unified way both side-by-side and head-to-tail condensates. In the former case we will consider $J = J_\perp$, since the tunneling occurs along the whole length of the system, while the latter case is represented by $J = 2J_\parallel L\,\delta(x)$, since tunneling occurs only in the origin of the system.

To implement an effective description of the relative phase of the quasicondensates, we first introduce a phase-amplitude parametrization by rewriting the bosonic fields $\psi_j(x,t)$ as

$$\psi_j(x,t) = [\rho_j(x,t)]^{1/2}\, e^{i\phi_j(x,t)}, \tag{5.31}$$

where $\rho_j(x,t)$ is the (number) density field, while $\phi_j(x,t)$ is the phase field. In this way, the Lagrangian density of Eq. (5.28) can be expressed as

$$\begin{aligned}\mathcal{L} = \sum_{j=1,2}\Big[&-\hbar\rho_j\,\dot{\phi}_j - \frac{\hbar^2\rho_j}{2m}\,(\partial_x\phi_j)^2 - \frac{\hbar^2}{8m\rho_j}\,(\partial_x\rho_j)^2 - \frac{g}{2}\rho_j^2\Big] \\ &+ J\sqrt{\rho_1\rho_2}\,\cos\left(\phi_1-\phi_2\right),\end{aligned} \tag{5.32}$$

which does not require any additional approximation of the initial equations. Then,

we introduce the following fields:

$$\bar{\phi} = \phi_1 + \phi_2, \qquad \phi = \phi_1 - \phi_2, \tag{5.33}$$

$$\bar{\rho} = \frac{\rho_1 + \rho_2}{2}, \qquad \zeta = \frac{\rho_1 - \rho_2}{2\,\bar{\rho}}\ , \tag{5.34}$$

which are, respectively, the total and relative phase, the total density, and the imbalance. Substituting these fields into Eq. (5.32), the resulting Lagrangian density can be rewritten as a sum of three contributions. Before writing them explicitly, we shift the total density as

$$\bar{\rho} \to \bar{\rho} + \delta\rho, \tag{5.35}$$

where we assume that $\bar{\rho}$ is the uniform mean density around which the total density fluctuates with (space and time dependent) amplitude $\delta\rho$. The first contribution to the Lagrangian density contains only the total fields, and reads

$$\mathcal{L}_{\rm tot} = -\hbar\,\delta\rho\,\zeta\,\dot{\bar{\phi}} - \frac{\hbar^2(\bar{\rho}+\delta\rho)}{4m}\,(\partial_x\bar{\phi})^2 - g\,\delta\rho^2 - 2g\bar{\rho}\,\delta\rho, \tag{5.36}$$

while the second one contains the relative fields

$$\begin{aligned}\mathcal{L}_{\rm rel} = &-\hbar\bar{\rho}\,\zeta\dot{\phi} - \frac{\hbar^2\bar{\rho}}{4m}\,(\partial_x\phi)^2 - \frac{\hbar^2\bar{\rho}}{4m}\,\frac{(\partial_x\zeta)^2}{1-\zeta^2} - g\bar{\rho}^2\zeta^2 \\ &+ J\,\bar{\rho}\,\sqrt{1-\zeta^2}\,\cos\phi\ ,\end{aligned} \tag{5.37}$$

and the final contribution includes all the coupling terms:

$$\begin{aligned}\mathcal{L}_{\rm coupl} = &-\hbar\bar{\rho}\,\zeta\dot{\bar{\phi}} - \hbar\,\delta\rho\,\zeta\dot{\phi} - \frac{\hbar^2\delta\rho}{4m}\,(\partial_x\phi)^2 - \frac{\hbar^2(\bar{\rho}+\delta\rho)}{2m}\,(\partial_x\bar{\phi})(\partial_x\phi) \\ &- \frac{\hbar^2\delta\rho}{4m}\,\frac{(\partial_x\zeta)^2}{1-\zeta^2} - \frac{\hbar^2}{4m(\bar{\rho}+\delta\rho)}\,\frac{(\partial_x\zeta)^2}{(1-\zeta)^2} - \frac{\hbar^2}{2m}\,\frac{(\partial_x\delta\rho)(\partial_x\zeta)}{1+\zeta} \\ &- g\,\delta\rho^2\zeta^2 - 2g\,\bar{\rho}\,\delta\rho\,\zeta^2 + J\,\delta\rho\,\sqrt{1-\zeta^2}\,\cos\phi\ ,\end{aligned} \tag{5.38}$$

so that, in full generality, $\mathcal{L} = \mathcal{L}_{\rm tot} + \mathcal{L}_{\rm rel} + \mathcal{L}_{\rm coupl}$.

The previous Lagrangian densities determine the full time evolution of the tunneling quasicondensates at zero temperature. Two different issues, however, emerge at this point. On the one hand, any experiment is performed at a finite temperature T, which sets a typical time $\tau = \hbar/(k_{\rm B}T)$ over which the dynamics of the system is not governed by quantum effects, but by thermal ones. This implies that our model is capable of predicting the dynamics of the system at times $t < \tau$, to which we limit our next results, and after which thermal decoherence occurs. On the other

hand, even the zero-temperature solution is impossible to get analytically, and we must simplify the problem. For this goal, we neglect the spatial dependence of the total fields by assuming $\delta\rho = 0$ and $\bar{\phi} = \text{const}$, under the implicit hypothesis that the interaction energy $g\bar{\rho}$ is sufficiently high and that the quantum fluctuations are suppressed. In this case, the coupling Lagrangian density can be neglected and the motion of the total and relative degrees of freedom is decoupled. Therefore, we focus on the dynamics of the relative modes, which is governed by the Lagrangian

$$\mathfrak{L}_{\rm rel} = \int_0^L \mathrm{d}x\, \mathcal{L}_{\rm rel}, \tag{5.39}$$

and we ignore the dynamics of the center-of-mass degrees of freedom.

The Euler-Lagrange equations of the relative variables are given by

$$\hbar\dot{\phi} = -J\frac{\zeta}{\sqrt{1-\zeta^2}}\cos\phi - 2g\bar{\rho}\,\zeta + \frac{\hbar^2}{2m}\left[\frac{\partial_x^2\zeta}{1-\zeta^2} + \frac{\zeta\,(\partial_x\zeta)^2}{(1-\zeta^2)^2}\right], \tag{5.40}$$

$$\hbar\dot{\zeta} = J\sqrt{1-\zeta^2}\sin\phi - \frac{\hbar^2}{2m}\,\partial_x^2\phi\,, \tag{5.41}$$

and extend those of Refs. [174, 180] to a nonuniform system in which the relative phase and the imbalance, as well as the tunneling amplitude, depend on space.

Side-by-side parallel quasicondensates

We consider side-by-side parallel quasicondensates and set $J = J_\perp$. Imposing reflecting boundary conditions at the system boundaries, we decompose the relative fields in the basis of cosines as

$$\phi(x,t) = \frac{\sqrt{2}}{L}\sum_{k\geq 0}\phi_k(t)\,\cos(kx), \quad \phi_k(t) = \alpha_k\int_0^L \mathrm{d}x\,\phi(x,t)\cos(kx), \tag{5.42}$$

$$\zeta(x,t) = \frac{\sqrt{2}}{L}\sum_{k\geq 0}\zeta_k(t)\,\cos(kx), \quad \zeta_k(t) = \alpha_k\int_0^L \mathrm{d}x\,\zeta(x,t)\cos(kx), \tag{5.43}$$

where $k = \pi n/L$ is the wave vector, with n integer, and where we set $\alpha_0 = 1/\sqrt{2}$ and $\alpha_k = \sqrt{2}$ for $k > 0$. Substituting this decomposition into the relative Lagrangian of Eq. (5.39), the resulting expression will depend both on ϕ_k and on ζ_k. To get an effective description of the phase degrees of freedom, we calculate the Euler-Lagrange equation for ζ and we substitute it in the Lagrangian. As a final step, we perform a Legendre transformation, obtaining

$$H = \sum_k\left[\frac{p_k^2}{2M_k} + \frac{M_k}{2}\omega_k^2\phi_k^2\right], \tag{5.44}$$

which is the Hamiltonian of a system of harmonic oscillators, with $p_k = M_k\dot{\phi}_k$. These oscillators represent the noninteracting modes in which we have decomposed the dynamics of the relative degrees of freedom of the parallel condensates. In particular, the mass of the oscillators is given by

$$M_k = \frac{\hbar^2\bar{\rho}}{L}\frac{1}{(J_\perp + 2g\bar{\rho}) + \hbar^2k^2/(2m)}, \tag{5.45}$$

while the excitations spectrum reads

$$\hbar\omega_k = \sqrt{J_\perp(J_\perp + 2g\bar{\rho}) + \frac{\hbar^2k^2}{2m}\left[\frac{\hbar^2k^2}{2m} + 2(J_\perp + g\bar{\rho})\right]}\,, \tag{5.46}$$

and is in the form of a gapped Bogoliubov-like spectrum.

Head-to-tail parallel quasicondensates

To study the head-to-tail configuration, we consider in this section the tunneling energy $J(x) = 2J_\parallel L\delta(x)$. To tackle the problem analytically, we limit ourselves to the analysis of the following Lagrangian density

$$\mathcal{L}_{\rm rel} = -\hbar\bar{\rho}\,\zeta\dot{\phi} - \frac{\hbar^2\bar{\rho}}{4m}\,(\partial_x\phi)^2 - \frac{\hbar^2\bar{\rho}}{4m}\,(\partial_x\zeta)^2 - \frac{(2g\bar{\rho}^2 + J\bar{\rho})}{2}\,\zeta^2 - \frac{J\bar{\rho}}{2}\,\phi^2, \tag{5.47}$$

which is the linearized version of the Lagrangian density that appears in Eq. (5.39). As a further approximation, we also neglect the term $\propto (\partial_x\zeta)^2$, which requires us to work in the Josephson regime of $g\bar{\rho} \gg J_\parallel$ that is pertinent to most experiments [181, 182]. As before, we proceed with substituting into Eq. (5.47) the Euler-Lagrange equation for ϕ, considering the effective phase-only Lagrangian

$$\mathcal{L}_{\rm rel} = \frac{\hbar^2}{4g}\,\dot{\phi}^2 - \frac{\hbar^2\bar{\rho}}{4m}\,(\partial_x\phi)^2 - J_\parallel\bar{\rho}\,L\delta(x)\,\phi^2, \tag{5.48}$$

and, by writing the relative phase field as

$$\phi(x,t) = \frac{1}{\sqrt{L}}\sum_n q_n(t)\;\phi_n(x)\;, \tag{5.49}$$

we calculate the Hamiltonian $H = \sum_n P_n\dot{q}_n - \mathcal{L}_{\rm rel}$, where $P_n = M\dot{q}_n$ are the momenta, obtaining

$$H = \sum_n\left[\frac{P_n^2}{2M} + \frac{M}{2}\Omega_n^2\phi_n^2\right]\,, \tag{5.50}$$

which is the Hamiltonian of the quasiparticles in the system of mass $M = \hbar^2/(2gL)$.

To diagonalize the Hamiltonian into the previous form and, therefore, to calculate the eigenfunctions ϕ_n and the oscillator energies $\hbar\Omega_n$, it is necessary to solve the following eigenproblem

$$\left[-\frac{\hbar^2}{2m}\partial_x^2 + 2J_\parallel L\delta(x)\right]\phi_n(x) = \epsilon_n\,\phi_n(x), \tag{5.51}$$

where we impose, as in the side-by-side case, reflecting conditions at the system boundaries. Note in particular that, once the eigenenergies ϵ_n are known, the oscillator energies are given by $\Omega_n = (2g\bar{\rho}\,\epsilon_n/\hbar^2)^{1/2}$. The eigenenergies we aim to determine can be equivalently obtained from the numerical solution of the following equation [183]

$$\sqrt{\frac{2mL^2\epsilon_n}{\hbar^2}}\ \tan\left(\sqrt{\frac{2mL^2\epsilon_n}{\hbar^2}}\right) = \frac{2mL^2J_\parallel}{\hbar^2}, \tag{5.52}$$

which admits some analytical approximations in the different regimes of n and $J_\parallel$. In the regime where the tunneling energy $J_\parallel$ is very small, the eigenenergies read [85]

$$\epsilon_n = \frac{1}{4}\left(\sqrt{4J_\parallel + \frac{\hbar^2\pi^2n^2}{2mL^2}} + \sqrt{\frac{\hbar^2\pi^2n^2}{2mL^2}}\right)^2, \tag{5.53}$$

and the oscillator energies are, therefore, given by

$$\hbar\Omega_k = \sqrt{2g\bar{\rho}\,J_\parallel + \frac{g\bar{\rho}}{2}\,\frac{\hbar^2k^2}{2m}} + \sqrt{\frac{g\bar{\rho}}{2}\,\frac{\hbar^2k^2}{2m}}, \tag{5.54}$$

where we introduce the wave vector $k = \pi n/L$. For other analytical approximations of Eq. (5.52), valid in other regimes, we refer to Ref. [85].

5.2.2 Dynamics of the coherence factor

We now model theoretically the dynamics of the relative-phase correlators after a quenching procedure. In particular, we consider here the following preparation of the initial state: we suppose that a single bosonic tube is quickly split in half, either in the side-by-side configuration, or in the head-to-tail one. Then, we suppose that the tunneling amplitude is restored and we discuss how the phase coherence evolves at short times after the quench. Let us then model this procedure, analyzing the typical times, and justifying our choice for the initial state of the parallel tubes.

We suppose that the single condensate tube is split in half in a time $\tau_s \ll \xi/c_s$, where $\xi = (\hbar^2/mg\bar{\rho})^{1/2}$ is the healing length, and c_s is the sound velocity in the

system. Dividing the system in L/ξ independent grains of length ξ and assuming a symmetric splitting, we consider the imbalance ζ_i in the ith grain of the system. Due to the fast splitting, we assume that the probability distribution is given by

$$|\Psi_i(\zeta_i)|^2 \propto \exp\left(-\frac{\zeta_i^2}{\bar{\rho}\xi}\right) \tag{5.55}$$

and is therefore a Gaussian with zero average (due to the symmetric splitting) and with variance equal to the number of atoms in the grain $\bar{\rho}\xi$. Since the relative phase ϕ_i is canonically conjugated to the imbalance ζ_i, its probability is[1]

$$|\Psi_i(\phi_i)|^2 \propto \exp(-\bar{\rho}\xi\,\phi_i^2), \tag{5.56}$$

namely, it is also Gaussian but with the inverse of the variance. Since the grains are statistically independent, the probability of splitting the quasicondensates with the series of initial relative phases $\phi_1, ..., \phi_{L/\xi}$ is the product of factors in the form of Eq. (5.56), for $i = 1, ..., L/\xi$. Considering a continuum notation, the sum over i in the exponentials can be performed as an integral, and the probability amplitude of having an initial relative phase $\phi(x)$ is given by the wave function

$$\Psi[\phi(x), t = 0] \propto \exp\left[-\frac{\bar{\rho}}{2}\int_0^L \mathrm{d}x\,\phi(x)^2\right], \tag{5.57}$$

which represents the state of the system at the time $t = 0$ of the splitting procedure. Fixing the normalization, and working in the Fourier space, we can rewrite it as

$$\Psi[\{\phi_k\}, t = 0] \simeq \prod_k \Psi_k(\phi_k, t = 0), \tag{5.58}$$

where we define the wave function of the single Fourier mode as

$$\Psi_k(\phi_k, t = 0) = \frac{1}{\pi^{1/4}\sigma^{1/2}}\, e^{-\frac{\phi_k^2}{2\sigma^2}}\ , \tag{5.59}$$

where $\sigma^2 = L/\bar{\rho}$ is the new variance.

The time evolution of the initial Gaussian state is given by the Hamiltonian of the quasiparticles of the system at the Eqs. (5.44) (5.50). In this case, each of the oscillators evolve independently according to the Schrödinger equation, and the probability of each oscillator at time t reads [184]

$$|\Psi_k(\phi_k, t)|^2 = \frac{1}{\pi^{1/2}\sigma_k(t)} e^{-\frac{\phi_k^2}{\sigma_k^2(t)}}, \tag{5.60}$$

[1]To understand the factors in the exponentials, consider the Fourier transform of a Gaussian wave function, and its associated probability.

namely, it remain Gaussian, but with a time-dependent variance given by

$$\sigma_k^2(t) = \sigma^2 \cos^2(\omega_k t) + \left(\frac{\hbar^2}{M_k^2 \omega_k^2 \sigma^2} \right) \sin^2(\omega_k t), \tag{5.61}$$

which depends on the oscillator frequency ω_k and on the mass M_k.

Given the previous knowledge, we calculate the coherence factor $\mathcal{C}(t) = \langle \cos(\phi) \rangle_t$, defined as the average of the cosine of the relative phase [177, 185]. After some simple steps, the coherence factor can be expressed as [177]

$$\mathcal{C}(t) = e^{-\frac{1}{4L^2} \sum_k \sigma_k^2(t)}, \tag{5.62}$$

which is completely determined by the variance at Eq. (5.61) and, therefore, by the excitation spectra ω_k and by the oscillator masses M_k previously derived. In the remaining part of this chapter, through the calculation of $\mathcal{C}(t)$, which is an observable quantity, we discuss the dynamics of the system in which, considering the initial state (5.58), the tunneling energy is quickly quenched to the nonzero value J.

Side-by-side parallel quasicondensates

We analyze the time evolution of the coherence factor of Eq. (5.62), considering side-by-side quasicondensates with the excitation spectrum of Eq. (5.46) and mass of the oscillators given by Eq. (5.45).

In Fig. 5.7 we show the coherence factor as a function of time, implementing the sum in Eq. (5.62) for the realistic experimental values of the system length, density and interactions [181, 186] described in the figure caption. The coherence factor $\mathcal{C}(t)$ performs time oscillations during its dynamics which, since $\mathcal{C}(t)$ models the overall time evolution of the relative phase, testifies the dephasing and rephasing of the noninteracting quasiparticles. This peculiar behavior is crucially due to the nonzero tunneling amplitude between the parallel quasicondensates, which opens a gap in the quasiparticle energy, see Eq. (5.46). In this configuration, the system is essentially performing Josephson oscillations, and the inclusion of the spatial degrees of freedom in the relative phase field $\phi(x)$ produces quantitative changes in the dynamics.

The crucial role of the nonzero tunneling energy $J_\perp$ is testified by Fig. 5.8, where we plot the adimensional variance $\sigma_k^2(t)/\sigma^2$ of the oscillators as a function of time. We first note that the oscillation period is practically determined by the lowest-energy oscillator, $\sigma_0^2(t)/\sigma^2$, while the higher-energy modes constitute higher harmonics

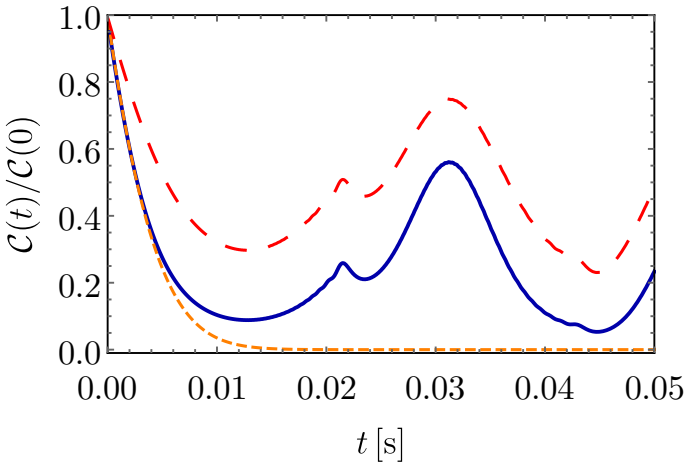

Figure 5.7: Dynamics of the coherence factor after the sudden splitting of two parallel quasicondensates in a side-by-side configuration. In the absence of tunneling, i. e. for $J_\perp = 0$, the two subsystems dephase [177] (orange dashed line), while for $J_\perp/\hbar = 5/(2\pi)\,\mathrm{Hz}$, the system dephases and rephases periodically. For a tube of length $L = 100\,\mu\mathrm{m}$ (red dashed line), the coherence factor acquires a higher value with respect to a shorter tube, with length $L = 50\,\mu\mathrm{m}$ (blue solid line). In this plot, we consider ^{87}Rb atoms with density $\bar{\rho} = 50\,\mu\mathrm{m}^{-1}$, and interaction strength $g = 2(\hbar^2/m)(a_s/l_\perp)$, where $a_s = 5\,\mathrm{nm}$, and $l_\perp = 0.24\,\mu\mathrm{m}$ is the thickness of the tubes. From Ref. [85].

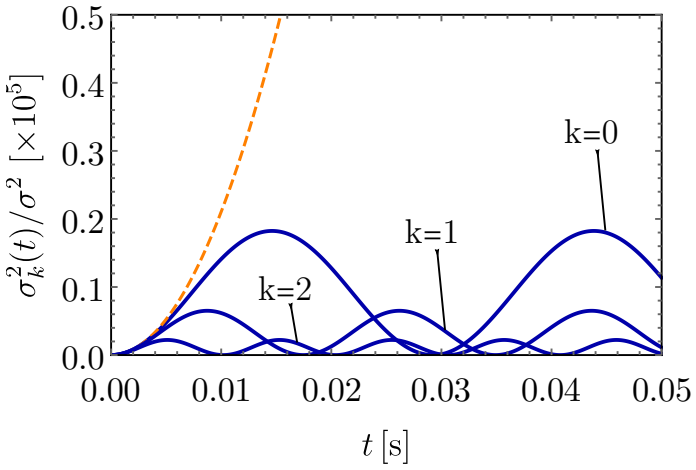

Figure 5.8: Evolution of the quasiparticle widths of Eq. (5.63) for different values of the wave vector k, where, to simplify the notation in the figure, $k = \{0, 1, 2, ...\}$ denotes actually $k = (\pi/L)\{0, 1, 2, ...\}$. While, in the absence of tunneling, the $k = 0$ mode grows quadratically (orange dashed line), for nonzero $J_\perp$ the widths oscillate in time (blue solid lines). In this plot, we use the same parameters of the blue curve in Fig. 5.7. From Ref. [85].

that are responsible for the small bumps in Fig. 5.7. Thus, we focus on the low wave vector limit of the oscillator variance Eq. (5.61), which reads

$$\sigma(t)^2 \sim \sigma^2 \cos^2(\omega_0 t) + \lim_{k\to 0} \left(\frac{\hbar^2}{M_k^2 \omega_k^2 \sigma^2} \right) \sin^2(\omega_k t). \tag{5.63}$$

If the excitation spectrum is gapped, so that ω_0 is finite, $\sigma(t)^2$ oscillates in time as the sum of sines and cosines with different weights. However, in the case of a gapped excitation spectrum for which $\omega_0 = 0$, the previous equation goes as

$$\sigma(t)^2 \sim \sigma^2 + \frac{\hbar^2}{M_0^2 \sigma^2}\, t^2, \tag{5.64}$$

and, therefore, grows quadratically in time and leads the coherence factor $\mathcal{C}(t)$ of Eq. (5.62) to decay exponentially.

Head-to-tail parallel quasicondensates

In the regimes considered here, pertinent to most experiments, the mechanism of dephasing and rephasing of the coherence factor occurs also in head-to-tail parallel quasicondensates. Indeed, this behavior is a general consequence of the

nonzero gap in the excitation spectrum derived in Eq. (5.54). Thus, by repeating the steps implemented in side-by-side quasicondensates also in the configuration of head-to-tail ones, we plot the coherence factor $\mathcal{C}(t)$ as a function of time in Fig. 5.9. As before, the coherence factor oscillates in time with a period which is essentially determined by the lowest-energy mode.

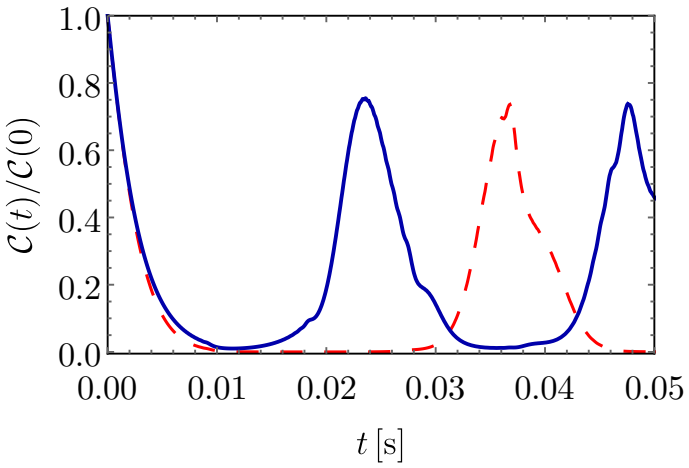

Figure 5.9: Time evolution of the coherence factor of two parallel head-to-tail quasicondendensates. The different rephasing times are controlled by the tunneling amplitude, either $J_{\parallel}/\hbar = 8/(2\pi)$ Hz (blue solid line), or $J_{\parallel}/\hbar = 2/(2\pi)$ Hz (red dashed line). We use in this plot the same parameters of Fig. 5.6, except for $\bar{\rho} = 30\,\mu\text{m}^{-1}$, and $L = 30\,\mu$m. From Ref. [85].

It is important to stress that the initial Gaussian state can be engineered in the head-to-tail quasicondensates by splitting a single tube into two side-by-side quasicondensates that tunnel only in the origin. Indeed, our formalism does not model the actual spatial position and the angle between the tubes, and this is the most practical way to ensure the desired initial condition.

6

Conclusions and outlook

The study of ultracold atomic gases in reduced dimensionalities and, particularly, the analysis of novel geometries, has often led to new discoveries and applications. In this thesis, we have focused our attention on discussing the physics of one- and two-dimensional systems, analyzing thoroughly the case of two-dimensional bubble-trapped condensates in spherical and in ellipsoidal configurations.

Shell-shaped condensates are an experimentally-relevant prototype of a curved quantum gas, and display rich equilibrium and nonequilibrium properties. Throughout their study, we have analyzed how finite size and curvature influence the transition of Bose-Einstein condensation, and we have derived a renormalization group description of the Berezinskii-Kosterlitz-Thouless transition in the spherical case. In this specific configuration, our results on the interplay of Bose-Einstein condensation and superfluidity, and the study of finite-temperature hydrodynamic modes, will offer analytical insight to benchmark future and ongoing experiments. Most of our findings are tailored on the specific conditions of microgravity research facilities, but can also be extended to model other experimental realizations of shell-shaped condensates that may be developed in the future.

Another major research direction of the present work is the study of sound propagation in two-dimensional uniform superfluids. To consider the Landau two-fluid model a valid description of a weakly-interacting gas, it is necessary to detect experimentally both sound modes, which should agree with the predictions of the model. This proof has been recently obtained in two-dimensional box-trapped bosons, but, in two-dimensional uniform fermions, the second sound velocity and its vanishing at the BKT transition is still undetected. This evidence, for a textbook configuration as that of a quantum gas in a box, would demonstrate the validity of the two-fluid picture in fermions across the whole BCS-BEC crossover. We also

hope to trigger future experimental investigations for observing the hybridization of first and second sound in box-trapped bosons. Our works, in particular, offer new theoretical predictions for the hybridization temperature in three- and two-dimensional weakly-interacting bosons, and for the behavior of the sound modes at low temperatures, where other theories do not apply.

In the last ten years, the field of ultracold quantum gases has also been stimulated by the experimental implementation of new interatomic interactions and by the engineering of artificial gauge fields. Actually, most of the results of the present thesis, concerning both shell-shaped condensates and other configurations, are obtained for zero-range interatomic interactions. Including in our theories long-range (i. e. dipolar) or higher-order effective interactions, could lead to a richer phenomenology.

In bubble-trapped condensates, new physics could stem from the complex interplay of fluctuations, interactions, temperature, topology, and curvature. Curvature, in particular, deserves further refined investigations. Most theoretical discoveries in the physico-mathematical context can be usually reframed as a direct consequence of the assumptions of the problem: this consideration, instead of proving worthless the analysis of the right postulates, implies that researching new results coincides, in a broad sense, with the precise identification of the correct initial definitions. In this sense, we believe that a better understanding of the concept of curvature of a quantum gas can lead to exciting developments in the field of ultracold atoms.

Acknowledgments

It may happen, and in my case it often occurred, that the continuous flow of conferences, discussions, peer reviews and publications prevents from acknowledging properly collaborators and friends. It is thus the right moment, at the end of a long path, to think about all the interactions that occurred in the past years and that determined my personal growth.

I want to thank my supervisor Luca Salasnich, who guided and animated my scientific interests, allowing me to grow as a scientist. Despite spending most of my PhD time confined due to the Covid-19 pandemic, he helped me to lead a productive and healthy activity. Another important guide in the last years has been Axel Pelster, whose scientific and personal advices were always supportive and complemented those of my supervisor.

I also gratefully acknowledge Fabio Cinti, Dmitry Petrov, Flavio Toigo, Yueming Wang, and Sandro Wimberger for productive and interesting collaborations. In addition, the possibility to talk informally about research and personal issues with close colleagues as Giacomo Bighin and Alberto Cappellaro, has always been fruitful.

It is also important, I believe, to thank the physicists to whom I sent emails during these years, and who replied carefully and with useful information that allowed me to solve difficult research issues.

Moving towards my peer group, I am happy that I could spend the (pre-lockdown) first year of the PhD with my colleagues: Timo Felser, Stefano Garlaschi, Alfredo Guarrera, Jay Kalinani, Sarah Libanore, Luca Mattiazzi, Leonardo Pacciani Mori, Giorgio Nicoletti, Dario Partipilo, Giovanni Verza. Their physical presence, their jokes and the casual discussions made working long hours in the office fun and productive.

My deep gratitude and some apologies are for my parents, my relatives, and my friend Giorgio: they have not seen me much in the last years, as I spent most of the time carrying on my studies in Padova. I dedicate this thesis to Federica.

Appendix A

Laplace equation in spherical coordinates

In this appendix, we derive the Green's function of Laplace equation in spherical coordinates. The Green's function $G(\theta, \varphi, \theta', \varphi')$ satisfies the following Poisson equation

$$-\frac{\hat{L}^2}{\hbar^2} G(\theta, \varphi, \theta', \varphi') = q \left[\delta(\cos\theta - \cos\theta')\, \delta(\varphi - \varphi') - \frac{1}{4\pi} \right], \tag{A.1}$$

where $\hat{L}^2$ is the angular momentum operator in spherical coordinates, and where the additional term $-1/(4\pi)$ eliminates the divergences in the following steps. We expand $G(\theta, \varphi, \theta', \varphi')$ and the delta functions in a basis of spherical harmonics as

$$G(\theta, \varphi, \theta', \varphi') = \sum_{l=0}^{\infty} \sum_{m_l=-l}^{l} g_{lm_l}(\theta', \varphi') \mathcal{Y}_l^{m_l}(\theta, \varphi), \tag{A.2}$$

$$\delta(\cos\theta - \cos\theta')\, \delta(\varphi - \varphi') = \sum_{l=0}^{\infty} \sum_{m_l=-l}^{l} \mathcal{Y}_l^{m_l *}(\theta', \varphi') \mathcal{Y}_l^{m_l}(\theta, \varphi). \tag{A.3}$$

where $g_{lm_l}(\theta', \varphi')$ are unknown coefficients. To determine them, we substitute these decompositions in Eq. (A.1), and using the properties of the spherical harmonics, we find that

$$g_{lm_l}(\theta', \varphi') = \frac{q}{l(l+1)} \mathcal{Y}_l^{m_l *}(\theta', \varphi'). \tag{A.4}$$

Then, substituting $g_{lm_l}(\theta', \varphi')$ into the Green's function of Eq. (A.2), and summing over m_l, we find

$$G(\theta, \varphi, \theta', \varphi') = \frac{q}{4\pi} \left[\sum_{l=1}^{\infty} \frac{1}{l} P_l(\cos\gamma) + \sum_{l=1}^{\infty} \frac{1}{l+1} P_l(\cos\gamma) \right], \tag{A.5}$$

with $P_l(\cos\gamma)$ the Legendre polynomia, and $\cos\gamma = \cos\theta\cos\theta' + \sin\theta\sin\theta'\cos(\varphi - \varphi')$. The sums in Eq. (A.5) can be performed analytically, see for instance Ref. [187], obtaining the Green's function as

$$G(\theta, \varphi, \theta', \varphi') = \frac{q}{4\pi} + \frac{q}{2\pi} \ln\left(\sqrt{\frac{1-\cos\gamma}{2}}\right),$$

which allows to determine the stream function of a spherical superfluid film, as discussed in section 3.3.

Bibliography

[1] J. R. McRae (translator), *The Platform Sutra of the sixth patriarch* (Numata Center for Buddhist Translation and Research, Berkeley, 2000).

[2] P. Feyerabend, *Against method* (London, 1975).

[3] S. N. Bose, *Plancks Gesetz und Lichtquantenhypothese*, Z. Phys. **26**, 178 (1924).

[4] A. Einstein, *Quantentheorie des einatomigen idealen Gases*, Sitzber. Kgl. Preuss. Akad. Wiss. 261 (1924).

[5] A. Einstein, *Quantentheorie des einatomigen idealen Gases. Zweite Abhandlung*, Sitzungsber. Preuss. Akad. Wiss. **1**, 3 (1925).

[6] W. Pauli, *Zur Frage der theoretischen Deutung der Satelliten einiger Spektrallinien und ihrer Beeinflussung durch magnetische Felder*, Naturwissenschaften **12**, 741 (1924).

[7] P. Godfrey-Smith, *Theory and reality: An introduction to the philosophy of science* (University of Chicago Press, 2009).

[8] T. S. Kuhn, *The Structure of Scientific Revolutions* (University of Chicago Press, 1962).

[9] P. Kapitza, *Viscosity of Liquid Helium below the λ-Point*, Nature **141**, 74 (1938).

[10] F. London, *The λ-Phenomenon of Liquid Helium and the Bose-Einstein Degeneracy*, Nature **141**, 643 (1938).

[11] S. Balibar, *The Discovery of Superfluidity*, J. Low. Temp. Phys. **146**, 441 (2007).

[12] L. D. Landau, *The Theory of Superfluidity of Helium II*, J. Phys. U.S.S.R. **5**, 71 (1941).

[13] L. Tisza, *Transport Phenomena in Helium II*, Nature **141**, 913 (1938).

[14] L. Tisza, *Sur la supraconductibilité thermique de l'hèlium II liquide et la statistique de Bose-Einstein*, C. r. hebd. séances Acad. sci. Paris **207**, 1035 (1938).

[15] L. Tisza, *La viscosité de l'hèlium liquide et la statistique de Bose-Einstein*, C. r. hebd. séances Acad. sci. Paris **207**, 1186 (1938).

[16] N. N. Bogoliubov, *On the theory of superfluidity*, J. Phys. USSR **11**, 23 (1947).

[17] A. J. Leggett, *Superfluidity*, Rev. Mod. Phys. **71**, S318 (1999).

[18] M. H. Anderson, J. R. Ensher, M. R. Matthews, C. E. Wieman, and E. A. Cornell *Observation of Bose-Einstein Condensation in a Dilute Atomic Vapor*, Science **269**, 198 (1995).

[19] K. B. Davis, M. -O. Mewes, M. R. Andrews, N. J. van Druten, D. S. Durfee, D. M. Kurn, and W. Ketterle, *Bose-Einstein Condensation in a Gas of Sodium Atoms*, Phys. Rev. Lett. **75**, 3969 (1995).

[20] C. C. Bradley, C. A. Sackett, J. J. Tollett, and R. G. Hulet, *Evidence of Bose-Einstein Condensation in an Atomic Gas with Attractive Interactions*, Phys. Rev. Lett. **75**, 1687 (1995). Erratum: C. C. Bradley, C. A. Sackett, and R. G. Hulet, *Bose-Einstein Condensation of Lithium: Observation of Limited Condensate Number*, Phys. Rev. Lett. **78**, 985 (1997).

[21] W. D. Phillips and H. Metcalf, *Laser Deceleration of an Atomic Beam*, Phys. Rev. Lett. **48**, 596 (1982).

[22] T. W. Hänsch and A. L. Schawlow, *Cooling of gases by laser radiation*, Opt. Commun. **13**, 68 (1975).

[23] D. J. Wineland, H. Dehmelt, *Proposed 1014 delta upsilon less than upsilon laser fluorescence spectroscopy on t1+ mono-ion oscillator iii*, Bull. Am. Phys. Soc. **20**, 637 (1975).

[24] S. Chu, L. Hollberg, J. E. Bjorkholm, A. Cable, and A. Ashkin, *Three-dimensional viscous confinement and cooling of atoms by resonance radiation pressure*, Phys. Rev. Lett. **55**, 48 (1985).

[25] A. L. Migdall, J. V. Prodan, W. D. Phillips, T. H. Bergeman, and H. J. Metcalf, *First Observation of Magnetically Trapped Neutral Atoms*, Phys. Rev. Lett. **54**, 2596 (1985).

[26] S. Chu, J. E. Bjorkholm, A. Ashkin, and A. Cable, *Experimental Observation of Optically Trapped Atoms*, Phys. Rev. Lett. **57**, 314 (1986).

[27] V. S. Bagnato, G. P. Lafyatis, A. G. Martin, E. L. Raab, R. N. Ahmad-Bitar, and D. E. Pritchard, *Continuous Stopping and Trapping of Neutral Atoms*, Phys. Rev. Lett. **58**, 2194 (1987).

[28] P. D. Lett, R. N. Watts, C. I. Westbrook, W. D. Phillips, P. L. Gould, and H. J. Metcalf, *Observation of Atoms Laser Cooled below the Doppler Limit*, Phys. Rev. Lett. **61**, 169 (1988).

[29] A. Aspect, E. Arimondo, R. Kaiser, N. Vansteenkiste, and C. Cohen-Tannoudji, *Laser Cooling below the One-Photon Recoil Energy by Velocity-Selective Coherent Population Trapping*, Phys. Rev. Lett. **61**, 826 (1988).

[30] E. L. Raab, M. Prentiss, A. Cable, S. Chu, and D. E. Pritchard, *Trapping of Neutral Sodium Atoms with Radiation Pressure*, Phys. Rev. Lett. **59**, 2631 (1987).

[31] N. Masuhara, J. M. Doyle, J. C. Sandberg, D. Kleppner, T. J. Greytak, H. F. Hess, and G. P. Kochanski, *Evaporative Cooling of Spin-Polarized Atomic Hydrogen*, Phys. Rev. Lett. **61**, 935 (1988).

[32] W. Ketterle and N. J. Van Druten, *Evaporative Cooling of Trapped Atoms*, Adv. At. Mol. Opt. Phys. **37**, 181 (1996).

[33] I. Bloch, J. Dalibard, and W. Zwerger, *Many-body physics with ultracold gases*, Rev. Mod. Phys. **80**, 885 (2008).

[34] I. Bloch, J. Dalibard, and S. Nascimbène, *Quantum simulations with ultracold quantum gases*, Nature Phys. **8**, 267 (2012).

[35] T. Lahaye, C. Menotti, L. Santos, M. Lewenstein, and T. Pfau, *The physics of dipolar bosonic quantum gases*, Rep. Prog. Phys. **72**, 126401 (2009).

[36] R. P. Feynman, *Simulating physics with computers*, Int. J. Theor. Phys. **21**, 467 (1982).

[37] S. Lloyd, *Universal Quantum Simulators*, Science **273**, 1073 (1996).

[38] I. M. Georgescu, S. Ashhab, and F. Nori, *Quantum simulation*, Rev. Mod. Phys. **86**, 153 (2014).

[39] A. Görlitz, J. M. Vogels, A. E. Leanhardt, C. Raman, T. L. Gustavson, J. R. Abo-Shaeer, A. P. Chikkatur, S. Gupta, S. Inouye, T. Rosenband, and W. Ketterle, *Realization of Bose-Einstein Condensates in Lower Dimensions*, Phys. Rev. Lett. **87**, 130402 (2001).

[40] D. S. Petrov, D. M. Gangardt, and G. V. Shlyapnikov, *Low-dimensional trapped gases*, J. Phys. IV **116**, 5 (2004).

[41] D. S. Petrov, *Bose-Einstein condensation in low-dimensional trapped gases*, Ph.D. thesis, University of Amsterdam, 2003.

[42] F. Dalfovo, S. Giorgini, L. P. Pitaevskii, and S. Stringari, *Theory of Bose-Einstein condensation in trapped gases*, Rev. Mod. Phys. **71**, 463 (1999).

[43] O. Zobay and B. M. Garraway, *Two-Dimensional Atom Trapping in Field-Induced Adiabatic Potentials*, Phys. Rev. Lett. **86**, 1195 (2001).

[44] E. R. Elliott, M. C. Krutzik, J. R. Williams, J. R. Thompson, and D. C. Aveline, *NASA's Cold Atom Lab (CAL): system development and ground test status*, npj Microgravity **4**, 16 (2018).

[45] D. C. Aveline, J. R. Williams, E. R. Elliott, C. Dutenhoffer, J. R. Kellogg, J. M. Kohel, N. E. Lay, K. Oudrhiri, R. F. Shotwell, N. Yu, and R. J. Thompson, *Observation of Bose-Einstein condensates in an Earth-orbiting research lab*, Nature **582**, 193 (2020).

[46] T. van Zoest, et al. *Bose-Einstein Condensation in Microgravity*, Science **328**, 1540 (2010).

[47] H. Müntinga, et al., *Interferometry with Bose-Einstein Condensates in Microgravity*, Phys. Rev. Lett. **110**, 093602 (2013).

[48] C. Vogt, M. Woltmann, S. Herrmann, C. Lämmerzahl, H. Albers, D. Schlippert, and E. M. Rasel, *Evaporative cooling from an optical dipole trap in microgravity*, Phys. Rev. A **101**, 013634 (2020).

[49] D. Becker, et al., *Space-borne Bose–Einstein condensation for precision interferometry*, Nature **562**, 391 (2018).

[50] G. Condon, M. Rabault, B. Barrett, L. Chichet, R. Arguel, H. Eneriz-Imaz, D. Naik, A. Bertoldi, B. Battelier, P. Bouyer, and A. Landragin, *All-Optical Bose-Einstein Condensates in Microgravity*, Phys. Rev. Lett. **123**, 240402 (2019).

[51] R. A. Carollo, D. C. Aveline, B. Rhyno, S. Vishveshwara, C. Lannert, J. D. Murphree, E. R. Elliott, J. R. Williams, R. J. Thompson, and N. Lundblad, *Observation of ultracold atomic bubbles in orbital microgravity*, arXiv:2108.05880.

[52] N. Lundblad, R. A. Carollo, C. Lannert, M. J. Gold, X. Jiang, D. Paseltiner, N. Sergay, and D. C. Aveline, *Shell potentials for microgravity Bose-Einstein condensates*, npj Microgravity **5**, 30 (2019).

[53] K. Frye, et al. *The Bose-Einstein Condensate and Cold Atom Laboratory*, EPJ Quantum Technol. **8**, 1 (2021).

[54] A. Tononi and L. Salasnich, *Bose-Einstein Condensation on the Surface of a Sphere*, Phys. Rev. Lett. **123**, 160403 (2019).

[55] A. Tononi, A. Pelster, and L. Salasnich, *Topological superfluid transition in bubble-trapped condensates*, arXiv:2104.04585.

[56] A. Tononi, F. Cinti, and L. Salasnich, *Quantum bubbles in microgravity*, Phys. Rev. Lett. **125**, 010402 (2020).

[57] K. Padavić, K. Sun, C. Lannert, and S. Vishveshwara, *Vortex-antivortex physics in shell-shaped Bose-Einstein condensates*, Phys. Rev. A **102**, 043305 (2020).

[58] S. J. Bereta, M. A. Caracanhas, and A. L. Fetter, *Superfluid vortex dynamics on a spherical film*, Phys. Rev. A **103**, 053306 (2021).

[59] C.-H. Song, Q.-C. Gao, X.-Y. Hou, X. Wang, Z. Zhou, Y. He, and H. Guo, *Machine learning of XY model on a spherical Fibonacci lattice*, arXiv:2109.00254.

[60] B. Rhyno, N. Lundblad, D. C. Aveline, C. Lannert, and S. Vishveshwara, *Thermodynamics in expanding shell-shaped Bose-Einstein condensates*, arXiv:2106.00835.

[61] C. Lannert, T.-C. Wei, and S. Vishveshwara, *Dynamics of condensate shells: Collective modes and expansion*, Phys. Rev. A **75**, 013611 (2007).

[62] K. Sun, K. Padavić, F. Yang, S. Vishveshwara, and C. Lannert, *Static and dynamic properties of shell-shaped condensates*, Phys. Rev. A **98**, 013609 (2018).

[63] K. Padavić, K. Sun, C. Lannert, and S. Vishveshwara, *Physics of hollow Bose-Einstein condensates*, EPL **120**, 20004 (2018).

[64] P. C. Diniz, E. A. B. Oliveira, A. R. P. Lima, and E. A. L. Henn, *Ground state and collective excitations of a dipolar Bose-Einstein condensate in a bubble trap*, Sci. Rep. **10**, 4831 (2020).

[65] M. Arazo, R. Mayol, and M. Guilleumas, *Shell-shaped condensates with gravitational sag: contact and dipolar interactions*, arXiv:2107.04577.

[66] S. Prestipino and P. V. Giaquinta, *Ground state of weakly repulsive soft-core bosons on a sphere*, Phys. Rev. A **99**, 063619 (2019).

[67] N. S. Móller, F. E. A. dos Santos, V. S. Bagnato, and A. Pelster, *Bose-Einstein condensation on curved manifolds*, New J. Phys. **22**, 063059 (2020).

[68] A. Andriati, L. Brito, L. Tomio, and A. Gammal, *Stability of a Bose condensed mixture on a bubble trap*, arXiv:2107.04130.

[69] V. L. Berezinskii, *Destruction of Long-range Order in One-dimensional and Two-dimensional Systems Possessing a Continuous Symmetry Group. II. Quantum Systems*, Sov. Phys. JETP **34**, 610 (1972).

[70] J. M. Kosterlitz and D. Thouless, *Ordering, metastability and phase transitions in two-dimensional systems*, J. Phys. C **5**, L124 (1972).

[71] J. M. Kosterlitz and D. J. Thouless, *Ordering, metastability and phase transitions in two-dimensional systems*, J. Phys. C **6**, 1181 (1973).

[72] J. M. Kosterlitz, *The critical properties of the two-dimensional xy model*, J. Phys. C: Solid State Phys. **7**, 1046 (1974).

[73] D. R. Nelson and J. M. Kosterlitz, *Universal Jump in the Superfluid Density of Two-Dimensional Superfluids*, Phys. Rev. Lett. **39**, 1201 (1977).

[74] D. J. Bishop and J. D. Reppy, *Study of the Superfluid Transition in Two-Dimensional ^{4}He Films*, Phys. Rev. Lett. **40**, 1727 (1978).

[75] Z. Hadzibabic, P. Krüger, M. Cheneau, B. Battelier, and J. Dalibard, *Berezinski-Kosterlitz-Thouless crossover in a trapped atomic gas*, Nature **441**, 1118 (2006).

[76] P. Christodoulou, M. Gałka, N. Dogra, R. Lopes, J. Schmitt, and Z. Hadzibabic, *Observation of first and second sound in a BKT superfluid*, Nature **594**, 191 (2021).

[77] M. Bohlen, L. Sobirey, N. Luick, H. Biss, T. Enss, T. Lompe, and H. Moritz, *Sound Propagation and Quantum-Limited Damping in a Two-Dimensional Fermi Gas*, Phys. Rev. Lett. **124**, 240403 (2020).

[78] W. Zwerger, (editor) in *BCS–BEC Crossover and the Unitary Fermi Gas* (Lecture Notes in Physics, Springer, 2012).

[79] G. Calvanese Strinati, P. Pieri, G. Röpke, P. Schuck, and M. Urban, *The BCS–BEC crossover: From ultra-cold Fermi gases to nuclear systems*, Phys. Rep. **738**, 1 (2018).

[80] T. Giamarchi, *Quantum Physics in One Dimension* (Oxford University, New York, 2004).

[81] E. P. Gross, *Structure of a quantized vortex in boson systems*, Nuovo Cim. **20**, 454 (1961).

[82] L. P. Pitaevskii, *Vortex lines in an imperfect Bose gas*, Sov. Phys. JETP **13**, 451 (1961).

[83] D. S. Petrov, *Quantum Mechanical Stabilization of a Collapsing Bose-Bose Mixture*, Phys. Rev. Lett. **115**, 155302 (2015).

[84] D. S. Petrov and G. E. Astrakharchik, *Ultradilute Low-Dimensional Liquids*, Phys. Rev. Lett. **117**, 100401 (2016).

[85] A. Tononi, F. Toigo, S. Wimberger, A. Cappellaro, and L. Salasnich, *Dephasing-rephasing dynamics of one-dimensional tunneling quasicondensates*, New J. Phys. **22**, 073020 (2020).

[86] P. W. Anderson, *Measurement in Quantum Theory and the Problem of Complex Systems*, in J. de Boer, E. Dal, and O. Ulfbeck in *The Lesson of Quantum Theory*, (Elsevier, Amsterdam 1986)

[87] A. J. Leggett and F. Sols, *On the concept of spontaneously broken gauge symmetry in condensed matter physics*, Found. Phys. **21**, 353 (1990).

[88] Y. Castin and J. Dalibard, *Relative phase of two Bose-Einstein condensates* Phys. Rev. A **55**, 4330 (1997).

[89] K. Huang, *Statistical mechanics, 2nd edition* (Wiley, 1987).

[90] N. D. Mermin and H. Wagner, *Absence of Ferromagnetism or Antiferromagnetism in One- or Two-Dimensional Isotropic Heisenberg Models*, Phys. Rev. Lett. **17**, 1133 (1966).

[91] P. C. Hohenberg, *Existence of Long-Range Order in One and Two Dimensions*, Phys. Rev. **158**, 383 (1967).

[92] S. J. Bereta, L. Madeira, V. S. Bagnato, and M. A. Caracanhas, *Bose–Einstein condensation in spherically symmetric traps*, Am. J. Phys. **87**, 924 (2019).

[93] L. Salasnich, *Quantum Physics of Light and Matter* (Springer, 2017).

[94] R. P. Feynman, *Space-Time Approach to Non-Relativistic Quantum Mechanics*, Rev. Mod. Phys. **20**, 367 (1948).

[95] J. W. Negele and H. Orland, *Quantum Many-Particle Systems* (CRC Press, 2018).

[96] A. Tononi, *Bose-Einstein Condensation and Superfluidity in 3D and 2D bosons*, M.Sc. thesis, Università degli Studi di Padova, 2018.

[97] A. Tononi, A. Cappellaro, and L. Salasnich, *Condensation and superfluidity of dilute Bose gases with finite-range interaction*, New J. Phys. **20**, 125007 (2018).

[98] A. Tononi, *Zero-Temperature Equation of State of a Two-Dimensional Bosonic Quantum Fluid with Finite-Range Interaction*, Condens. Matter **4(1)**, 20 (2019).

[99] C. Chin, R. Grimm, P. Julienne, and E. Tiesinga, *Feshbach resonances in ultracold gases*, Rev. Mod. Phys. **82**, 1225 (2010).

[100] N. Nagaosa, *Quantum Field Theory in Condensed Matter Physics*, (Springer, Berlin, 1999).

[101] L. N. Cooper, *Bound electron pairs in a degenerate Fermi gas*, Phys. Rev. **104**, 1189 (1956).

[102] J. Tempere and J. P. A. Devreese, *Path-Integral Description of Cooper Pairing*, in *Superconductors– Materials, Properties and Applications*, edited by A. Gabovich (IntechOpen Ltd., London, UK, 2012).

[103] R. B. Diener, R. Sensarma, and M. Randeria, *Quantum fluctuations in the superfluid state of the BCS-BEC crossover*, Phys. Rev. A **77**, 023626 (2008).

[104] L. D. Landau and E. M. Lifshits, *Statistical physics, Part 1* (Pergamon, Oxford, 1980).

[105] W. Ketterle, D. S. Durfee, and D. M. Stamper-Kurn, in *Making, Probing and Understanding Bose-Einstein Condensates*, Proceedings of the International School of Physics "Enrico Fermi", edited by M. Inguscio, S. Stringari, and C. Wieman [arXiv:cond-mat/9904034v2 (1999)].

[106] B. M. Garraway and H. Perrin, *Recent developments in trapping and manipulation of atoms with adiabatic potentials*, J. Phys. B: At. Mol. Opt. Phys. **49**, 172001 (2016).

[107] E. Majorana, *Atomi orientati in campo magnetico variabile*, Il Nuovo Cimento (1924-1942) **9**, 43 (1932).

[108] T. Schumm, S. Hofferberth, L. M. Andersson, S. Wildermuth, S. Groth, I. Bar-Joseph, J. Schmiedmayer, and P. Krüger, *Matter-wave interferometry in a double well on an atom chip*, Nature Phys. **1**, 57 (2005).

[109] Y. Colombe, E. Knyazchyan, O. Morizot, B. Mercier, V. Lorent, and H. Perrin, *Ultracold atoms confined in rf-induced two-dimensional trapping potentials*, EPL **67**, 593 (2004).

[110] M. White, H. Gao, M. Pasienski, and B. DeMarco, *Bose-Einstein condensates in rf-dressed adiabatic potentials*, Phys. Rev. A **74**, 023616 (2006).

[111] B. E. Sherlock, M. Gildemeister, E. Owen, E. Nugent, and C. J. Foot, *Time-averaged adiabatic ring potential for ultracold atoms*, Phys. Rev. A **83**, 043408 (2011).

[112] Y. Guo, R. Dubessy, M. de Goër de Herve, A. Kumar, T. Badr, A. Perrin, L. Longchambon, and H. Perrin, *Supersonic Rotation of a Superfluid: A Long-Lived Dynamical Ring*, Phys. Rev. Lett. **124**, 025301 (2020).

[113] M. de Goër de Herve, Y. Guo, C. de Rossi, A. Kumar, T. Badr, R. Dubessy, L. Longchambon, and H. Perrin, *A versatile ring trap for quantum gases*, arXiv:2103.14310.

[114] Y. Guo, E. M. Gutierrez, D. Rey, T. Badr, A. Perrin, L. Longchambon, V. Bagnato, H. Perrin, and R. Dubessy, *An annular quantum gas induced by dimensional reduction on a shell*, arXiv:2105.12981.

[115] V. N. Popov, *On the theory of the superfluidity of two- and one-dimensional bose systems*, Theor. Math. Phys. **11**, 354 (1972).

[116] A. Altland and B. Simons, *Condensed Matter Field Theory* (Cambridge University Press, Cambridge, 2010).

[117] L. Salasnich and F. Toigo, *Zero-point energy of ultracold atoms*, Phys. Rep. **640**, 1 (2016).

[118] H. Kleinert, S. Schmidt, and A. Pelster, *Reentrant Phenomenon in the Quantum Phase Transitions of a Gas of Bosons Trapped in an Optical Lattice*, Phys. Rev. Lett. **93**, 160402 (2004).

[119] H. Kleinert, S. Schmidt, and A. Pelster, *Quantum phase diagram for homogeneous Bose-Einstein condensate*, Ann. Phys. **14**, 214 (2005).

[120] M. Schick, *Two-Dimensional System of Hard-Core Bosons*, Phys. Rev. A **3**, 1067 (1971).

[121] B. A. Lippmann and J. Schwinger, *Variational Principles for Scattering Processes. I*, Phys. Rev. **79**, 469 (1950).

[122] H. K. Stoof, K. B. Gubbels, and D. B. M. Dickerscheid, *Ultracold Quantum Fields* (Springer, Dordrecht, 2009).

[123] M. Born, *Zur Quantenmechanik der Stoßvorgänge*, Z. Phys. **37**, 863 (1926).

[124] L. Pricoupenko, *Isotropic contact forces in arbitrary representation: Heterogeneous few-body problems and low dimensions*, Phys. Rev. A **83**, 062711 (2011).

[125] C. Mora and Y. Castin, *Extension of Bogoliubov theory to quasicondensates*, Phys. Rev. A **67**, 053615 (2003).

[126] C. Mora and Y. Castin, *Ground State Energy of the Two-Dimensional Weakly Interacting Bose Gas: First Correction Beyond Bogoliubov Theory*, Phys. Rev. Lett. **102**, 180404 (2009).

[127] J. Zhang and T.-L. Ho, *Potential scattering on a spherical surface*, J. Phys. B **51**, 115301 (2018).

[128] L. D. Landau and E. M. Lifshitz, *Quantum Mechanics Non-Relativistic Theory* (Pergamon Press, New York, 1981).

[129] D. S. Petrov and G. V. Shlyapnikov, *Interatomic collisions in a tightly confined Bose gas*, Phys. Rev. A **64**, 012706 (2001).

[130] L. Onsager, *Statistical hydrodynamics*, Nuovo Cim. **6**, 279 (1949).

[131] R. P. Feynman,*Chapter II Application of quantum mechanics to liquid helium*, Progress in low temperature physics **1**, 17 (1955).

[132] E. Babaev and H. Kleinert, *Nonperturbative XY-model approach to strong coupling superconductivity in two and three dimensions*, Phys. Rev. B **59**, 12083 (1999).

[133] A. M. Turner, V. Vitelli, and D. R. Nelson, *Vortices on curved surfaces*, Rev. Mod. Phys. **82**, 1301 (2010).

[134] V. Kotsubo and G. A. Williams, *Kosterlitz-Thouless Superfluid Transition for Helium in Packed Powders*, Phys. Rev. Lett. **53**, 691 (1984).

[135] V. Kotsubo and G. A. Williams, *Superfluid transition of ^{4}He films adsorbed in porous materials*, Phys. Rev. B **33**, 6106 (1986).

[136] A. P. Young, *On the theory of the phase transition in the two-dimensional planar spin model*, J. Phys. C **11**, L453 (1978).

[137] J. M. Kosterlitz, *Kosterlitz-Thouless physics: a review of key issues*, *Rep. Prog. Phys.* **79**, 026001 (2016).

[138] I. Maccari, N. Defenu, L. Benfatto, C. Castellani, and T. Enss, *Interplay of spin waves and vortices in the two-dimensional XY model at small vortex-core energy*, Phys. Rev. B **102**, 104505 (2020).

[139] C. J. Foster, P. B. Blakie, and M. J. Davis, *Vortex pairing in two-dimensional Bose gases*, Phys. Rev. A **81**, 023623 (2010).

[140] K. Y. Szeto and G. Dresselhaus, *Zero-field susceptibility of finite-size Kosterlitz-Thouless systems*, Phys. Rev. B **32**, 3142 (1985).

[141] S. T. Bramwell and P. C. W. Holdsworth, *Magnetization: A characteristic of the Kosterlitz-Thouless-Berezinskii transition*, Phys. Rev. B **49**, 8811 (1994).

[142] Y. Komura and Y. Okabe, *Large-Scale Monte Carlo Simulation of Two-Dimensional Classical XY Model Using Multiple GPUs*, J. Phys. Soc. Japan **81**, 113001 (2012).

[143] A. Griffin, *Conserving and gapless approximations for an inhomogeneous Bose gas at finite temperatures*, Phys. Rev. B **53**, 9341 (1996).

[144] S. Giorgini, L. P. Pitaevskii, and S. Stringari, *Thermodynamics of a Trapped Bose-Condensed Gas*, J. Low Temp. Phys. **109**, 309 (1997).

[145] L. Salasnich, *Self-Consistent Derivation of the Modified Gross-Pitaevskii Equation with Lee-Huang-Yang Correction*, Appl. Sci. **8(10)**, 1998 (2018).

[146] A. Tononi, A. Cappellaro, G. Bighin, and L. Salasnich, *Propagation of first and second sound in a two-dimensional Fermi superfluid*, Phys. Rev. A **103**, L061303 (2021).

[147] G. Bighin and L. Salasnich, *Finite-temperature quantum fluctuations in two-dimensional Fermi superfluids*, Phys. Rev. B **93**, 014519 (2016).

[148] S. N. Klimin, J. T. Devreese, and J. Tempere, *Pseudogap and preformed pairs in the imbalanced Fermi gas in two dimensions*, New J. Phys. **14**, 103044 (2012).

[149] G. Bighin, *Mean field and fluctuations for fermionic systems: from ultracold Fermi gases to cuprates*, Ph.D. thesis, Università degli Studi di Padova, 2016.

[150] L. Salasnich, *Low-temperature thermodynamics of the unitary Fermi gas: Superfluid fraction, first sound, and second sound*, Phys. Rev. A **82**, 063619 (2010).

[151] L. Verney, L. Pitaevskii, and S. Stringari, *Hybridization of first and second sound in a weakly interacting Bose gas*, EPL **111**, 40005 (2015).

[152] G. Bighin and L. Salasnich, *Vortices and antivortices in two-dimensional ultracold Fermi gases*, Sci. Rep. **7**, 45702 (2017).

[153] N. Luick, L. Sobirey, M. Bohlen, V. Pal Singh, L. Mathey, T. Lompe, and H. Moritz, *An ideal Josephson junction in an ultracold two-dimensional Fermi gas*, Science **369**, 89 (2020).

[154] E. Arahata and T. Nikuni, *Propagation of second sound in a superfluid Fermi gas in the unitary limit*, Phys. Rev. A **80**, 043613 (2009).

[155] P. Noziéres and D. Pines, *The Theory of Quantum Liquids II: Superfluid Bose Liquids* (Westview Press, Boulder, 1999).

[156] T. Ozawa and S. Stringari, *Discontinuities in the First and Second Sound Velocities at the Berezinskii-Kosterlitz-Thouless Transition*, Phys. Rev. Lett. **112**, 025302 (2014).

[157] L. A. Sidorenkov, M. Tey, R. Grimm, Y.-H. Hou, L. Pitaevskii, and S. Stringari, *Second sound and the superfluid fraction in a Fermi gas with resonant interactions*, Nature **498**, 78 (2013).

[158] K. Furutani, A. Tononi, and L. Salasnich, *Sound modes in collisional superfluid Bose gases*, New J. Phys. **23**, 043043 (2021).

[159] S. Stringari, *Second sound seen*, Nat. Phys. **17**, 770 (2021).

[160] J. Dalibard, *Fluides quantiques de basse dimension et transition de Kosterlitz-Thouless*, (Collège de France Lecture Notes, 2016)

[161] N. Prokof'ev and B. Svistunov, *Two-dimensional weakly interacting Bose gas in the fluctuation region*, Phys. Rev. A **66**, 043608 (2002).

[162] J. Machta and R. Guyer, *Superfluid films on a cylindrical surface*, J. Low Temp. Phys. **74**, 231 (1989).

[163] A. Tononi, Y. Wang, and L. Salasnich, *Quantum Solitons in Spin-Orbit Coupled Bose-Bose Mixtures*, Phys. Rev. A **99**, 063618 (2019).

[164] S. Stringari and L. P. Pitaevskii, *Bose-Einstein Condensation and Superfluidity, 2nd edition* (Oxford Univ. Press, 2016).

[165] C. R. Cabrera, L. Tanzi, J. Sanz, B. Naylor, P. Thomas, P. Cheiney, and L. Tarruell, *Quantum liquid droplets in a mixture of Bose-Einstein condensates*, Science **359**, 301 (2018).

[166] G. Semeghini, G. Ferioli, L. Masi, C. Mazzinghi, L. Wolswijk, F. Minardi, M. Modugno, G. Modugno, M. Inguscio, and M. Fattori, *Self-Bound Quantum*

Droplets of Atomic Mixtures in Free Space, Phys. Rev. Lett. **120**, 235301 (2018).

[167] Y. L. Lin, K. Jiménez-García, and I. Spielman, *Spin-orbit-coupled Bose-Einstein condensates*, Nature **471**, 83 (2011).

[168] T.-L. Ho and S. Zhang, *Bose-Einstein Condensates with Spin-Orbit Interaction*, Phys. Rev. Lett. **107**, 150403 (2011).

[169] D. J. Korteweg and G. de Vries, *XLI. On the change of form of long waves advancing in a rectangular canal, and on a new type of long stationary waves*, London, Edinburgh Dublin Philos. Mag. J. Sci. **39:240**, 422 (1895).

[170] V. Achilleos, D. J. Frantzeskakis, P. G. Kevrekidis, and D. E. Pelinovsky, *Matter-Wave Bright Solitons in Spin-Orbit Coupled Bose-Einstein Condensates*, Phys. Rev. Lett. **110**, 264101 (2013).

[171] G. E. Astrakharchik and B. A. Malomed, *Dynamics of one-dimensional quantum droplets*, Phys. Rev. A **98**, 013631 (2018).

[172] A. Cappellaro, T. Macrì, G. F. Bertacco, and L. Salasnich, *Equation of state and self-bound droplet in Rabi-coupled Bose mixtures*, Sci. Rep. **7**, 13358 (2017).

[173] A. Cappellaro, T. Macrì, and L. Salasnich, *Collective modes across the soliton-droplet crossover in binary Bose mixtures*, Phys. Rev. A **97**, 053623 (2018).

[174] B. D. Josephson, *Possible new effects in superconductive tunnelling*, Phys. Lett. **1**, 251 (1962).

[175] A. Streltsov, G. Adesso, and M. B. Plenio, *Colloquium: Quantum coherence as a resource*, Rev. Mod. Phys. **89**, 041003 (2017).

[176] A. D. Cronin, J. Schmiedmayer, and D. E. Pritchard, *Optics and interferometry with atoms and molecules*, Rev. Mod. Phys. **81**, 1051 (2009).

[177] R. Bistritzer and E. Altman, *Intrinsic dephasing in one-dimensional ultracold atom interferometers*, Proc. Natl Acad. Sci. USA **104**, 9955 (2007).

[178] E. G. Dalla Torre, E. Demler, and A. Polkovnikov, *Universal Rephasing Dynamics after a Quantum Quench via Sudden Coupling of Two Initially Independent Condensates*, Phys. Rev. Lett. **110**, 090404 (2013).

[179] M. Gring, M. Kuhnert, T. Langen, T. Kitagawa, B. Rauer, M. Schreitl, I. Mazets, D. Adu Smith, E. Demler, and J. Schmiedmayer, *Relaxation and Prethermalization in an Isolated Quantum System*, Science **337**, 1318 (2012).

[180] A. Smerzi, S. Fantoni. S. Giovanazzi, and S. R. Shenoy, *Quantum Coherent Atomic Tunneling between Two Trapped Bose-Einstein Condensates*, Phys. Rev. Lett. **79**, 4950 (1997).

[181] M. Pigneur, T. Berrada, M. Bonneau, T. Schumm, E. Demler, and J. Schmiedmayer, *Relaxation to a Phase-Locked Equilibrium State in a One-Dimensional Bosonic Josephson Junction*, Phys. Rev. Lett. **120**, 173601 (2018).

[182] T. Betz, S. Manz, R. Bücker, T. Berrada, Ch. Koller, G. Kazakov, I. E. Mazets, H.-P. Stimming, A. Perrin, T. Schumm, and J. Schmiedmayer, *Two-Point Phase Correlations of a One-Dimensional Bosonic Josephson Junction*, Phys. Rev. Lett. **106**, 020407 (2011).

[183] D. A. Atkinson, *An exact treatment of the Dirac delta function potential in the Schrödinger equation*, Am. J. Phys. **43**, 301 (1975).

[184] R. Robinett and L. Bassett, *Analytic Results for Gaussian Wave Packets in Four Model Systems: I. Visualization of the Kinetic Energy*, Found. Phys. Lett. **17**, 607 (2004).

[185] A. Polkovnikov, E. Altman, and E. Demler, *Interference between independent fluctuating condensates*, Proc. Natl. Acad. Sci. USA **103**, 6125 (2006).

[186] S. Hofferberth, I. Lesanovsky, B. Fischer, T. Schumm, and J. Schmiedmayer, *Non-equilibrium coherence dynamics in one-dimensional Bose gases*, Nature **449**, 324 (2007).

[187] I. S. Gradshteyn and I. M. Ryzhik, *Table of Integrals, Series, and Products* (Academic Press, 1996).